



Measurements of electroweak $W^\pm Z$ boson pair production in association with two jets in pp collisions at $\sqrt{s} = 13$ TeV with the ATLAS detector

The ATLAS Collaboration

Measurements of integrated and differential cross-sections for electroweak $W^\pm Z$ production in association with two jets ($W^\pm Zjj$) in proton–proton collisions are presented. The data collected by the ATLAS detector at the Large Hadron Collider from 2015 to 2018 at a centre-of-mass energy of $\sqrt{s} = 13$ TeV are used, corresponding to an integrated luminosity of 140 fb^{-1} . The $W^\pm Zjj$ candidate events are reconstructed using leptonic decay modes of the gauge bosons. Events containing three identified leptons, either electrons or muons, and two jets are selected. Processes involving pure electroweak $W^\pm Zjj$ production at Born level are separated from $W^\pm Zjj$ production involving a strong coupling. The measured integrated fiducial cross-section of electroweak $W^\pm Zjj$ production per lepton flavour is $\sigma_{WZjj\text{-EW}\rightarrow\ell'\nu\ell\ell jj} = 0.368 \pm 0.037$ (stat.) ± 0.059 (syst.) ± 0.003 (lumi.) fb. Respective cross-sections of electroweak and strong $W^\pm Zjj$ production are measured separately for events with exactly two jets or with more than two jets, and in three bins of the invariant mass of the two jets. The inclusive $W^\pm Zjj$ production cross-section, without separating electroweak and strong production, is also measured to be $\sigma_{WZjj\rightarrow\ell'\nu\ell\ell jj} = 1.462 \pm 0.063$ (stat.) ± 0.118 (syst.) ± 0.012 (lumi.) fb, per lepton flavour. The inclusive $W^\pm Zjj$ production cross-section is measured differentially for several kinematic observables. Finally, the measurements are used to constrain anomalous quartic gauge couplings by extracting 95% confidence level intervals on dimension-8 operators.

Contents

1	Introduction	2
2	ATLAS detector	4
3	Phase space for cross-section measurements	4
4	Signal and background simulation	5
5	Event selection	7
6	Background estimation	9
7	Measurements methodology	10
7.1	$WZjj$ -EW and $WZjj$ -strong integrated measurements	10
7.2	$WZjj$ -EW and $WZjj$ -strong differential measurements	12
7.3	$W^\pm Zjj$ differential measurements	12
8	Systematic uncertainties	13
9	Results	15
9.1	$WZjj$ -EW and $WZjj$ -strong integrated measurements	15
9.2	$WZjj$ -EW and $WZjj$ -strong differential measurements	18
9.3	$W^\pm Zjj$ differential measurements	19
10	Limits on anomalous quartic gauge couplings	25
11	Conclusion	28

1 Introduction

Vector boson scattering (VBS), $VV \rightarrow VV$ with $V = W/Z/\gamma$, is a key process with which to probe the $SU(2)_L \times U(1)_Y$ gauge symmetry of the electroweak (EW) theory that determines the self-couplings of the vector bosons. New phenomena beyond the Standard Model (SM) can alter the couplings of vector bosons, generating additional contributions to quartic gauge couplings (QGC) compared with the SM predictions [1–3].

In proton–proton collisions, VBS is initiated by an interaction of two vector bosons radiated from the initial-state quarks, yielding a final state with two bosons and two jets, $VVjj$, in a purely electroweak process [4]. VBS diagrams are not independently gauge invariant and cannot be studied separately from other processes leading to the same $VVjj$ final state [5]. Two categories of processes give rise to $VVjj$ final states. The first category, which includes VBS contributions, involves exclusively weak interactions at Born level of order α_{EW}^6 including the boson decays, where α_{EW} is the electroweak coupling constant. It is referred to as EW production. The second category involves both the quantum chromodynamics (QCD) and electroweak interactions at Born level of order $\alpha_s^2 \alpha_{EW}^4$, where α_s is the strong interaction coupling constant. It is referred to as QCD production. According to the SM a small interference occurs between

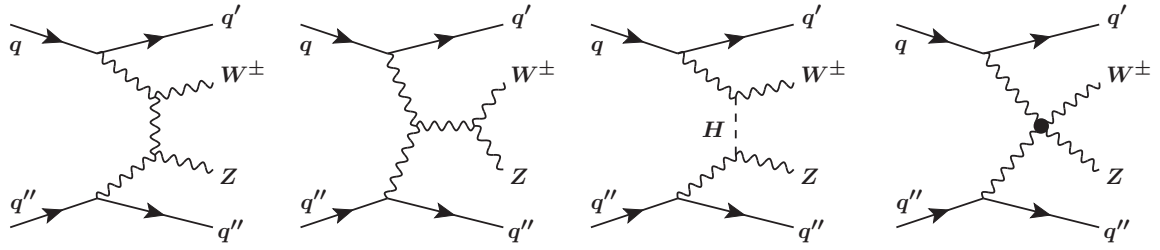


Figure 1: Representative diagrams at LO of the $WZjj$ -EW production in pp collisions.

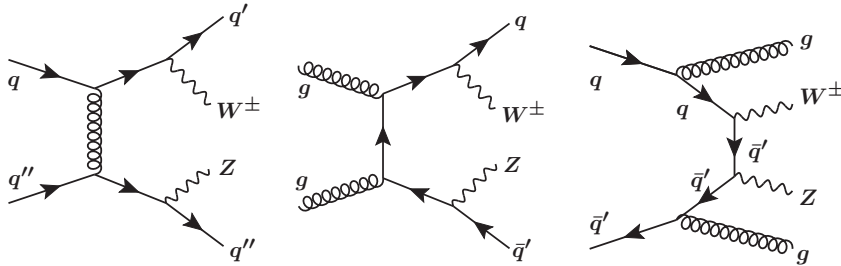


Figure 2: Representative diagrams at LO of the $WZjj$ -QCD production in pp collisions.

electroweak and QCD production that also involves both the strong and electroweak interactions at Born level of orders $\alpha_s \alpha_{EW}^5$. The sum of QCD and interference contributions are referred to as strong production, as opposite to the pure EW production. Representative diagrams at LO of $WZjj$ -EW and $WZjj$ -QCD production are presented in Figures 1 and 2, respectively.

A first observation of $W^\pm Zjj$ electroweak production was reported by the ATLAS Collaboration [6] using an integrated luminosity of 36 fb^{-1} of pp collision data collected at a centre-of-mass energy of 13 TeV. The observation was then confirmed by the CMS Collaboration using data corresponding to an integrated luminosity of 137 fb^{-1} [7]. In these two results only integrated measurements of the electroweak $W^\pm Zjj$ production cross-section were made, without further attempts to verify the modelling of key kinematic observables of the electroweak $W^\pm Zjj$ processes by theory predictions. The CMS and ATLAS Collaborations also used the measured $W^\pm Zjj$ events to obtain constraints on the structure of quartic vector boson interactions in an Effective Field Theory (EFT) framework [7, 8].

This paper presents measurements of integrated and differential cross-sections for electroweak and inclusive $W^\pm Zjj$ production, exploiting the fully leptonic decays of the Z and W bosons where final state charged leptons are electrons or muons. The pp collision data were collected with the ATLAS detector from 2015 to 2018 at a centre-of-mass energy of $\sqrt{s} = 13 \text{ TeV}$ and correspond to an integrated luminosity of 140 fb^{-1} . A multivariate discriminant constructed from a boosted decision tree (BDT) is used to separate electroweak and strong $W^\pm Zjj$ production modes. Their respective cross-sections are measured integrated over a fiducial phase space. They are also measured differentially in three bins of the invariant mass of the two tagging jets, m_{jj} , and separately for events with exactly two jets or with more than two jets. The cross-section of inclusive $W^\pm Zjj$ production is also measured differentially as a function of various kinematic observables sensitive to the modelling from Monte Carlo (MC) event generators or to new physics effects. The distributions of the transverse mass of the $W^\pm Z$ system, m_T^{WZ} , and of the BDT score are used in an EFT interpretation to constrain dimension-8 operators.

2 ATLAS detector

The ATLAS experiment [9] at the Large Hadron Collider (LHC) [10] is a multipurpose particle detector with a forward–backward symmetric cylindrical geometry and a near 4π coverage in solid angle.¹ It consists of an inner tracking detector (ID) surrounded by a thin superconducting solenoid providing a 2 T axial magnetic field, electromagnetic and hadron calorimeters and a muon spectrometer (MS). The inner tracking detector covers the pseudorapidity range $|\eta| < 2.5$. It consists of silicon pixel, silicon microstrip and transition radiation tracking detectors. Lead/liquid-argon (LAr) sampling calorimeters provide electromagnetic (EM) energy measurements with high granularity. A steel/scintillator-tile hadron calorimeter covers the central pseudorapidity range ($|\eta| < 1.7$). The endcap and forward regions are instrumented with LAr calorimeters for both the EM and hadronic energy measurements up to $|\eta| = 4.9$. The muon spectrometer surrounds the calorimeters and is based on three large superconducting air-core toroidal magnets with eight coils each. The field integral of the toroids ranges between 2.0 and 6.0 T m across most of the detector. The muon spectrometer includes a system of precision tracking chambers and fast detectors for triggering. A two-level trigger system is used to select events. The first-level trigger is implemented in hardware and uses a subset of the detector information to accept events at a rate below 100 kHz. This is followed by a software-based trigger that reduces the accepted event rate to 1 kHz on average depending on the data-taking conditions. An extensive software suite [11] is used in the reconstruction and analysis of real and simulated data, in detector operations, and in the trigger and data acquisition systems of the experiment.

3 Phase space for cross-section measurements

The $W^\pm Z jj$ cross-sections are measured in a fiducial phase space that is defined by the kinematics of the final-state leptons, electrons or muons, associated with the W^\pm and Z boson decays. Leptons produced in the decay of a hadron, a τ -lepton, or their descendants are not considered in the definition of the fiducial phase space and are treated as background. At particle level, the kinematics of the charged leptons after quantum electrodynamics (QED) final-state radiation (FSR) are ‘dressed’ by including contributions from photons with an angular distance $\Delta R < 0.1$ from the lepton. Dressed charged leptons, and final-state neutrinos that do not originate from hadron or τ -lepton decays, are matched to the W^\pm and Z boson decay products using a MC generator-independent algorithmic approach, called the ‘resonant shape’ algorithm [12]. This algorithm is based on the value of an estimator expressing the product of the nominal line-shapes of the W and Z resonances,

$$P = \left| \frac{1}{m_{(\ell^+, \ell^-)}^2 - (m_Z^{\text{PDG}})^2 + i \Gamma_Z^{\text{PDG}} m_Z^{\text{PDG}}} \right|^2 \times \left| \frac{1}{m_{(\ell', \nu_{\ell'})}^2 - (m_W^{\text{PDG}})^2 + i \Gamma_W^{\text{PDG}} m_W^{\text{PDG}}} \right|^2,$$

where m_Z^{PDG} (m_W^{PDG}) and Γ_Z^{PDG} (Γ_W^{PDG}) are the world average mass and total width of the Z (W) boson, respectively, as reported by the Particle Data Group [13]. The input to the estimator is the invariant mass m of all possible pairs (ℓ^+, ℓ^-) and $(\ell', \nu_{\ell'})$ satisfying the fiducial selection requirements defined in the

¹ ATLAS uses a right-handed coordinate system with its origin at the nominal interaction point (IP) in the centre of the detector and the z -axis along the beam pipe. The x -axis points from the IP to the centre of the LHC ring, and the y -axis points upwards. Cylindrical coordinates (r, ϕ) are used in the transverse plane, ϕ being the azimuthal angle around the z -axis. The pseudorapidity is defined in terms of the polar angle θ as $\eta = -\ln \tan(\theta/2)$. Angular distance is measured in units of $\Delta R \equiv \sqrt{(\Delta\eta)^2 + (\Delta\phi)^2}$.

next paragraph. The final choice of which leptons are assigned to the W or Z bosons corresponds to the configuration exhibiting the largest value of the estimator. Using this association algorithm, the gauge boson kinematics can be computed using the kinematics of the associated leptons independently of any internal MC generator details.

The fiducial phase space of the measurement is the same as used in Ref. [6]. It is defined at particle level by the following requirements: the charged leptons from the Z boson decay are required to have transverse momentum $p_T > 15$ GeV, the charged lepton from the W^\pm decay is required to have transverse momentum $p_T^\ell > 20$ GeV, the charged leptons from the W^\pm and Z bosons are required to have $|\eta| < 2.5$ and the invariant mass of the two leptons from the Z boson decay must be within 10 GeV of the nominal Z boson mass, taken from the world average value, $m_Z^{\text{PDG}} = 91.1876$ GeV [13]. The W boson transverse mass, defined as $m_T^W = \sqrt{2 \cdot p_T^\nu \cdot p_T^\ell \cdot [1 - \cos \Delta\phi(\ell, \nu)]}$, where $\Delta\phi(\ell, \nu)$ is the angle between the lepton and the neutrino in the transverse plane and p_T^ν is the transverse momentum of the neutrino, is required to be $m_T^W > 30$ GeV. The angular distance between the charged lepton from the W^\pm decay and each of the charged leptons from the Z decay is required to be $\Delta R > 0.3$, and the angular distance between the two leptons from the Z decay is required to be $\Delta R > 0.2$.

In addition to these requirements that define an inclusive phase space, at least two jets with $p_T > 40$ GeV and $|\eta_j| < 4.5$ are required. These particle-level jets are reconstructed from stable particles with a lifetime of $\tau > 30$ ps in the simulation after parton showering, hadronisation, and decay of particles with $\tau < 30$ ps. Muons, electrons, neutrinos and photons associated with W and Z decays are excluded. The particle-level jets are reconstructed using the anti- k_r [14, 15] algorithm with a radius parameter $R = 0.4$. The angular distance between all selected leptons and jets is required to be $\Delta R(j, \ell) > 0.3$. If this requirement is not satisfied, the jet is discarded. The invariant mass, m_{jj} , of the two highest- p_T jets in opposite hemispheres, $\eta_{j1} \cdot \eta_{j2} < 0$, is required to be $m_{jj} > 500$ GeV to enhance the sensitivity to VBS processes. These two jets are referred to as tagging jets. Finally, processes with a b -quark in the initial state, such as tZj production, are not considered as part of the $WZjj$ -EW events. The production of tZj results from a t -channel exchange of a W boson between a b - and a u -quark giving a final state with a t -quark, a Z boson and a light-quark jet, but does not include diagrams with gauge boson couplings.

4 Signal and background simulation

The MADGRAPH5_AMC@NLO 2.6.5 [16] MC event generator, interfaced with PYTHIA 8.240 [17] using the A14 tune [18] for the modelling of the parton shower (PS), hadronisation and underlying event, was used to model $W^\pm Zjj$ events. The NNPDF3.0NLO [19] parton distribution function (PDF) set was used for the hard-scattering process, while the NNPDF2.3LO [19] PDF set was used for the PS. The dipole recoil scheme [20] is used for the PS. The default dynamic renormalisation and factorisation scales set by MADGRAPH5_AMC@NLO [21] were used. A first MC event sample, referred to as $WZjj$ -EW, includes processes of order six (zero) in α_{EW} (α_s). In this sample, which includes VBS diagrams, two additional jets originating from electroweak vertices from matrix-element partons are included in the final state. Diagrams with a b -quark in either the initial or final state, i.e. b -quarks in the matrix-element calculation, are not considered. This sample provides a LO prediction for the $WZjj$ -EW signal process. A second MC event sample, referred to as $WZjj$ -QCD, includes processes of order four in α_{EW} in the matrix-element. Matrix elements containing three leptons, one neutrino and up to two jets in the final state were calculated at NLO QCD and merged with the PS from PYTHIA 8.210 using the FxFx scheme [22]. This $WZjj$ -QCD sample includes matrix-element b -quarks. Interferences between the $WZjj$ -EW and $WZjj$ -QCD processes,

labelled $WZjj$ -INT, include only contributions to the squared matrix-element of order one in α_s . Their contribution is simulated at LO in a third MC sample using MADGRAPH5_AMC@NLO 2.6.5 [16] and the same parameters as used for $WZjj$ -EW events. The contribution of interferences is found to be positive and approximately 6% of the $WZjj$ -EW cross-section in the fiducial phase space at particle level and maximally 12% of the $WZjj$ -EW cross-section for events with three or more jets of $p_T > 25$ GeV.

For the estimate of the PS uncertainties in the simulation of the $WZjj$ -EW process, an alternative MC sample was simulated using MADGRAPH5_AMC@NLO 2.6.5 interfaced with HERWIG 7.1 [23, 24]. For the estimate of modelling uncertainties and comparisons to data, alternative MC samples of $WZjj$ -QCD and $WZjj$ -EW processes were generated with the SHERPA 2.2.12 [25] MC event generator. For $WZjj$ -QCD processes, the matrix elements contain all diagrams with four electroweak vertices. They were calculated for up to one parton at next-to-leading-order (NLO) in QCD and up to three partons at leading-order (LO) using Comix [26] and OPENLOOPS [27], and merged with the SHERPA PS [28] according to the ME+PS@NLO prescription [29]. The NNPDF3.0NNLO PDF set was used along with the associated set of tuned parton-shower parameters developed by the SHERPA authors. For $WZjj$ -EW production, processes of order six (zero) in α_{EW} (α_s) are included. Two additional jets originating from electroweak vertices from matrix-element partons are included in the final state. Diagrams with a b -quark in either the initial or final state are not considered. The LO-accurate matrix elements for up to one additional parton were matched to a PS based on Catani-Seymour dipole factorisation [26, 28] using the MEPS@LO prescription [29–32]. The contribution of interferences is not simulated using SHERPA 2.2.12 but the $WZjj$ -INT prediction from MADGRAPH5_AMC@NLO 2.6.5 is added to the $WZjj$ -EW and $WZjj$ -QCD SHERPA 2.2.12 predictions to form the $W^\pm Zjj$ SHERPA 2.2.12 prediction.

The background sources include processes with two or more electroweak gauge bosons, namely ZZ , WW and VVV ($V = W, Z$); processes with top quarks, such as $t\bar{t}$ and $t\bar{t} + V$, single top and tZj ; and processes with gauge bosons associated with jets or photons ($Z + j$ and $Z\gamma$). MC simulation is used to estimate the contribution from background processes with three or more prompt leptons. Background processes with at least one misidentified lepton are evaluated using data-driven techniques and simulated events are used to assess the systematic uncertainties of these backgrounds.

The SHERPA 2.2.2 event generator was used to simulate both the $q\bar{q}$ and gg -initiated ZZ processes, including $H \rightarrow ZZ$ production, using the NNPDF3.0NNLO PDF set. It provides a matrix element calculation accurate to NLO in α_s for 0- and 1-jet final states, and LO accuracy for 2- and 3-jet final states. The $ZZjj$ -EW production was modelled using the MADGRAPH5_AMC@NLO 2.6.7 generator with matrix elements calculated at LO in QCD and with the NNPDF3.0NNLO PDF set. The events were interfaced with PYTHIA 8.230 using the A14 tune and the NNPDF2.3LO PDF set.

The production of $t\bar{t} + V$ events was modelled using the MADGRAPH5_AMC@NLO 2.3.3 [16] generator at NLO with the NNPDF3.0NNLO PDF. The events were interfaced to PYTHIA 8.210 using the A14 tune and the NNPDF2.3LO PDF set. The tZj process was modelled using the MADGRAPH5_AMC@NLO 2.3.3 [16] generator at NLO with the NNPDF3.0NNLO PDF. The events were interfaced with PYTHIA 8.230 using the A14 tune and the NNPDF2.3LO PDF set. Finally, the on-shell production of triboson events with fully leptonic decays were simulated by the SHERPA 2.2.2 event generator at NLO accuracy with zero additional partons and at LO accuracy with one and two additional partons and using the NNPDF3.0NNLO PDF set. The decays of bottom and charm hadrons were simulated using the EVTGEN 1.2.0 program [33], except for processes modelled using SHERPA.

All generated MC events were passed through the ATLAS detector simulation [34], based on GEANT4 [35], and processed using the same reconstruction software as used for the data. The event samples include the

simulation of additional pp interactions (pile-up) generated with PYTHIA 8.186 using the NNPDF2.3LO PDF set and the A3 [36] set of tuned parameters. Simulated events were reweighted to match the pile-up conditions observed in the data. Furthermore, the lepton and jet momentum scale and resolution, the lepton reconstruction, identification, isolation and trigger efficiencies and the pile-up jets and b -jet veto efficiencies in the simulation were corrected to match those measured in data.

5 Event selection

Only data recorded with stable beam conditions and with all relevant detector subsystems operational are considered. Candidate events are selected using triggers requiring at least one electron or muon [37–39]. These triggers require leptons to satisfy different transverse momentum thresholds and isolation criteria, which depend on the data-taking run period and the instantaneous luminosity. The combined efficiency of these triggers is 99% for $W^\pm Zjj$ events satisfying the offline selection criteria. Events are required to have a primary vertex compatible with the LHC luminous region inside the ATLAS detector. The primary vertex is defined as the reconstructed vertex with at least two charged-particle tracks that has the largest sum of the p_T^2 for the associated tracks.

Muon candidates are identified by tracks reconstructed in the MS and matched to tracks reconstructed in the ID. Muons are required to satisfy a ‘medium’ identification selection [40, 41]. The efficiency of this selection averaged over p_T and η is larger than 98%. The muon momentum is measured by combining the MS measurement, corrected for the energy deposited in the calorimeters, and the ID measurement. The p_T of the muon must be greater than 15 GeV and its pseudorapidity must satisfy $|\eta| < 2.5$.

Electron candidates are reconstructed from energy clusters in the electromagnetic calorimeter matched to ID tracks. Electrons are identified using a discriminant that is the value of a likelihood function constructed with information about the shape of the electromagnetic showers in the calorimeter, the track properties and the quality of the track-to-cluster matching for the candidate [42]. Electrons must satisfy a ‘medium’ likelihood requirement, which provides an overall identification efficiency of 90%. The electron momentum is computed from the cluster energy and the direction of the track. The p_T of the electron must be greater than 15 GeV and the pseudorapidity of the cluster must satisfy $|\eta| < 1.37$ or $1.52 < |\eta| < 2.47$.

Electron and muon candidates are required to originate from the primary vertex. Thus, the significance of the track’s transverse impact parameter calculated relative to the beam line, $|d_0/\sigma_{d_0}|$, must be smaller than 3.0 for muons and less than 5.0 for electrons. Furthermore, the longitudinal impact parameter, z_0 (the difference between the value of z of the point on the track at which d_0 is defined and the longitudinal position of the primary vertex), is required to satisfy $|z_0 \cdot \sin(\theta)| < 0.5$ mm.

Electrons and muons are required to be isolated from other particles using both calorimeter-cluster and ID-track information. The isolation requirement for electrons is tuned for an efficiency of at least 90% for $p_T > 25$ GeV and at least 99% for $p_T > 60$ GeV [41], while particle-flow-based isolation variables are used for muons, providing an efficiency above 90% for $p_T > 15$ GeV and at least 99% for $p_T > 60$ GeV [42].

Jets of hadrons are reconstructed using a particle-flow algorithm based on noise-suppressed positive-energy topological clusters in the calorimeters [43]. Energy deposited in the calorimeters by charged particles is subtracted and replaced by the momenta of tracks which are matched to those topological clusters. Tracks which are not matched to the primary vertex are not used in jet reconstruction, which effectively removes contribution from charged particle pile-up. The jets are clustered using the anti- k_r algorithm with a radius parameter $R = 0.4$. They are calibrated according to in situ measurements of the jet energy scale [44].

All jets must have $p_T > 25$ GeV and be reconstructed in the pseudorapidity range $|\eta| < 4.5$. To reduce the impact of jets originating from pile-up interactions, jets with $|\eta| < 2.4$ and $p_T < 60$ GeV, or with $2.5 < |\eta| < 4.5$ and $p_T < 120$ GeV, are required to satisfy the ‘tight’ and ‘loose’ working points of the jet vertex [45] and forward jet vertex [46] tagging algorithms, respectively. Jets with $|\eta| < 2.5$ containing a b -hadron are identified with a deep-learning neural network (NN) [47] which uses distinctive features of b -hadron decays in terms of the impact parameters of the tracks and the displaced vertices reconstructed in the inner detector. Jets initiated by b -quarks are selected by setting the algorithm’s output threshold such that an 70% b -jet selection efficiency is achieved in simulated $t\bar{t}$ events, with a rejection factor of 40 against light-flavour jets. Corrections to the flavour-tagging efficiencies are based on data-driven calibration analyses [47].

The transverse momentum of the neutrino is estimated from the missing transverse momentum in the event, E_T^{miss} , calculated as the negative vector sum of the transverse momentum of all identified hard physics objects (electrons, muons, jets), with a contribution from an additional soft term. This soft term is calculated from ID tracks matched to the primary vertex and not assigned to any of the hard objects [48].

Events are required to contain exactly three lepton candidates satisfying the selection criteria described above. To ensure that the trigger efficiency is well determined, at least one of the candidate leptons is required to have $p_T > 25$ GeV for 2015 and $p_T > 27$ GeV for 2016–2018 data, as well as being geometrically matched to a lepton that was selected by the trigger. This detector-level requirement that the transverse momentum of the leading lepton be above 27 GeV is not present in the definition of the fiducial phase space. It would reduce the acceptance of the fiducial phase space by only 0.02%.

To suppress background processes with at least four prompt leptons, events with a fourth lepton candidate satisfying looser selection criteria are rejected. For this looser selection, the lepton p_T requirement is lowered to $p_T > 5$ GeV, electrons are allowed to be reconstructed in the region $1.37 < |\eta| < 1.52$ and ‘loose’ identification requirements [41, 42] are used for both the electrons and muons. A less stringent requirement is applied for electron isolation and is based only on ID track information. No dedicated identification algorithm is used to suppress events with electrons and muons originating from the decay of τ -leptons.

Candidate events are required to have at least one pair of leptons with the same flavour and opposite charge, with an invariant mass that is consistent with m_Z^{PDG} to within 10 GeV. This pair is considered to be the Z boson candidate. If more than one pair can be formed, the pair whose invariant mass is closest to m_Z^{PDG} is taken as the Z boson candidate. The remaining third lepton is assigned to the W boson decay. The transverse mass of the W candidate, computed using E_T^{miss} and the p_T of the associated lepton, is required to be greater than 30 GeV.

Backgrounds originating from misidentified leptons are suppressed by requiring the lepton associated with the W boson to satisfy more stringent selection criteria. The transverse momentum of this lepton is therefore required to be greater than 20 GeV. This lepton is also required to satisfy the ‘tight’ identification and isolation requirements [41, 42], which results in an efficiency between 90% and 98% depending on p_T for muons and an overall efficiency of 85% for electrons.

To select $W^\pm Z jj$ candidates, events are further required to be associated with at least two ‘tagging’ jets. The leading tagging jet is selected as the highest- p_T jet in the event with $p_T > 40$ GeV. The second tagging jet is selected as the one with the highest p_T among the remaining jets that have a pseudorapidity of opposite sign to the first tagging jet and a $p_T > 40$ GeV. These two jets are required to satisfy $m_{jj} > 150$ GeV, in order to minimise the contamination from triboson processes.

The final signal region (SR) for VBS processes is defined by requiring that the invariant mass of the two tagging jets, m_{jj} , be greater than 500 GeV and that no b -jet be present in the event.

6 Background estimation

The background sources are classified into two groups: events where all candidates are prompt leptons or are produced in the decay of a τ -lepton (irreducible background) and events where at least one of the candidate leptons is not a prompt lepton (reducible background). Candidates that are not prompt leptons are also called ‘misidentified’ or ‘fake’ leptons.

The main sources of irreducible background arise from ZZ and $t\bar{t} + V$ (where $V = Z$ or W). These irreducible backgrounds are modelled using MC simulations. Data in two dedicated control regions (CR), referred to as ZZ -CR and b -CR, respectively, are used to constrain the normalisations of the $ZZjj$ -QCD and $t\bar{t} + V$ backgrounds. The control region ZZ -CR, enriched in ZZ events, is defined by applying the $W^\pm Zjj$ event selection defined in Section 5, but instead of vetoing a fourth lepton, events must have at least a fourth lepton candidate with looser identification requirements. This region is dominated by $ZZjj$ -QCD events with a small contribution of $ZZjj$ -EW events. The control region b -CR, enriched in $t\bar{t} + V$ and tZj events, is defined by selecting $W^\pm Zjj$ candidate events having at least one reconstructed b -jet. The remaining sources of irreducible background are $ZZjj$ -EW and VVV events. Their contributions in the control and signal regions are estimated from MC simulations.

The reducible backgrounds originate from $Z + j$, $Z\gamma$, $t\bar{t}$, Wt and WW production processes. These backgrounds are estimated by using a data-driven method based on the inversion of a global matrix containing the efficiencies and the misidentification probabilities for prompt and fake leptons [12, 49–51]. The method exploits the classification of the leptons as loose or tight candidates and the probability that a fake lepton is misidentified as a loose or tight lepton candidate. Tight lepton candidates are signal lepton candidates as defined in Section 5. Loose lepton candidates are leptons that do not meet the isolation and identification criteria of signal lepton candidates but satisfy only looser criteria. The misidentification probabilities for misidentified leptons are determined from data using dedicated control samples each enriched in misidentified leptons from light- or heavy-flavour jets and from photon conversions, respectively. The lepton efficiencies for prompt leptons are determined as detailed in Refs. [40–42]. The lepton efficiencies and misidentification probabilities are combined with event rates in data samples of $W^\pm Zjj$ candidate events where at least one and up to three of the leptons are loose. Then, solving a system of linear equations, the number of events with at least one misidentified lepton is obtained, which represents the amount of reducible background in the $W^\pm Zjj$ sample. The method allows the shape of any kinematic distribution of reducible background events to be estimated. Another independent method of assessing the reducible background was also considered. This method estimates the amount of reducible background using MC simulations scaled to data by process-dependent factors determined from the data-to-MC comparison in dedicated control regions. Agreement within 20% with the matrix method estimate is obtained in both yield and shape of the distributions of irreducible background events. This level of agreement is compatible with the systematic uncertainties determined for the matrix method estimate.

The number of expected and observed events is summarised in Table 1 for the signal region and the two control regions. All sources of uncertainties, as described in Section 8, are included. The expected contribution of $WZjj$ -EW events in the $W^\pm Zjj$ signal region is about 16% while 64% of the events are expected to arise from $WZjj$ -QCD production.

Table 1: Expected and observed numbers of events in the $W^\pm Zjj$ signal region and in the two control regions, before the fit described in Section 7.1. The expected number of $WZjj$ -EW, $WZjj$ -QCD and $WZjj$ -INT events and the estimated number of background events from the other processes are shown. The sum of the backgrounds containing misidentified leptons is labelled ‘Misid. leptons’. The total systematic uncertainties are quoted.

	SR, $N_{\text{jets}} = 2$		SR, $N_{\text{jets}} \geq 3$		b -CR		ZZ-CR	
Data	169		477		666		210	
Total pred.	231	± 12	550	± 50	660	± 40	205	± 11
$WZjj$ -EW	65.0	± 3.5	60	± 6	4.82	± 0.28	0.725	± 0.014
$WZjj$ -QCD	125	± 9	380	± 50	77	± 18	6.2	± 0.7
$WZjj$ -INT	1.3	± 0.6	5.3	± 2.6	0.58	± 0.29	0.22	± 0.11
$t\bar{t} + V$	0.66	± 0.04	20.2	± 0.7	289	± 10	9.89	± 0.28
tZj	8.78	± 0.34	19.7	± 1.2	134	± 4	0.432	± 0.005
ZZ-QCD	9.6	± 0.4	32.0	± 2.5	10.1	± 0.6	159	± 9
ZZ-EW	2.2	± 0.6	4.4	± 1.1	0.25	± 0.06	23	± 6
VVV	0.41	± 0.10	2.0	± 0.5	0.39	± 0.10	4.1	± 1.1
Misid. leptons	18	± 4	28	± 7	150	± 40	1.7	± 0.5

7 Measurements methodology

7.1 $WZjj$ -EW and $WZjj$ -strong integrated measurements

Events associated to $WZjj$ -EW production are separated from other $W^\pm Zjj$ events originating from $WZjj$ -QCD production and from the interference $WZjj$ -INT, based on their kinematic properties as modelled by MC predictions. The production cross-section of the two populations of events, $\sigma_{WZjj\text{-EW}}$ and $\sigma_{WZjj\text{-strong}}$, are then measured simultaneously.

Given the small contribution to the signal region of $WZjj$ -EW processes, a multivariate discriminant is used to separate the signal from the backgrounds. A BDT, as implemented in the TMVA package [52], is used to exploit the kinematic differences between the $WZjj$ -EW signal and the $WZjj$ -QCD and other backgrounds. The BDT is trained and optimised on simulated events to separate $WZjj$ -EW events from all other processes.

Similarly to Ref. [6], 15 variables are used as inputs to the BDT discriminant. The variables can be classified into three categories: jet-kinematics variables, vector-bosons-kinematics variables, and variables related to both jets and leptons kinematics. The variables related to the kinematic properties of the two tagging jets are the invariant mass of the two jets, m_{jj} , the transverse momenta of the jets, p_{Tj1} and p_{Tj2} , the difference in pseudorapidity and azimuthal angle between the two jets, $\Delta\eta_{jj}$ and $\Delta\phi_{jj}$, the rapidity of the leading jet and the jet multiplicity. The variables related to the kinematic properties of the vector bosons are the transverse momenta of the W and Z bosons, the pseudorapidity of the W boson, the absolute difference between the rapidities of the Z boson and the lepton from the decay of the W boson, $|y_Z - y_{\ell,W}|$, and the transverse mass of the $W^\pm Z$ system m_T^{WZ} . The pseudorapidity of the W boson is reconstructed using an estimate of the longitudinal momentum of the neutrino obtained using the neural-network based method developed in Ref. [50]. The m_T^{WZ} observable is reconstructed following Ref. [12]. The variables that relate the kinematic properties of jets and leptons are the distance in the pseudorapidity–azimuth plane between the Z boson and the leading jet, $\Delta R(j_1, Z)$, the event balance $R_{p_T}^{\text{hard}}$, defined as the transverse component

of the vector sum of the WZ bosons and tagging jets momenta, normalised to their scalar p_T sum, and, finally the centrality of the WZ system relative to the tagging jets, defined as $\zeta_{\text{lep.}} = \min(\Delta\eta_-, \Delta\eta_+)$, with $\Delta\eta_- = \min(\eta_\ell^W, \eta_{\ell_2}^Z, \eta_{\ell_1}^Z) - \min(\eta_{j_1}, \eta_{j_2})$ and $\Delta\eta_+ = \max(\eta_{j_1}, \eta_{j_2}) - \max(\eta_\ell^W, \eta_{\ell_2}^Z, \eta_{\ell_1}^Z)$. The good modelling by MC simulations of the distribution shapes and the correlations of all input variables to the BDT is verified in a validation region defined by requiring $150 < m_{jj} < 500$ GeV. The modelling of input variables to the BDT, and in particular of the m_{jj} distribution, is also verified in a sub-signal region enriched in $WZjj$ -QCD events. An Adversarial Neural Network (ANN) is developed to separate $WZjj$ -QCD from $WZjj$ -EW events in the SR, without introducing a bias in the shape of the m_{jj} distribution. The output score of this ANN is used to select a sub-sample of events in the SR enriched in $WZjj$ -QCD production. For these events, a good modelling of the shapes of the m_{jj} distribution and of the other BDT input observables is observed. Finally the good modelling by MC simulations of the kinematic of $W^\pm Zjj$ events is verified independently by the measurement of differential cross-sections of key observables as presented in Section 7.3 and whose results are shown in Section 9.3.

To better separate the $t\bar{t} + V$ and tZj events in the b -CR and to constrain the normalisation of both contributions using data in this CR, a second BDT discriminant, labelled b -CR BDT, is built using 16 input variables. The input variables used are related to the kinematics of tagging jets: $p_{Tj1}, \eta_{j1}, \phi_{j1}, p_{Tj2}, \Delta\eta_{jj}$ and $\Delta\phi_{jj}$; to the kinematics of vector bosons: $p_T^Z, \eta_Z, \phi_Z, p_T^W, m_{WZ}, \Delta\eta(W, Z)$ and $\Delta\phi(W, Z)$; to the jet multiplicites: $N_{\text{jets}}, N_{b\text{-jets}}$; and to the invariant mass of final state particles: $m(3\ell, \text{jets})$, defined as the invariant mass of the three charged leptons and all jets with a $p_T > 25$ GeV. The BDT is trained and optimised on simulated events to separate tZj from $t\bar{t} + V$ events. Its discriminant output is labelled b -CR BDT score.

The distribution of the BDT score in the $W^\pm Zjj$ signal region is used in a maximum-likelihood fit to separate $WZjj$ -EW events from $WZjj$ -strong events and to measure their respective fiducial cross-sections. To minimise the dependency of the measurement on possible mis-modelling of $WZjj$ -QCD and $WZjj$ -EW events by the MC generators, the $W^\pm Zjj$ SR is divided in two categories corresponding to events with exactly two jets of $p_T > 25$ GeV or with three or more jets. An extended likelihood is built from the product of four likelihoods corresponding to the BDT score distributions in the two event categories of the $W^\pm Zjj$ SR, the b -CR BDT distribution in the b -CR and the m_{jj} distribution in the ZZ -CR. The inclusion of the two control regions in the fit allows the yields of the $t\bar{t} + V, tZj$ and $ZZjj$ -QCD backgrounds to be constrained by data. The shapes of these backgrounds are taken from MC predictions and can vary within the uncertainties affecting the measurement as described in Section 8. The normalisations of these backgrounds are introduced in the likelihood as parameters, labelled $\mu_{t\bar{t}+V}, \mu_{tZj}$ and μ_{ZZ} for $t\bar{t} + V, tZj$ and $ZZjj$ -QCD backgrounds, respectively. They are treated as unconstrained nuisance parameters that are determined mainly by the data in the respective control region. The normalisation and shape of the other irreducible backgrounds are taken from MC simulations and are allowed to vary within their respective uncertainties. The distribution of the reducible background is estimated from data using the matrix method presented in Section 6 and is allowed to vary within its uncertainty. Each source of systematic uncertainty is implemented in the likelihood function as a nuisance parameter with a Gaussian constraint.

The fiducial cross-sections $\sigma_{WZjj\text{-EW}}$ and $\sigma_{WZjj\text{-strong}}$ integrated over the two event categories in N_{jets} are determined as parameters of a binned fit to data. The fit parameters are directly linked to normalisation factors of the $WZjj$ -EW, $WZjj$ -QCD and $WZjj$ -INT MC templates as

$$\begin{aligned}
\sigma_{WZjj\text{-EW}} &= \mu_{WZjj\text{-EW}} \cdot \sigma_{WZjj\text{-EW}}^{\text{th. MC}}, \\
\sigma_{WZjj\text{-strong}} &= \mu_{WZjj\text{-QCD}} \cdot \sigma_{WZjj\text{-QCD}}^{\text{th. MC}} + \mu_{WZjj\text{-INT}} \cdot \sigma_{WZjj\text{-INT}}^{\text{th. MC}}, \\
&= \mu_{WZjj\text{-QCD}} \cdot \sigma_{WZjj\text{-QCD}}^{\text{th. MC}} + \sqrt{\mu_{WZjj\text{-EW}}} \cdot \sqrt{\mu_{WZjj\text{-QCD}}} \cdot \sigma_{WZjj\text{-INT}}^{\text{th. MC}},
\end{aligned} \tag{1}$$

where $\sigma_{WZjj\text{-EW}}^{\text{th. MC}}$, $\sigma_{WZjj\text{-QCD}}^{\text{th. MC}}$ and $\sigma_{WZjj\text{-INT}}^{\text{th. MC}}$ are the theoretical cross-section predicted by the MC for the respective processes. By convention, the measured fiducial cross-sections correspond to a given decay channel $W^\pm Z \rightarrow \ell'^\pm \nu \ell^+ \ell^-$, where ℓ and ℓ' are either an electron or a muon. The contribution of the interference between $WZjj\text{-EW}$ and $WZjj\text{-QCD}$ production processes, $WZjj\text{-INT}$, is introduced in the fit using a separate MC template. Its contribution is estimated to be very low at detector level, of the order of 5.3% of the $WZjj\text{-EW}$ contribution as predicted by MADGRAPH+PYTHIA8. The kinematics and shape of the BDT score distribution of $WZjj\text{-INT}$ events is very close to the one of $WZjj\text{-QCD}$ events. Therefore, with the statistical sensitivity of the present data sample, this contribution can not be extracted alone from data. The normalisation of the interference contribution, $\mu_{WZjj\text{-INT}}$, is not fixed in the fit to the predicted MADGRAPH+PYTHIA8 cross-section but is linked to the measured $\sigma_{WZjj\text{-EW}}$ and $\sigma_{WZjj\text{-strong}}$ cross-section as $\mu_{WZjj\text{-INT}} = \sqrt{\mu_{WZjj\text{-EW}}} \cdot \sqrt{\mu_{WZjj\text{-QCD}}}$, and the $WZjj\text{-INT}$ contribution is included into the measured $\sigma_{WZjj\text{-strong}}$ cross-section.

7.2 $WZjj\text{-EW}$ and $WZjj\text{-strong}$ differential measurements

Events in the SR are separated in bins as a function of N_{jets} , the exclusive multiplicity of jets with a $p_T > 25$ GeV or as a function of m_{jj} , the invariant mass of the two tagging jets. Two bins in N_{jets} , separating events with $N_{\text{jets}} = 2$ and $N_{\text{jets}} \geq 3$ and three bins in m_{jj} are used. In each of the bins, the BDT score distribution is used to separate $WZjj\text{-EW}$ events and $WZjj\text{-strong}$ events and therefore measure differentially the separate $\sigma_{WZjj\text{-EW}}$ and $\sigma_{WZjj\text{-strong}}$ production cross-sections. A simultaneous fit to data of the BDT score distributions of events in each bin is performed to measure the fiducial cross-section in each bin. For e.g. $WZjj\text{-EW}$ events, the fiducial cross-section is defined in each bin i as

$$\sigma_{WZjj\text{-EW}}^i = \mu_{WZjj\text{-EW}}^i \cdot \sigma_{WZjj\text{-EW}}^{i, \text{th. MC}} = \frac{N_{\text{fit}}^i}{\mathcal{L} \cdot C_i}, \quad C_i = \frac{N_{\text{MC, det.}}^i}{N_{\text{MC, part.}}^i}, \tag{2}$$

where $\mu_{WZjj\text{-EW}}^i$ is the normalisation factor of the $WZjj\text{-EW}$ MC template in bin i , N_{fit}^i is the number of extracted $WZjj\text{-EW}$ events in data, \mathcal{L} is the integrated luminosity of data and C_i is a bin-by-bin correction factor for detector inefficiency and resolution. The term $N_{\text{MC, det.}}^i$ is the number of $WZjj\text{-EW}$ events predicted by the MC at detector level and $N_{\text{MC, part.}}^i$ is the corresponding number of MC events predicted at particle level in the fiducial phase space. Correction factors are calculated using the MADGRAPH+PYTHIA8 MC simulations. The same control regions and a similar parameterisation of the fit as described in Section 7.1 are used. Correlations between bins of experimental and background systematic uncertainties detailed in Section 8 are taken into account in the simultaneous fit.

7.3 $W^\pm Zjj$ differential measurements

Events in the SR are also used to measure the $W^\pm Zjj$ differential production cross-section in the VBS fiducial phase space. The differential detector-level distributions are corrected for detector efficiency and

resolution effects using an iterative Bayesian unfolding method [53], as implemented in the RooUnfold toolkit [54]. Three iterations were used for the unfolding of each variable. The width of the bins in each distribution is chosen according to the experimental resolution and to the statistical significance of the expected number of events in that bin. The fraction of signal MC events reconstructed in the same bin as generated is always greater than 40% and around 70% on average.

For each distribution, simulated $W^\pm Zjj$ events are used to obtain a response matrix that accounts for bin-to-bin migration effects between the reconstruction-level and particle-level distributions. The MADGRAPH+PYTHIA8 MC samples for $WZjj$ -EW, $WZjj$ -INT and $WZjj$ -QCD production are added together to model $W^\pm Zjj$ production. Because of differences in event kinematics, the response matrix for separate $WZjj$ -EW and $WZjj$ -QCD processes are close but not similar. To better model the data and to minimise unfolding uncertainties, their predicted cross-sections are rescaled by the signal strengths of 1 and 0.71 for the $WZjj$ -EW and $WZjj$ -strong contributions, respectively, as measured by the maximum-likelihood fit described in Section 7.1 applied to data in Section 9.1. The background contributions from $ZZjj$ -QCD, $t\bar{t} + V$ and tZj are also rescaled according to the result of the maximum-likelihood fit of Section 7.1, following constraints from data in the CRs.

8 Systematic uncertainties

Systematic uncertainties in the signal and control regions affecting the shape and normalisation of the BDT score, m_{jj} and b -CR BDT distributions for the individual backgrounds, as well as the acceptance of the $WZjj$ -EW, $WZjj$ -QCD and $WZjj$ -INT events and the shape of their templates are considered. Shape and normalisation uncertainties affecting $WZjj$ -EW, $WZjj$ -QCD and $WZjj$ -INT contributions in control regions are also considered. A bootstrapping procedure [55] is used to ensure statistically significant variations as a function of considered distributions.

Systematic uncertainties due to the theoretical modelling in the event generator used to evaluate the $WZjj$ -QCD and $WZjj$ -EW templates are considered. Uncertainties due to higher order QCD corrections are evaluated by varying the renormalisation, μ_R , and factorisation, μ_F , scales independently by factors of two and one-half, removing combinations where the variations differ by a factor of four. For the $WZjj$ -EW process, simulated only at LO in QCD, changes in the definition of μ_F are also considered: dedicated MC studies show that depending on the definition of μ_F the shape of the BDT score distribution is subject to changes not covered by the scaling of μ_F by factors half or one-half. In the SR, these uncertainties are of up to $\pm 5\%$ and of $\pm 20\%$ on the shape of the BDT score distribution for $WZjj$ -QCD and $WZjj$ -EW events, respectively. The uncertainties due to the PDF and the α_s value used in the PDF determination are evaluated using the PDF4LHC prescription [56] and are of the order of 1% to 2% in shape. A global modelling uncertainty in the $WZjj$ -QCD background template that includes effects of the parton shower model is estimated by comparing predictions of the BDT score distribution in the signal region from the MADGRAPH+PYTHIA8 and SHERPA MC event generators. The difference between the predicted shapes of the BDT score distribution from the two generators is considered as an uncertainty and affects the shape of the BDT score distribution of $WZjj$ -QCD events by up to 30% at larger values of the BDT score. A parton-shower uncertainty in the $WZjj$ -EW signal template is estimated by comparing predictions of the BDT score distribution in the signal region from MC simulations from MADGRAPH interfaced to PYTHIA or HERWIG. This parton-shower uncertainty affects the shape of the BDT score distribution of $WZjj$ -EW events by at most 10% at lower values of the BDT score. For the $WZjj$ -INT template, uncertainties due

to variations of the renormalisation and factorisation scales and due to the PDF and to the α_s value used in the PDF determination are considered. They affect the shape of the template by approximately 3%.

For the measurement of integrated and differential $\sigma_{WZjj\text{-EW}}$ and $\sigma_{WZjj\text{-strong}}$ cross-sections using a combined maximum-likelihood fit, all the uncertainties related to higher order QCD corrections, parton shower and modelling are considered as uncorrelated between bins in N_{jets} or m_{jj} in the SR and between the SR and the control regions. This leads to the most conservative fit approach for these uncertainties.

For the measurements of $W^\pm Zjj$ differential cross-sections, uncertainties in the unfolding due to imperfect modelling of the data by the MC simulation are evaluated using a data-driven method [57], where the MC differential distribution is corrected to match the data distribution and the resulting weighted MC distribution at reconstruction level is unfolded with the response matrix used in the data unfolding. The new unfolded distribution is compared with the weighted MC distribution at generator level and the difference is taken as the systematic uncertainty. The uncertainties obtained range from 0.1% to 16% depending on the resolution of the unfolded observables and on the quality of its description by MADGRAPH+PYTHIA8. They cover residual modelling uncertainties in the unfolded observables, which could still be present after the adjustment to data of the normalisation of $WZjj\text{-QCD}$ and $WZjj\text{-EW}$ contributions. It is also verified that, by construction, these uncertainties cover for possible EFT contributions being present in the data. An additional uncertainty is derived to account for more subtle differences between the MADGRAPH+PYTHIA8 and SHERPA generators (e.g. hadronisation models, additional soft objects, mis-modelling in other kinematic variables). The SHERPA generator is used to unfold the data and deviation from the nominal result is taken as the uncertainty. To remove effects already accounted for in the data-driven method, the SHERPA distributions were first reweighted to match MADGRAPH+PYTHIA8 distributions at particle level.

Systematic uncertainties affecting the reconstruction and energy calibration of jets, electrons and muons are propagated through the analysis. The dominant sources of uncertainties are the jet energy scale calibration, including the modelling of pile-up. The uncertainties in the jet energy scale are obtained from $\sqrt{s} = 13$ TeV simulations and *in situ* measurements [58]. The uncertainties in the jet energy resolution [58], in the suppression of jets originating from pile-up [45], in the b -tagging efficiency and in the mistag rate [47] are also considered. The uncertainty in the E_T^{miss} measurement is estimated by propagating the uncertainties in the transverse momenta of hard physics objects and by applying momentum scale and resolution uncertainties to the track-based soft term [48]. A variation in the pile-up reweighting of MC events is included in order to cover the uncertainty in the ratio of the predicted and measured pp inelastic cross-sections [59].

The uncertainties due to lepton reconstruction, identification, isolation requirements and trigger efficiencies as well as in the lepton momentum scale and resolution are assessed using tag-and-probe methods in $Z \rightarrow \ell\ell$ events [40–42].

The uncertainty in the amount of background from misidentified leptons takes into account the limited number of events in the control regions as well as the difference in background composition between the control region used to determine the lepton misidentification rate and the control regions used to estimate the yield in the signal region. This results in an uncertainty of about 25% in the total misidentified-lepton background yield and in the shape of the differential distributions of the reducible background events.

The uncertainty due to irreducible background sources that are not constraint by data in the dedicated CRs is evaluated by propagating the uncertainty in their MC cross-sections. These are 20% for VVV [60] and 25% for $ZZjj\text{-EW}$ to account for the potentially large impact of scale variations.

Table 2: Grouped impact of systematic uncertainties in the measured integrated fiducial cross-sections $\sigma_{WZjj\text{-EW}}$ and $\sigma_{WZjj\text{-strong}}$. The uncertainties are reported as percentages. The total systematic uncertainty does not correspond directly to the sum in quadrature of the distinct sources due to correlations introduced by the fit, in particular between $\sigma_{WZjj\text{-EW}}$ and $\sigma_{WZjj\text{-strong}}$.

Source	$\frac{\Delta\sigma_{WZjj\text{-EW}}}{\sigma_{WZjj\text{-EW}}}$ [%]	$\frac{\Delta\sigma_{WZjj\text{-strong}}}{\sigma_{WZjj\text{-strong}}}$ [%]
$WZjj\text{-EW}$ theory modelling	7	1.8
$WZjj\text{-QCD}$ theory modelling	2.8	8
$WZjj\text{-EW}$ and $WZjj\text{-QCD}$ interference	0.35	0.6
PDFs	1.0	0.06
Jets	2.3	5
Pile-up	1.1	0.6
Electrons	0.8	0.8
Muons	0.9	0.9
b -tagging	0.10	0.11
MC statistics	1.9	1.2
Misid. lepton background	2.3	2.3
Other backgrounds	0.9	0.23
Luminosity	0.7	0.9
All systematics	16	12
Statistics	10	6
Total	19	13

The uncertainty in the combined 2015–2018 integrated luminosity is 0.83% [61], obtained using the LUCID-2 detector [62] for the primary luminosity measurements, complemented by measurements using the inner detector and calorimeters.

The effect of the systematic uncertainties on the final results after the maximum-likelihood fit is shown in Table 2 where the breakdown of the contributions to the uncertainties in the measured fiducial cross-section $\sigma_{WZjj\text{-EW}}$ and $\sigma_{WZjj\text{-strong}}$ is presented. The individual sources of systematic uncertainty are combined into theory modelling and experimental categories. As shown in the table, the systematic uncertainties in the modelling of the $WZjj\text{-EW}$ and $WZjj\text{-QCD}$ processes play a dominant role, followed by the uncertainties in the jet reconstruction and calibration. Systematic uncertainties in the missing transverse momentum computation arise directly from the momentum and energy calibration of jets, electrons and muons and are included in the respective lines of Table 2. Systematic uncertainties in the modelling of the other backgrounds are also considered.

9 Results

9.1 $WZjj\text{-EW}$ and $WZjj\text{-strong}$ integrated measurements

The post-fit distributions of the BDT score in the signal region for events with $N_{\text{jets}} = 2$ and $N_{\text{jets}} \geq 3$ are presented in Figures 3(a) and (b), respectively. The background normalisations, signal normalisation

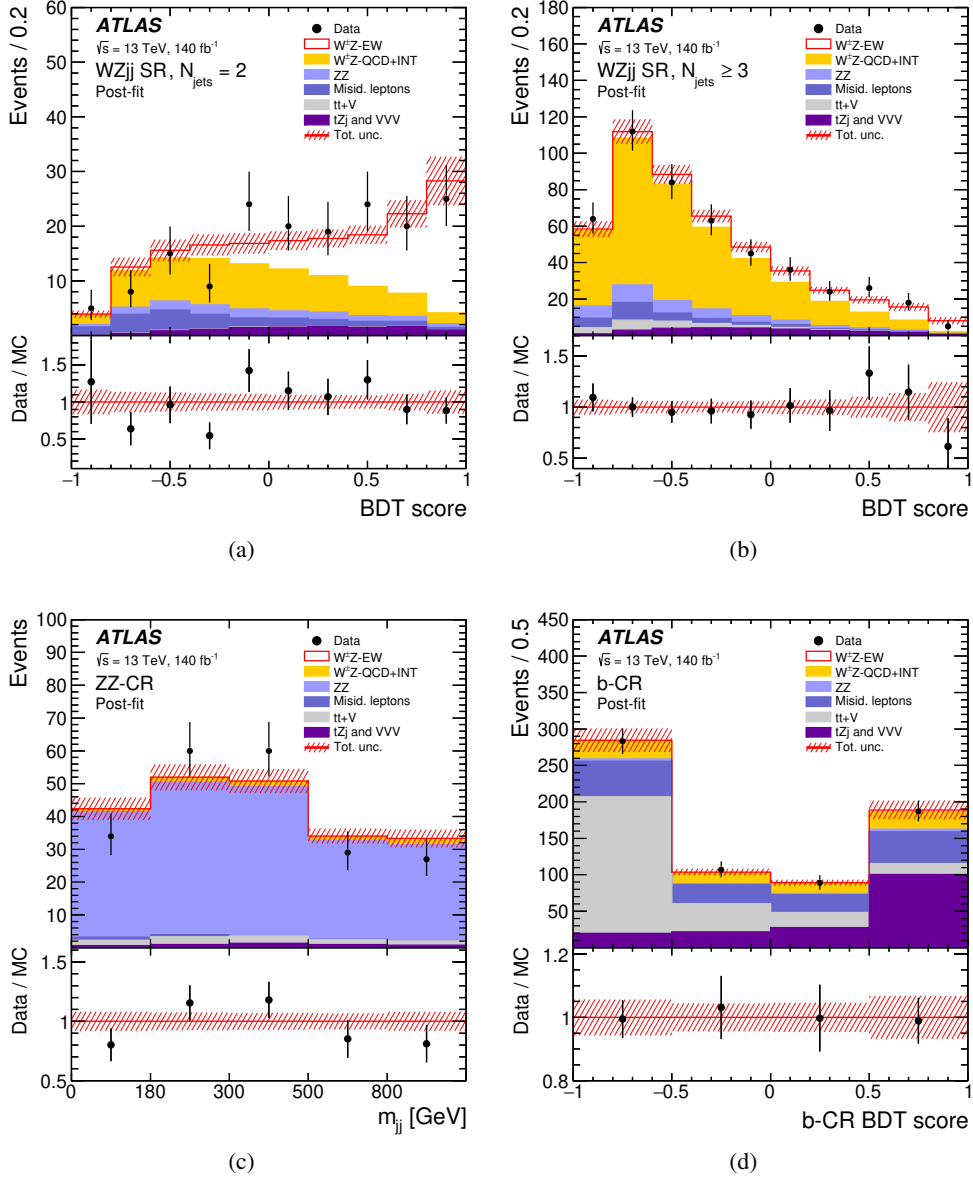


Figure 3: Post-fit distributions of (a) the BDT score distribution in the signal region, for $N_{\text{jets}} = 2$ and (b) $N_{\text{jets}} \geq 3$ categories, (c) m_{jj} in the ZZ-CR control region, (d) the b -CR BDT score in the b -CR. Signal and backgrounds are normalised to the expected number of events after the fit. The uncertainty band around the MC expectation includes all systematic uncertainties as obtained from the fit.

and nuisance parameters are adjusted by the profile-likelihood fit. The post-fit distributions of m_{jj} and of the b -CR BDT score in the ZZ-CR and b -CR, respectively, are also presented in Figures 3(c) and (d). The corresponding post-fit event yields are detailed in Table 3. The normalisation parameters of the $t\bar{t} + V$ and ZZ backgrounds constrained by data in the control and signal regions are measured to be $\mu_{t\bar{t}V} = 0.91 \pm 0.13$, $\mu_{tZj} = 1.26 \pm 0.22$ and $\mu_{ZZ} = 1.07 \pm 0.11$. No pull of nuisance parameters by more than 0.5σ is observed.

Table 3: Observed and expected numbers of events in the $W^\pm Z jj$ signal region and in the two control regions, after the fit. The expected number of $WZjj$ -EW, $WZjj$ -QCD and $WZjj$ -INT events and the estimated number of background events from the other processes are shown. The sum of the backgrounds containing misidentified leptons is labelled ‘Misid. leptons’. The total correlated post-fit systematic uncertainties are quoted.

	SR, $N_{\text{jets}} = 2$		SR, $N_{\text{jets}} \geq 3$		b -CR		ZZ-CR	
Data	169		477		666		210	
Total pred.	170	± 13	476	± 22	667	± 26	212	± 14
$WZjj$ -EW	68	± 14	55	± 18	4.84 ± 0.27		0.724 ± 0.014	
$WZjj$ -QCD	58	± 16	307	± 27	77 ± 18		6.3 ± 0.7	
$WZjj$ -INT	0.9 ± 0.4		4.4 ± 2.3		0.57 ± 0.29		0.22 ± 0.11	
$t\bar{t} + V$	0.59 ± 0.10		18.3 ± 2.4		262 ± 34		9.0 ± 1.3	
tZj	11.0 ± 1.9		25 ± 5		169 ± 30		0.54 ± 0.09	
ZZ-QCD	10.3 ± 1.0		34.6 ± 3.2		10.1 ± 0.5		171 ± 15	
ZZ-EW	1.9 ± 0.4		3.7 ± 0.9		0.21 ± 0.05		19 ± 5	
VVV	0.41 ± 0.10		2.0 ± 0.5		0.39 ± 0.10		4.2 ± 1.0	
Misid. leptons	18 ± 4		27 ± 6		143 ± 35		1.7 ± 0.5	

The integrated fiducial cross-sections $\sigma_{WZjj\text{-EW}}$ and $\sigma_{WZjj\text{-strong}}$, for a given decay channel $W^\pm Z \rightarrow \ell'^{\pm} \nu \ell^+ \ell^-$, where ℓ and ℓ' are either an electron or a muon, are measured to be

$$\begin{aligned}
\sigma_{WZjj\text{-EW}} &= 0.368 \pm 0.037 \text{ (stat.)} \pm 0.059 \text{ (syst.)} \pm 0.003 \text{ (lumi.) fb} \\
&= 0.37 \pm 0.07 \text{ fb,} \\
\sigma_{WZjj\text{-strong}} &= 1.093 \pm 0.066 \text{ (stat.)} \pm 0.131 \text{ (syst.)} \pm 0.009 \text{ (lumi.) fb} \\
&= 1.09 \pm 0.14 \text{ fb,}
\end{aligned}$$

where the uncertainties correspond to statistical, systematic, and luminosity uncertainties, respectively. Table 2 shows the main sources of uncertainty in the measured cross-sections. The precision of the measurements is limited by the systematic uncertainties, and in particular by the model uncertainties of the MC event generators. The corresponding predictions from MADGRAPH+PYTHIA8 are

$$\begin{aligned}
\sigma_{WZjj\text{-EW}}^{\text{MADGRAPH+PYTHIA8}} &= 0.370 \pm 0.001 \text{ (stat.)} \pm 0.006 \text{ (PDF)}^{+0.030}_{-0.026} \text{ (scale) fb,} \\
\sigma_{WZjj\text{-strong}}^{\text{MADGRAPH+PYTHIA8}} &= 1.537 \pm 0.009 \text{ (stat.)} \pm 0.016 \text{ (PDF)}^{+0.087}_{-0.149} \text{ (scale) fb,}
\end{aligned}$$

where the uncertainties correspond to statistical, PDF and QCD scale uncertainties, respectively, calculated as detailed in Section 8. The measured values of $\sigma_{WZjj\text{-EW}}$ and $\sigma_{WZjj\text{-strong}}$ are also compared to the predictions from MADGRAPH+PYTHIA8 and SHERPA 2.2.12 in Figure 4. A good agreement of the MC predictions with the measured $WZjj$ -EW integrated cross-section is observed, while the $WZjj$ -QCD integrated cross-section is measured to be lower than the prediction from both MC event generators by a factor of 0.7. Considering the theory uncertainty in the MADGRAPH+PYTHIA8 prediction, the present measurement and the MADGRAPH+PYTHIA8 prediction agree within 1.8σ . A similar observation regarding the modelling of $WZjj$ -QCD production was also made by the ATLAS Collaboration using a different measurement phase space [63]. It is also consistent with measurements done in previous ATLAS publications dedicated to $W^\pm Z jj$ and $W^\pm Z$ final states [6, 50].

faire

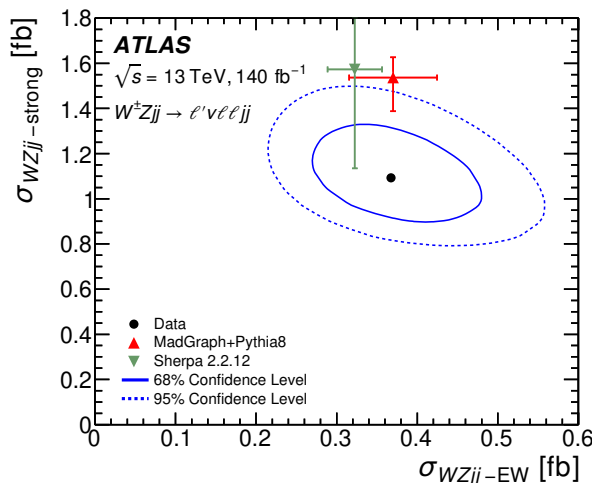


Figure 4: The measured $\sigma_{WZjj\text{-EW}}$ and $\sigma_{WZjj\text{-strong}}$ integrated cross-sections compared with predictions from MADGRAPH+PYTHIA8 (upward pointing triangle) and SHERPA 2.2.12 (downward pointing triangle). The full and dashed contours around the data points correspond to 68% and 95% CL, respectively.

The $W^\pm Zjj$ integrated cross-section in the fiducial phase space is also measured from the fit to be $\sigma_{WZjj} = 1.462 \pm 0.133 \text{ fb} = 1.462 \pm 0.063 \text{ (stat.)} \pm 0.118 \text{ (sys.)} \pm 0.012 \text{ (lumi.) fb}$. The corresponding prediction from MADGRAPH+PYTHIA8 for strong and electroweak production and including interference effects is $1.907 \pm 0.009 \text{ (stat.)} \pm 0.022 \text{ (PDF)}_{-0.175}^{+0.117} \text{ (scale) fb}$.

9.2 $WZjj\text{-EW}$ and $WZjj\text{-strong}$ differential measurements

Dividing the SR in events with $N_{\text{jets}} = 2$ and $N_{\text{jets}} \geq 3$ the $\sigma_{WZjj\text{-EW}}$ and $\sigma_{WZjj\text{-strong}}$ production cross-sections of these two categories of events are measured. The measurements are compared in Figure 5 to the prediction from MADGRAPH+PYTHIA8 and SHERPA 2.2.12. For $N_{\text{jets}} \geq 3$, the predicted $\sigma_{WZjj\text{-EW}}$ cross-sections are in good agreement with the measured value while the predicted $\sigma_{WZjj\text{-strong}}$ cross-section lie within about 2σ of the measurement. However, for $N_{\text{jets}} = 2$ the measured $\sigma_{WZjj\text{-strong}}$ cross-section is lower by a factor of two than the value predicted by both MADGRAPH+PYTHIA8 and SHERPA. The predicted values of $\sigma_{WZjj\text{-EW}}$ are found to be in agreement within 1σ of the measured value. The ratio $\frac{2}{3}$ of the number of events with $N_{\text{jets}} = 2$ to the number of events with $N_{\text{jets}} \geq 3$ is also extracted from data by the simultaneous fit of the two categories to be $R_{2/3}^{\text{EW}} = 1.70 \pm 0.71$ and $R_{2/3}^{\text{QCD}} = 0.21 \pm 0.06$ for $WZjj\text{-EW}$ and $WZjj\text{-QCD}$ events, respectively. In comparison, the values predicted by MADGRAPH+PYTHIA8 (SHERPA) are $R_{2/3}^{\text{EW}} = 1.43_{-0.02}^{+0.06}$ (1.67 ± 0.13) and $R_{2/3}^{\text{QCD}} = 0.36_{-0.04}^{+0.02}$ (0.38 ± 0.03), respectively.

The $\sigma_{WZjj\text{-EW}}$ and $\sigma_{WZjj\text{-strong}}$ production cross-sections are measured differentially in three bins of m_{jj} . The measurements are compared in Figure 6 to the prediction from MADGRAPH+PYTHIA8 and SHERPA 2.2.12. For $500 < m_{jj} < 1300 \text{ GeV}$, the MC predictions are found to overestimate the measured $\sigma_{WZjj\text{-strong}}$ value by a factor 1.4. For m_{jj} values above 1300 GeV, the MC predictions agree within approximately 2σ with the measurements, for both $\sigma_{WZjj\text{-EW}}$ and $\sigma_{WZjj\text{-strong}}$.

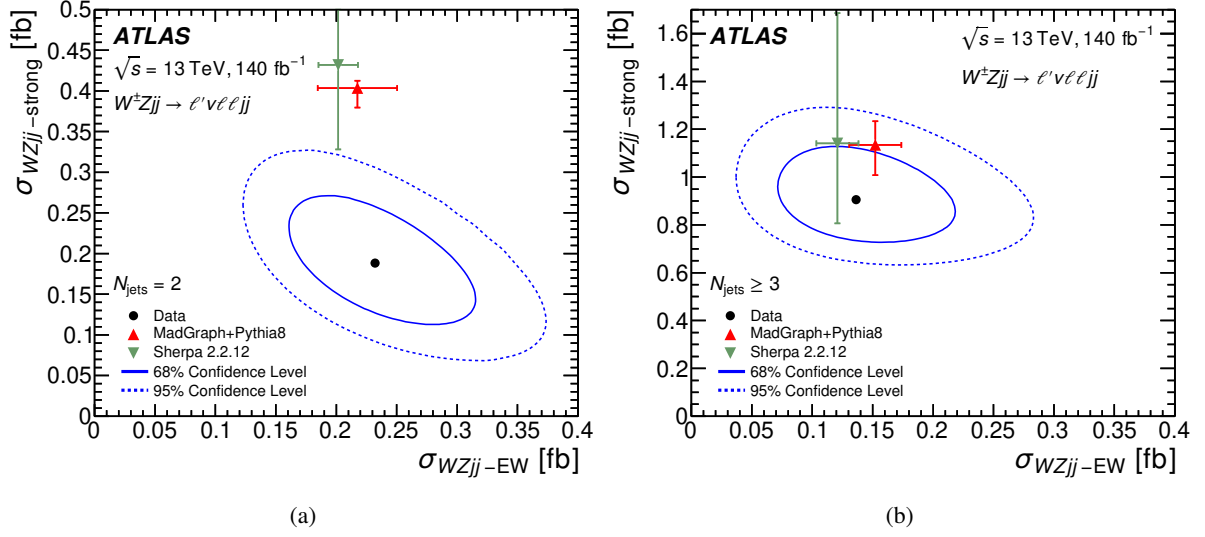


Figure 5: The measured $\sigma_{WZjj\text{-EW}}$ and $\sigma_{WZjj\text{-strong}}$ cross-sections (a) for $N_{\text{jets}} = 2$ and (b) $N_{\text{jets}} \geq 3$ compared with predictions from MADGRAPH+PYTHIA8 (upward pointing triangle) and SHERPA 2.2.12 (downward pointing triangle). The full and dashed contours around the data points correspond to 68% and 95% CL, respectively.

9.3 $W^\pm Zjj$ differential measurements

Differential measurements of $W^\pm Zjj$ production cross-section are performed as a function of three variables sensitive to anomalies in the quartic gauge coupling in $W^\pm Zjj$ events [12], namely the scalar sum of the transverse momenta of the three charged leptons associated with the W and Z bosons $\sum p_T^\ell$, the difference in azimuthal angle $\Delta\phi(W, Z)$ between the W and Z bosons' directions, and the transverse mass of the $W^\pm Z$ system m_T^{WZ} , defined following Ref. [12]. These are presented in Figure 7.

Measurements are also performed as a function of variables related to the kinematics of jets. The exclusive multiplicity of jets with $p_T > 40$ GeV, $N_{\text{jets}}^{p_T > 40 \text{ GeV}}$, the absolute difference in rapidity between the two tagging jets Δy_{jj} , the invariant mass of the tagging jets m_{jj} , the exclusive multiplicity $N_{\text{jets}}^{\text{gap}}$ of jets with $p_T > 25$ GeV in the gap in η between the two tagging jets, and the azimuthal angle between the two tagging jets $\Delta\phi_{jj}$ are shown in Figure 8.

Measurements related to the jet activity in the gap between the two tagging jets are also performed using the subset of events in the SR where a third jet with $p_T > 25$ GeV is present. The exclusive multiplicity $N_{\text{jets}}^{\text{gap}}$ of jets with $p_T > 25$ GeV in the gap in η between the two tagging jets and the Zeppenfeld variable [64], z_{j_3} , for the third jet with $p_T > 25$ GeV are presented in Figure 9. The z_{j_3} variable is defined as

$$z_{j_3} = \left| \frac{y_{j_3} - \frac{1}{2}(y_{j_1} + y_{j_2})}{y_{j_1} - y_{j_2}} \right|, \quad (3)$$

where y_{j_i} is the rapidity of the jet i .

Finally, a differential measurement of $W^\pm Zjj$ production cross-section is performed as a function of the BDT score and is presented in Figure 10. The particle-level BDT score prediction is evaluated using the same BDT as trained at detector level and evaluated using particle-level input observables.

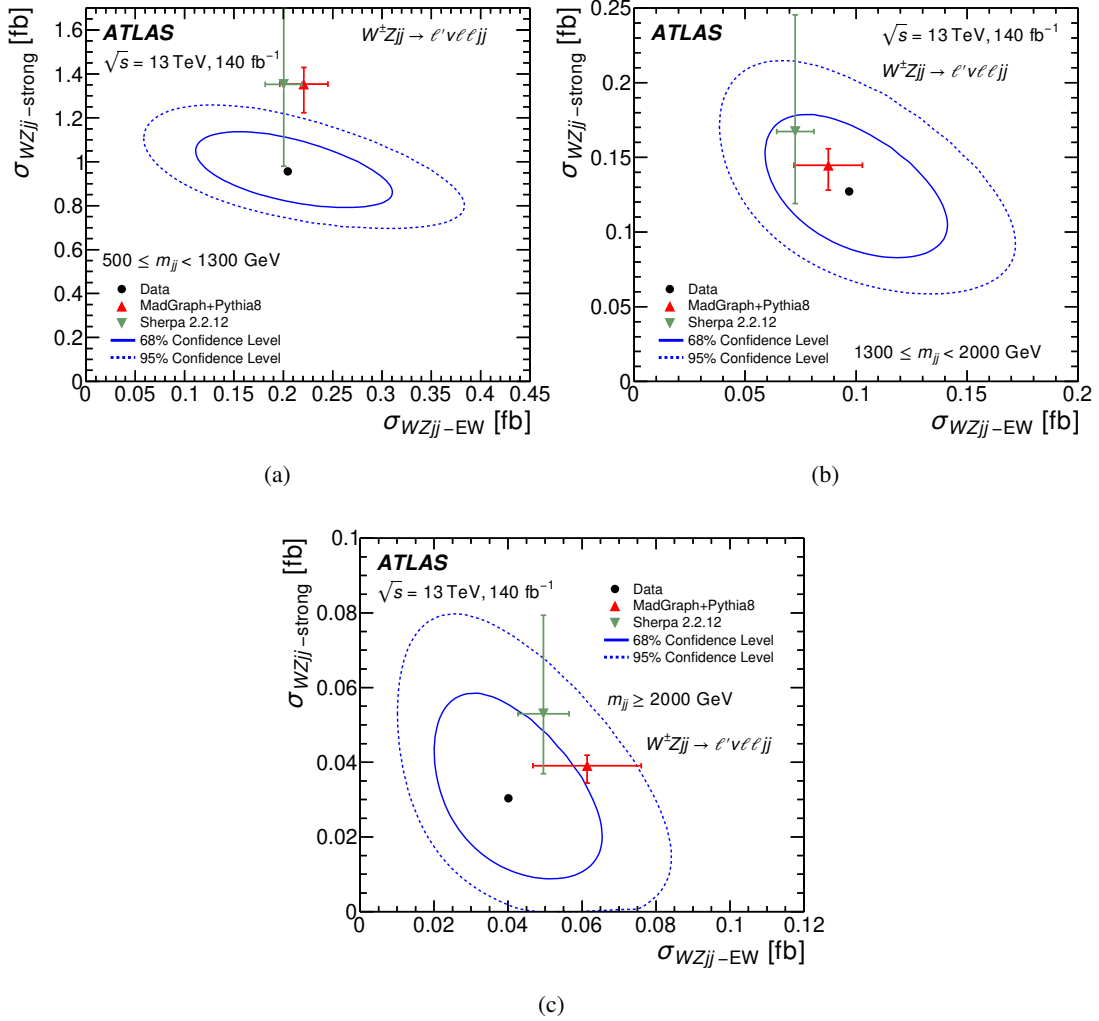


Figure 6: The measured $\sigma_{WZjj\text{-EW}}$ and $\sigma_{WZjj\text{-strong}}$ cross-sections per m_{jj} bin, (a) $500 \leq m_{jj} < 1300$ GeV, (b) $1300 \leq m_{jj} < 2000$ GeV, (c) $m_{jj} \geq 2000$ GeV, compared with predictions from MADGRAPH+PYTHIA8 (upward pointing triangle) and SHERPA 2.2.12 (downward pointing triangle). The full and dashed contours around the data points correspond to 68% and 95% CL, respectively.

Total uncertainties in the measurements are dominated by statistical uncertainties. The differential measurements are compared with the prediction from MADGRAPH+PYTHIA8, after having rescaled the separate $WZjj\text{-QCD}$ and $WZjj\text{-EW}$ components respectively to the inclusive $\sigma_{WZjj\text{-strong}}$ and $\sigma_{WZjj\text{-EW}}$ cross-sections obtained from the profile-likelihood fit to data. Interference effects between the $WZjj\text{-QCD}$ and $WZjj\text{-EW}$ processes are incorporated in the $WZjj\text{-QCD}$ prediction. The measurements are also compared with the predictions from SHERPA 2.2.12.

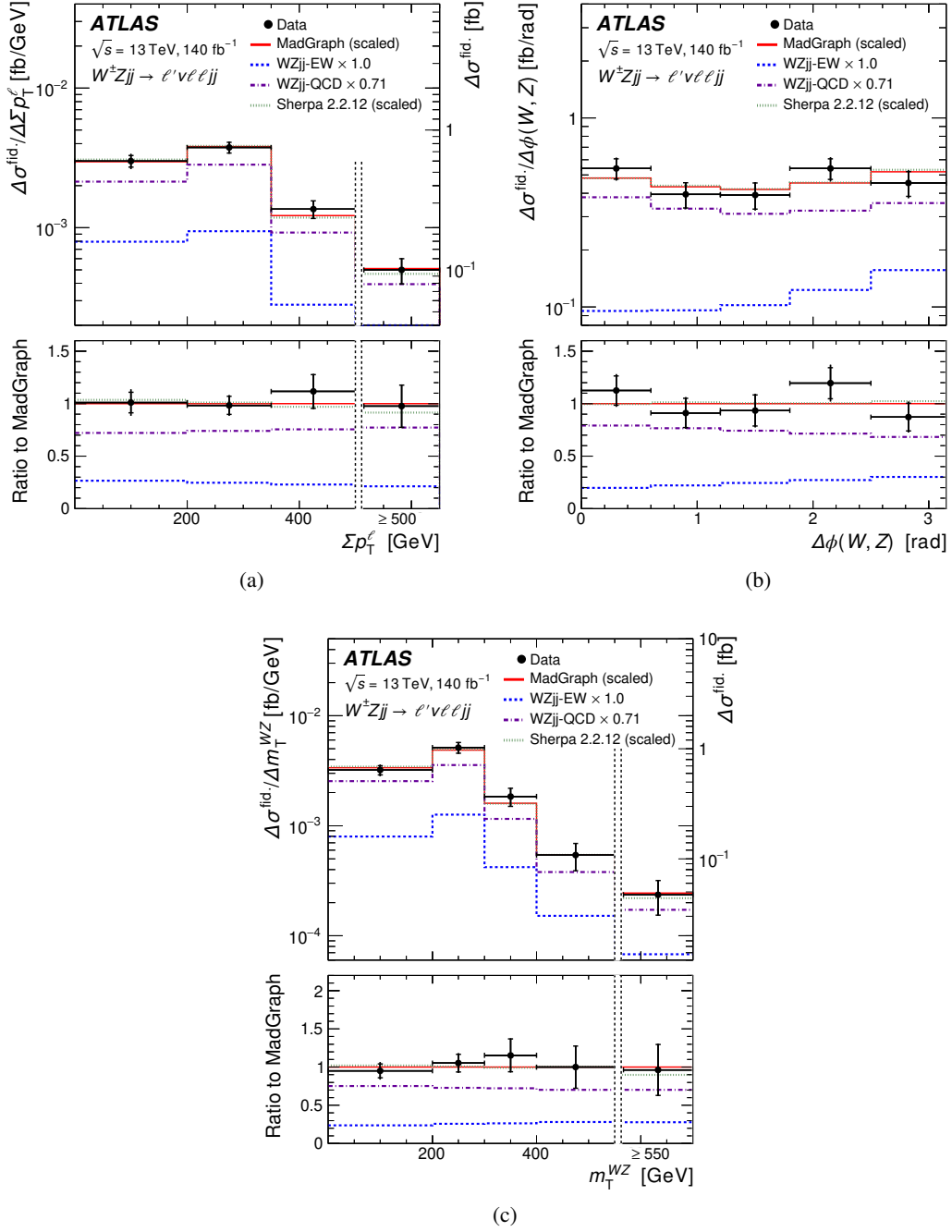


Figure 7: The measured $W^\pm Z jj$ differential cross-section in the VBS fiducial phase space as a function of (a) Σp_T^ℓ , (b) $\Delta\phi(W, Z)$ and (c) m_T^{WZ} . The inner and outer error bars on the data points represent the statistical and total uncertainties, respectively. The measurements are compared with the sum of the rescaled $WZjj$ -QCD and $WZjj$ -EW predictions from MADGRAPH+PYTHIA8 (solid line) and SHERPA 2.2.12 (dotted line). The $WZjj$ -EW and $WZjj$ -QCD contributions are also represented by dashed and dashed-dotted lines, respectively. In (a) and (c), the right y-axis refers to the last cross-section point, separated from the others by a vertical dashed line, as this last bin is integrated up to the maximum value reached in the phase space. The lower panels show the ratios of the data to the predictions from MADGRAPH+PYTHIA8.

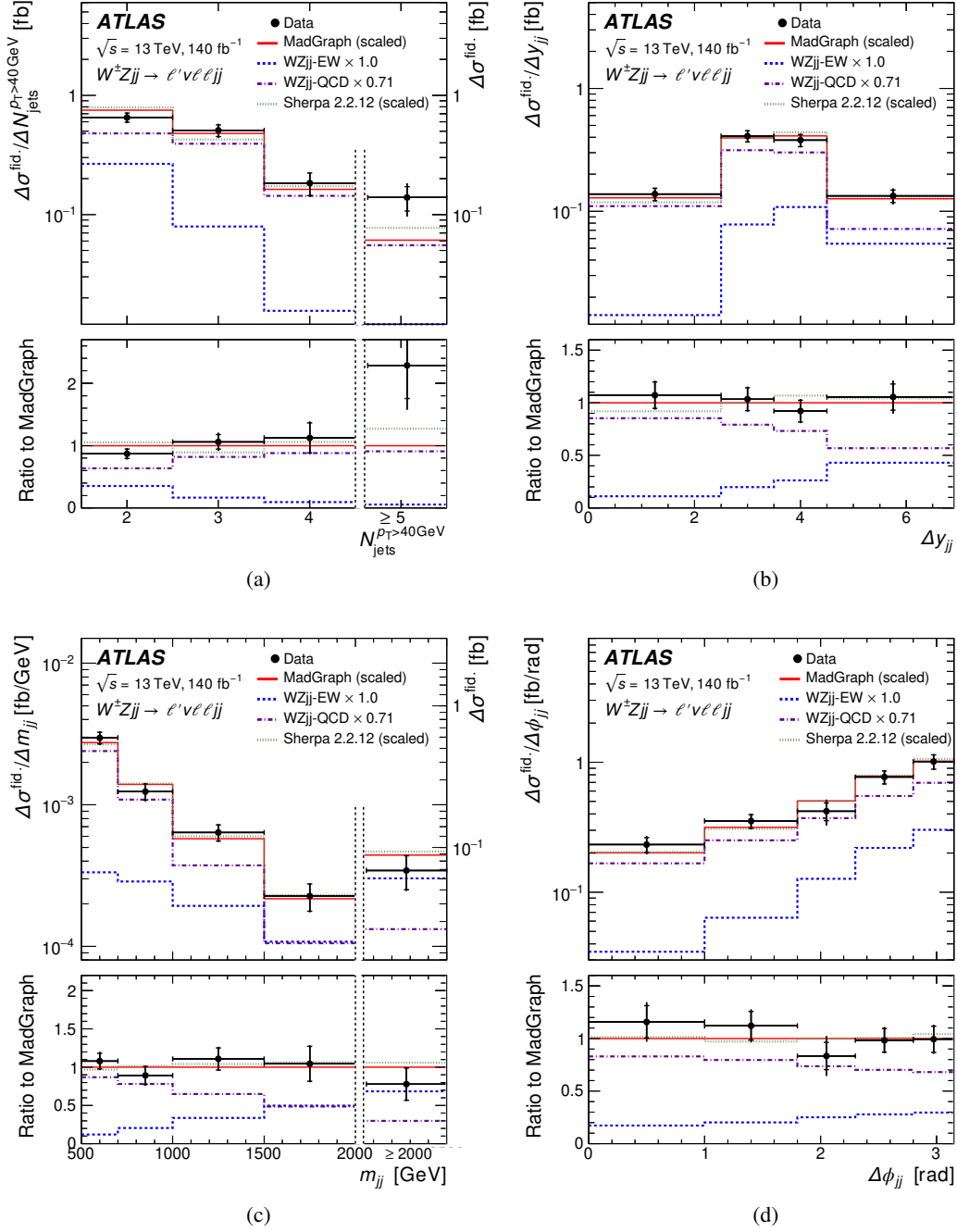


Figure 8: The measured $W^\pm Zjj$ differential cross-section in the VBS fiducial phase space as a function of (a) the exclusive jet multiplicity of jets with $p_T > 40$ GeV, $N_{\text{jets}}^{p_T > 40 \text{ GeV}}$, (b) the absolute difference in rapidity between the two tagging jets Δy_{jj} , (c) the invariant mass of the tagging jets m_{jj} , and (d) the azimuthal angle between the two tagging jets $\Delta\phi_{jj}$. The inner and outer error bars on the data points represent the statistical and total uncertainties, respectively. The measurements are compared with the sum of the rescaled $WZjj$ -QCD and $WZjj$ -EW predictions from MADGRAPH+PYTHIA8 (solid line) and SHERPA 2.2.12 (dotted line). The $WZjj$ -EW and $WZjj$ -QCD contributions are also represented by dashed and dashed-dotted lines, respectively. In (a) and (c), the right y-axis refers to the last cross-section point, separated from the others by a vertical dashed line, as this last bin is integrated up to the maximum value reached in the phase space. The lower panels show the ratios of the data to the predictions from MADGRAPH+PYTHIA8.

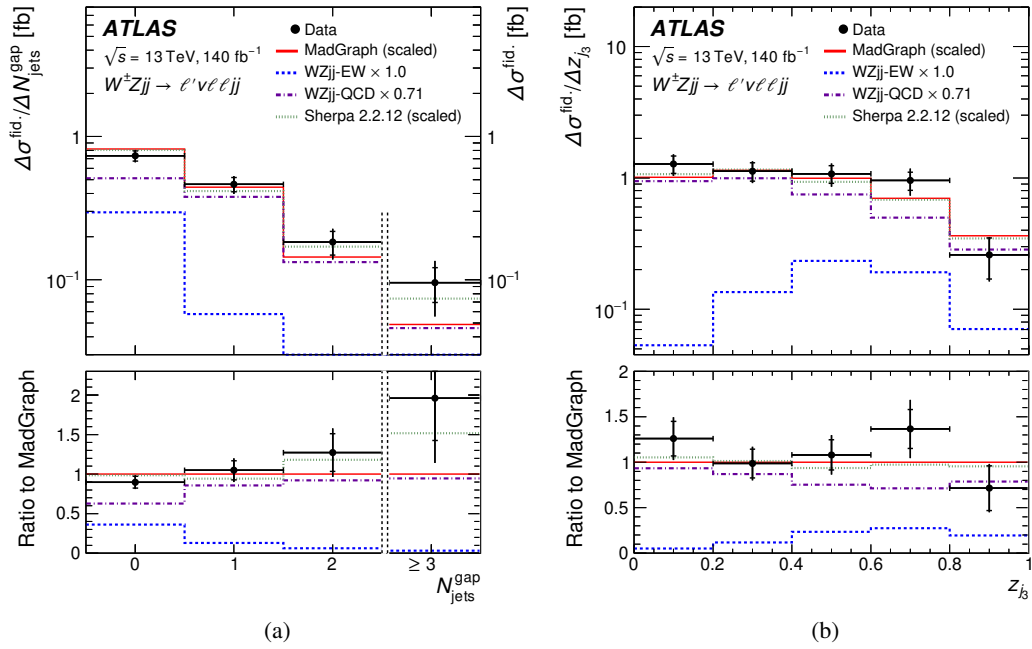


Figure 9: The measured $W^\pm Z j j$ differential cross-section in the VBS fiducial phase space as a function of (a) $N_{\text{jets}}^{\text{gap}}$ the exclusive jet multiplicity of jets with $p_T > 25$ GeV in the gap between the two tagging jets, and (b) z_{j_3} the Zeppenfeld variable. The inner and outer error bars on the data points represent the statistical and total uncertainties, respectively. The measurements are compared with the sum of the rescaled $WZ j j$ -QCD and $WZ j j$ -EW predictions from MADGRAPH+PYTHIA8 (solid line) and SHERPA 2.2.12 (dotted line). The $WZ j j$ -EW and $WZ j j$ -QCD contributions from MADGRAPH+PYTHIA8 are also represented separately by dashed and dashed-dotted lines, respectively. In (a) the right y-axis refers to the last cross-section point, separated from the others by a vertical dashed line, as this last bin is integrated up to the maximum value reached in the phase space. The lower panels show the ratios of the data to the predictions from MADGRAPH+PYTHIA8.

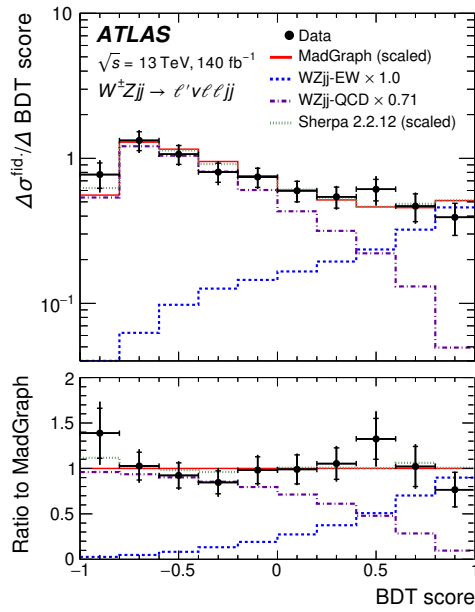


Figure 10: The measured $W^\pm Zjj$ differential cross-section in the VBS fiducial phase space as a function of the BDT score. The inner and outer error bars on the data points represent the statistical and total uncertainties, respectively. The measurements are compared with the sum of the rescaled $WZjj$ -QCD and $WZjj$ -EW predictions from MADGRAPH+PYTHIA8 (solid line) and SHERPA 2.2.12 (dotted line). The $WZjj$ -EW and $WZjj$ -QCD contributions from MADGRAPH+PYTHIA8 are also represented separately by dashed and dashed-dotted lines, respectively. The lower panels show the ratios of the data to the predictions from MADGRAPH+PYTHIA8.

10 Limits on anomalous quartic gauge couplings

The $WZjj$ -EW production can be sensitive to effects beyond the SM affecting the quartic interactions of weak bosons. The measured $W^\pm Zjj$ events are therefore used to search for anomalous quartic gauge couplings (aQGC) using an EFT framework [2, 65]. In this model the SM Lagrangian \mathcal{L}_{SM} is extended in an effective Lagrangian \mathcal{L}_{eff} adding higher order operators and their respective Wilson coefficients as:

$$\mathcal{L}_{\text{eff}} = \mathcal{L}_{\text{SM}} + \sum_i \frac{f_i^{(6)}}{\Lambda_i^2} O_i^{(6)} + \sum_j \frac{f_j^{(8)}}{\Lambda_j^4} O_j^{(8)} + \dots, \quad (4)$$

where $O_{i,j}^{(6),(8)}$ are dimension-6 and dimension-8 operators, respectively, and involve SM fields with respective dimensionless couplings $f_i^{(6)}$ and $f_j^{(8)}$, and Λ is the energy scale of the new processes. In this study only dimension-8 operators are considered and all dimension-6 couplings, affecting triple gauge boson couplings, are assumed to be equal to zero. Dimension-6 couplings are indeed already constrained by other processes, and especially by inclusive diboson production [66, 67]. The effect of dimension-6 operators in VBS processes is of interest on its own [68, 69], but is not studied here. Nine independent charge-conjugate and parity conserving dimension-8 operators are considered [2]. The $O_{S0,1,2}$ operators are constructed from the covariant derivative of the Higgs doublet. The $O_{T0,1,2}$ operators are constructed from the $SU_L(2)$ gauge fields. The mixed operators $O_{M0,1,7}$ involve the $SU_L(2)$ gauge fields and the Higgs doublet. Because the operators O_{S0} and O_{S2} are Hermitian conjugates of each other, they are varied simultaneously, with equal coefficient values $f_{S0} = f_{S2} = f_{S02}$.

The squared scattering amplitude of the effective field theory prediction for $W^\pm Zjj$ production can be written as:

$$\left| A_{\text{SM}} + \sum_i c_i A_i \right|^2 = |A_{\text{SM}}|^2 + \sum_i c_i 2 \text{Re}(A_{\text{SM}}^* A_i) + \sum_i c_i^2 |A_i|^2 + \sum_{ij, i \neq j} c_i c_j 2 \text{Re}(A_i A_j^*), \quad (5)$$

where $c_i = f_j^{(8)}/\Lambda^4$, A_{SM} is the SM scattering amplitude, $\sum_i c_i 2 \text{Re}(A_{\text{SM}}^* A_i)$ is the amplitude of the interference term between the SM and the dimension-8 operators, $\sum_i c_i^2 |A_i|^2$ is the pure dimension-8 contribution, and $\sum_{ij, i \neq j} c_i c_j 2 \text{Re}(A_i A_j^*)$ is the amplitude of interferences between two dimension-8 operators, called cross terms. The different terms are simulated separately using `MADGRAPH5_AMC@NLO 2.6.5` interfaced with `PYTHIA 8.240`, providing individual MC samples. The same PDF sets and PS modelling as for $W^\pm Zjj$ SM events and detailed in Section 4 are used. Generated events corresponding to a given value of the EFT coefficient c_i , or c_i and c_j for cross terms, are obtained by multiplying the respective MC samples by the coefficient value and adding them together.

As non-zero aQGC contributions will enhance the production cross-section of $WZjj$ -EW events at large diboson invariant masses, a two-dimensional combination of the BDT score, separating $WZjj$ -EW from $WZjj$ -QCD events, and m_T^{WZ} observables is used to look for dimension-8 EFT contributions. Four bins in BDT score ($[-1, -0.25, 0.17, 0.72, 1]$) and five bins in m_T^{WZ} ($[0, 400, 750, 1050, 1350, \infty]$ GeV) are used and arranged in a one-dimensional histogram of 20 statistically independent bins, as represented in Figure 11. The bin boundaries are optimised to obtain the best expected limits when no unitarisation cut-off are applied. The distribution is used to define an extended likelihood function, adding the same control regions as defined in Section 7.1. Experimental and theory uncertainties, as discussed in section 8,

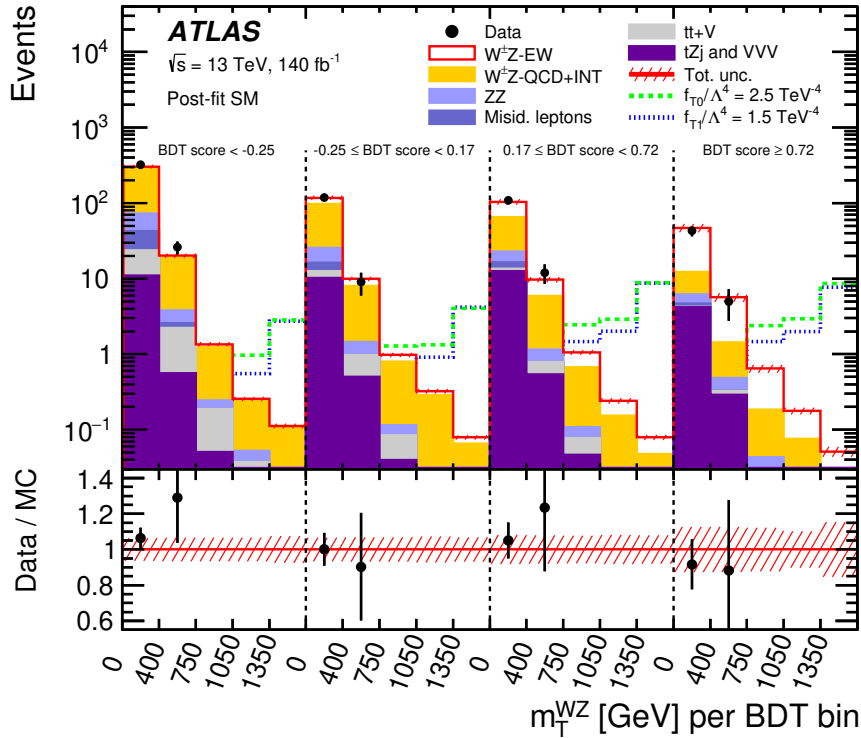


Figure 11: Detector-level one-dimension distribution of the two-dimensional combination of BDT score and m_T^{WZ} observables used to obtain limits on EFT coefficients. The SM predicted event yields resulting from the SM-only fit to data are shown. The uncertainty band around the MC expectation includes all systematic uncertainties as obtained from the fit. The contribution of the O_{T0} and O_{T1} operators with illustrative values of the corresponding Wilson coefficients are also represented.

are included as Gaussian-constrained nuisance parameters. A profile-likelihood ratio test statistic is constructed to estimate the confidence intervals for a given c_i . For each individual c_i , or pair (c_i, c_j) for two-dimensional limits, a maximum-likelihood fit to data is performed by setting other coefficients to zero. The same fit parameterisation as described in Section 7.1 is used.

No deviation with respect to the SM predictions is observed and the expected and observed 95% confidence level (CL) lower and upper limits on the given Wilson coefficients are presented in Table 4. Coefficients associated to the O_{T0} and O_{T1} operators are the most tightly constrained. The limits are dominated by the pure dimension-8 contribution in Eq. (5). These limits are similar to those obtained by the CMS experiment also using leptonic decay modes of $W^\pm Z j j$ events [7]. Two-dimensional limits at 95% CL on the pair of O_{T0} and O_{T1} operators are also obtained and presented in Figure 12. No unitarisation procedure is applied to obtain these results.

The EFT is not a complete model and the presence of non-zero dimension-8 operators violates tree-level unitarity at sufficiently high energy. More physical limits are obtained by removing the EFT contribution above the unitarity limit and keeping the SM prediction for all WZ invariant masses, even above the unitarity limit. The unitarity limits from Ref. [70] are used with only one non-zero Wilson coefficient. These unitarity limits are presented in Figure 13 for the Wilson coefficients f_{T0} and f_{T1} , together with the evolution of the expected and observed 95% CL intervals as a function of the cut-off scale m_{WZ} used in the unitarisation procedure.

Table 4: Expected and observed 95% CL intervals on the Wilson coefficients of the different dimension-8 operators, with no unitarisation procedure. The notation S02 is used to indicate that the coefficients corresponding to operators O_{S0} and O_{S2} are assigned the same value.

	Expected [TeV ⁻⁴]	Observed [TeV ⁻⁴]
f_{T0}/Λ^4	[-0.80, 0.80]	[-0.57, 0.56]
f_{T1}/Λ^4	[-0.52, 0.49]	[-0.39, 0.35]
f_{T2}/Λ^4	[-1.6, 1.4]	[-1.2, 1.0]
f_{M0}/Λ^4	[-8.3, 8.3]	[-5.8, 5.6]
f_{M1}/Λ^4	[-12.3, 12.2]	[-8.6, 8.5]
f_{M7}/Λ^4	[-16.2, 16.2]	[-11.3, 11.3]
f_{S02}/Λ^4	[-14.2, 14.2]	[-10.4, 10.4]
f_{S1}/Λ^4	[-42, 41]	[-30, 30]

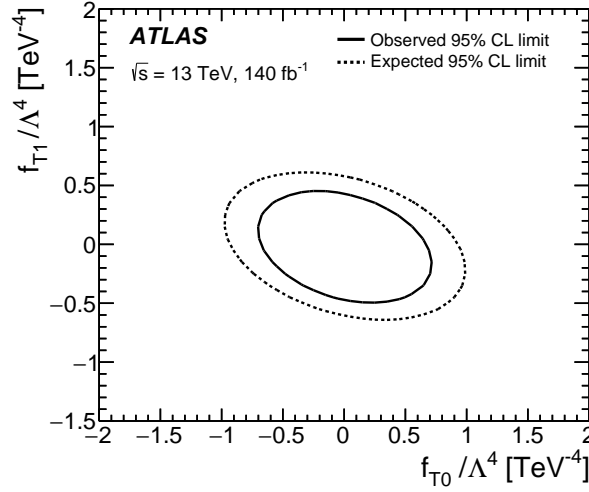


Figure 12: Two-dimensional expected (dashed line) and observed (solid line) 95% CL intervals on Wilson coefficients corresponding to the pair of O_{T0} and O_{T1} operators. No unitarisation procedure is used.

Table 5 shows the individual 95% CL intervals of each Wilson coefficients obtained when applying a unitarisation cut-off at the unitarity bound. For the O_{S1} operator no crossing with the unitarity bound was found in the scanned region above 600 GeV and therefore no limits are reported.

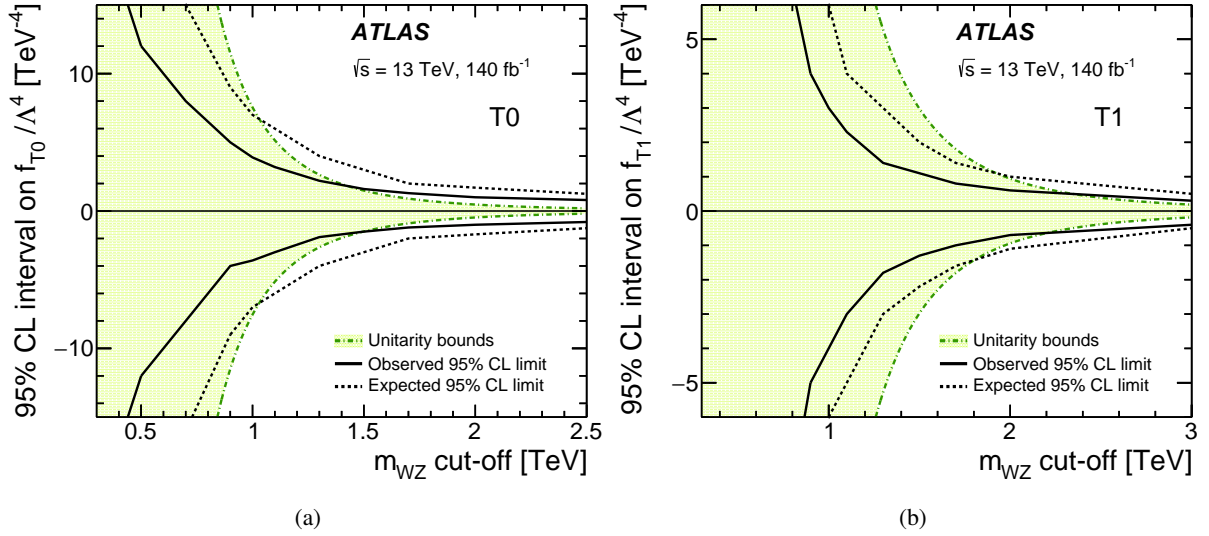


Figure 13: Evolution as a function of the cut-off scale of the individual expected (dashed lines) and observed (solid lines) limits at 95% CL on the Wilson coefficients corresponding to the operators (a) O_{T0} and (b) O_{T1} . The shaded area represents the unitarity allowed region. The unitarity bounds (dotted-dashed line) for each operator are defined for one non-zero Wilson coefficient following Ref. [70].

Table 5: Expected and observed 95% CL intervals on the Wilson coefficients of the different dimension-8 operators, with a unitarisation cut-off set at the unitarity bound, i.e. where the unitarity bound and the experimental bound cross. The notation S02 is used to indicate that the coefficients corresponding to operators O_{S0} and O_{S2} are assigned the same value.

	Expected [TeV ⁻⁴]	Observed [TeV ⁻⁴]
f_{T0}/Λ^4	[-7.0, 7.0]	[-1.5, 1.6]
f_{T1}/Λ^4	[-1.1, 1.0]	[-0.7, 0.6]
f_{T2}/Λ^4	[-12, 6]	[-2.4, 1.8]
f_{M0}/Λ^4	[-60, 60]	[-12, 12]
f_{M1}/Λ^4	[-32, 32]	[-15, 15]
f_{M7}/Λ^4	[-30, 30]	[-15, 15]
f_{S02}/Λ^4	[-41, 41]	[-18, 18]
f_{S1}/Λ^4	—	—

11 Conclusion

Measurements of integrated and differential cross-sections of electroweak production of a $W^\pm Z$ pair in association with two jets and measurements of its production cross-section in $\sqrt{s} = 13$ TeV pp collisions at the LHC are presented. The data were collected with the ATLAS detector and correspond to an integrated luminosity of 140 fb⁻¹. The measurements use leptonic decays of the gauge bosons into electrons or muons and are performed in a fiducial phase space approximating the detector acceptance that increases the sensitivity to $W^\pm Z jj$ electroweak production modes.

The measured integrated fiducial cross-sections for a single leptonic decay mode of electroweak and inclusive $W^\pm Zjj$ production are $\sigma_{WZjj-EW \rightarrow \ell' \nu \ell \ell jj} = 0.368 \pm 0.037$ (stat.) ± 0.059 (syst.) ± 0.003 (lumi.) fb and $\sigma_{WZjj \rightarrow \ell' \nu \ell \ell jj} = 1.462 \pm 0.063$ (stat.) ± 0.118 (syst.) ± 0.012 (lumi.) fb, respectively. This is the most precise measurement to date of the $WZjj$ -EW production cross-section. The electroweak $W^\pm Zjj$ production cross-section is found to agree with the LO SM prediction of 0.37 ± 0.03 fb as calculated with the MADGRAPH+PYTHIA8 MC event generator. However, the inclusive $W^\pm Zjj$ production cross-section is found to be smaller than the SM prediction from the MADGRAPH+PYTHIA8 generator of 1.91 ± 0.17 fb. The reason for this is that the $WZjj$ -QCD integrated cross-section is measured to be lower than the prediction from MADGRAPH+PYTHIA8 by a factor of 0.7, with a compatibility of 1.8σ between the measurement and the prediction.

Differential cross-sections of electroweak and strong $W^\pm Zjj$ production are measured for the first time separately for events with exactly two jets or with more than two jets, as well as in three bins of the invariant mass of the two tagging jets. For electroweak $W^\pm Zjj$ production, MC predictions from both MADGRAPH+PYTHIA8 or SHERPA 2.2.12 are found to agree with the measured cross-sections within two standard deviations in all sub-categories of signal region events. The strong $W^\pm Zjj$ production cross-section is however found to be largely mis-modelled by MC predictions from both MADGRAPH+PYTHIA8 or SHERPA 2.2.12 for events with exactly two jets of $p_T > 25$ GeV or with $500 < m_{jj} < 1300$ GeV. Differential cross-sections of $W^\pm Zjj$ production, including both the strong and electroweak processes, are also measured in the same fiducial phase space as a function of several kinematic observables.

Finally, the measured $W^\pm Zjj$ events are also used to constrain anomalous quartic gauge couplings by extracting 95% confidence level intervals on the dimension-8 operators T0, T1, T2, M0, M1, M7, S02 and S1, with and without consideration of tree-level unitarity violation. These constraints are similar to those obtained by the CMS Collaboration using the $W^\pm Zjj$ final state.

Acknowledgements

We thank CERN for the very successful operation of the LHC and its injectors, as well as the support staff at CERN and at our institutions worldwide without whom ATLAS could not be operated efficiently.

The crucial computing support from all WLCG partners is acknowledged gratefully, in particular from CERN, the ATLAS Tier-1 facilities at TRIUMF/SFU (Canada), NDGF (Denmark, Norway, Sweden), CC-IN2P3 (France), KIT/GridKA (Germany), INFN-CNAF (Italy), NL-T1 (Netherlands), PIC (Spain), RAL (UK) and BNL (USA), the Tier-2 facilities worldwide and large non-WLCG resource providers. Major contributors of computing resources are listed in Ref. [71].

We gratefully acknowledge the support of ANPCyT, Argentina; YerPhI, Armenia; ARC, Australia; BMWFW and FWF, Austria; ANAS, Azerbaijan; CNPq and FAPESP, Brazil; NSERC, NRC and CFI, Canada; CERN; ANID, Chile; CAS, MOST and NSFC, China; Minciencias, Colombia; MEYS CR, Czech Republic; DNRF and DNSRC, Denmark; IN2P3-CNRS and CEA-DRF/IRFU, France; SRNSFG, Georgia; BMBF, HGF and MPG, Germany; GSRI, Greece; RGC and Hong Kong SAR, China; ISF and Benozziyo Center, Israel; INFN, Italy; MEXT and JSPS, Japan; CNRST, Morocco; NWO, Netherlands; RCN, Norway; MEiN, Poland; FCT, Portugal; MNE/IFA, Romania; MESTD, Serbia; MSSR, Slovakia; ARRS and MIZŠ, Slovenia; DSI/NRF, South Africa; MICINN, Spain; SRC and Wallenberg Foundation, Sweden; SERI, SNSF and Cantons of Bern and Geneva, Switzerland; MOST, Taipei; TENMAK, Türkiye; STFC, United Kingdom; DOE and NSF, United States of America.

Individual groups and members have received support from BCKDF, CANARIE, CRC and DRAC, Canada; PRIMUS 21/SCI/017, Czech Republic; COST, ERC, ERDF, Horizon 2020, ICSC-NextGenerationEU and Marie Skłodowska-Curie Actions, European Union; Investissements d’Avenir Labex, Investissements d’Avenir IDEX and ANR, France; DFG and AvH Foundation, Germany; Herakleitos, Thales and Aristeia programmes co-financed by EU-ESF and the Greek NSRF, Greece; BSF-NSF and MINERVA, Israel; Norwegian Financial Mechanism 2014-2021, Norway; NCN and NAWA, Poland; La Caixa Banking Foundation, CERCA Programme Generalitat de Catalunya and PROMETEO and GenT Programmes Generalitat Valenciana, Spain; Göran Gustafssons Stiftelse, Sweden; The Royal Society and Leverhulme Trust, United Kingdom.

In addition, individual members wish to acknowledge support from CERN: European Organization for Nuclear Research (CERN PJA5); Chile: Agencia Nacional de Investigación y Desarrollo (FONDECYT 1190886, FONDECYT 1210400, FONDECYT 1230987); China: National Natural Science Foundation of China (NSFC - 12175119, NSFC 12275265); Czech Republic: Ministry of Education Youth and Sports (FORTE CZ.02.01.01/00/22_008/0004632); European Union: European Research Council (ERC - 948254, ERC 101089007), Horizon 2020 Framework Programme (MUCCA - CHIST-ERA-19-XAI-00), Italian Center for High Performance Computing, Big Data and Quantum Computing (ICSC, NextGenerationEU); France: Agence Nationale de la Recherche (ANR-20-CE31-0013, ANR-21-CE31-0022), Investissements d’Avenir Labex (ANR-11-LABX-0012); Germany: Baden-Württemberg Stiftung (BW Stiftung-Postdoc Eliteprogramme), Deutsche Forschungsgemeinschaft (DFG - 469666862, DFG - CR 312/5-2); Italy: Istituto Nazionale di Fisica Nucleare (ICSC, NextGenerationEU); Japan: Japan Society for the Promotion of Science (JSPS KAKENHI 22H01227, JSPS KAKENHI 22KK0227, JSPS KAKENHI JP21H05085, JSPS KAKENHI JP22H04944); Netherlands: Netherlands Organisation for Scientific Research (NWO Veni 2020 - VI.Veni.202.179); Norway: Research Council of Norway (RCN-314472); Poland: Polish National Agency for Academic Exchange (PPN/PPO/2020/1/00002/U/00001), Polish National Science Centre (NCN 2021/42/E/ST2/00350, NCN OPUS nr 2022/47/B/ST2/03059, NCN UMO-2019/34/E/ST2/00393, UMO-2020/37/B/ST2/01043, UMO-2021/40/C/ST2/00187, UMO-2022/47/O/ST2/00148); Slovenia: Slovenian Research Agency (ARIS grant J1-3010); Spain: Generalitat Valenciana (Artemisa, FEDER, IDIFEDER/2018/048), Ministry of Science and Innovation (RYC2019-028510-I, RYC2020-030254-I), PROMETEO and GenT Programmes Generalitat Valenciana (CIDEAGENT/2019/023, CIDEAGENT/2019/027); Sweden: Swedish Research Council (VR 2022-03845, VR 2023-03403), Knut and Alice Wallenberg Foundation (KAW 2022.0358); Switzerland: Swiss National Science Foundation (SNSF - PCEFP2_194658); United Kingdom: Leverhulme Trust (Leverhulme Trust RPG-2020-004); United States of America: Neubauer Family Foundation.

References

- [1] O. J. P. Éboli, M. C. Gonzalez-Garcia and S. M. Lietti, *Bosonic quartic couplings at CERN LHC*, *Phys. Rev. D* **69** (2004) 095005, arXiv: [hep-ph/0310141](#) [[hep-ph](#)].
- [2] O. J. P. Éboli, M. C. Gonzalez-Garcia and J. K. Mizukoshi, *$pp \rightarrow jje^\pm\mu^\pm\nu\nu$ and $jje^\pm\mu^\pm\nu\nu$ at $O(\alpha_{em}^6)$ and $O(\alpha_{em}^4\alpha_s^2)$ for the study of the quartic electroweak gauge boson vertex at CERN LHC*, *Phys. Rev. D* **74** (2006) 073005, arXiv: [hep-ph/0606118](#) [[hep-ph](#)].
- [3] C. Degrande et al., *Effective Field Theory: A Modern Approach to Anomalous Couplings*, *Annals Phys.* **335** (2013) 21, arXiv: [1205.4231](#) [[hep-ph](#)].

- [4] R. N. Cahn, S. D. Ellis, R. Kleiss and W. J. Stirling, *Transverse-momentum signatures for heavy Higgs bosons*, [Phys. Rev. D **35** \(1987\) 1626](#).
- [5] E. Accomando, A. Ballestrero, A. Belhouari and E. Maina, *Isolating vector boson scattering at the CERN LHC: Gauge cancellations and the equivalent vector boson approximation versus complete calculations*, [Phys. Rev. D **74** \(2006\) 073010](#), arXiv: [hep-ph/0608019 \[hep-ph\]](#).
- [6] ATLAS Collaboration, *Observation of electroweak $W^\pm Z$ boson pair production in association with two jets in pp collisions at $\sqrt{s} = 13$ TeV with the ATLAS detector*, [Phys. Lett. B **793** \(2019\) 469](#), arXiv: [1812.09740 \[hep-ex\]](#).
- [7] CMS Collaboration, *Measurements of production cross sections of WZ and same-sign WW boson pairs in association with two jets in proton-proton collisions at $\sqrt{s} = 13$ TeV*, [Phys. Lett. B **809** \(2020\) 135710](#), arXiv: [2005.01173 \[hep-ex\]](#).
- [8] ATLAS Collaboration, *Combined effective field theory interpretation of $W^\pm Z jj$ and $W^\pm W^\pm jj$ measurements using ATLAS 13 TeV data*, tech. rep. ATL-PHYS-PUB-2023-002, 2023, URL: <https://cds.cern.ch/record/2850667>.
- [9] ATLAS Collaboration, *The ATLAS Experiment at the CERN Large Hadron Collider*, [JINST **3** \(2008\) S08003](#).
- [10] L. Evans and P. Bryant, *LHC Machine*, [JINST **3** \(2008\) S08001](#).
- [11] ATLAS Collaboration, *The ATLAS Collaboration Software and Firmware*, ATL-SOFT-PUB-2021-001, 2021, URL: <https://cds.cern.ch/record/2767187>.
- [12] ATLAS Collaboration, *Measurements of $W^\pm Z$ production cross sections in pp collisions at $\sqrt{s} = 8$ TeV with the ATLAS detector and limits on anomalous gauge boson self-couplings*, [Phys. Rev. D **93** \(2016\) 092004](#), arXiv: [1603.02151 \[hep-ex\]](#).
- [13] Particle Data Group, *Review of Particle Physics*, [Phys. Rev. D **98** \(2018\) 030001](#).
- [14] M. Cacciari, G. P. Salam and G. Soyez, *The anti- k_t jet clustering algorithm*, [JHEP **04** \(2008\) 063](#), arXiv: [0802.1189 \[hep-ph\]](#).
- [15] M. Cacciari, G. P. Salam and G. Soyez, *FastJet user manual*, [Eur. Phys. J. C **72** \(2012\) 1896](#), arXiv: [1111.6097 \[hep-ph\]](#).
- [16] J. Alwall et al., *The automated computation of tree-level and next-to-leading order differential cross sections, and their matching to parton shower simulations*, [JHEP **07** \(2014\) 079](#), arXiv: [1405.0301 \[hep-ph\]](#).
- [17] T. Sjöstrand et al., *An introduction to PYTHIA 8.2*, [Comput. Phys. Commun. **191** \(2015\) 159](#), arXiv: [1410.3012 \[hep-ph\]](#).
- [18] ATLAS Collaboration, *ATLAS Pythia 8 tunes to 7 TeV data*, ATL-PHYS-PUB-2014-021, 2014, URL: <https://cds.cern.ch/record/1966419>.
- [19] NNPDF Collaboration, *Parton distributions for the LHC Run II*, [JHEP **04** \(2015\) 040](#), arXiv: [1410.8849 \[hep-ph\]](#).
- [20] B. Cabouat and T. Sjöstrand, *Some Dipole Shower Studies*, [Eur. Phys. J. C **78** \(2018\) 226](#), arXiv: [1710.00391 \[hep-ph\]](#).
- [21] V. Hirschi and O. Mattelaer, *Automated event generation for loop-induced processes*, [JHEP **10** \(2015\) 146](#), arXiv: [1507.00020 \[hep-ph\]](#).

- [22] R. Frederix and S. Frixione, *Merging meets matching in MC@NLO*, *JHEP* **12** (2012) 061, arXiv: [1209.6215 \[hep-ph\]](#).
- [23] J. Bellm et al., *Herwig 7.0/Herwig++ 3.0 release note*, *Eur. Phys. J. C* **76** (2016) 196, arXiv: [1512.01178 \[hep-ph\]](#).
- [24] J. Bellm et al., *Herwig 7.1 Release Note*, (2017), arXiv: [1705.06919 \[hep-ph\]](#).
- [25] E. Bothmann et al., *Event generation with Sherpa 2.2*, *SciPost Phys.* **7** (2019) 034, arXiv: [1905.09127 \[hep-ph\]](#).
- [26] T. Gleisberg and S. Höche, *Comix, a new matrix element generator*, *JHEP* **12** (2008) 039, arXiv: [0808.3674 \[hep-ph\]](#).
- [27] F. Cascioli, P. Maierhöfer and S. Pozzorini, *Scattering Amplitudes with Open Loops*, *Phys. Rev. Lett.* **108** (2012) 111601, arXiv: [1111.5206 \[hep-ph\]](#).
- [28] S. Schumann and F. Krauss, *A Parton shower algorithm based on Catani-Seymour dipole factorisation*, *JHEP* **03** (2008) 038, arXiv: [0709.1027 \[hep-ph\]](#).
- [29] S. Höche, F. Krauss, M. Schönherr and F. Siegert, *QCD matrix elements + parton showers. The NLO case*, *JHEP* **04** (2013) 027, arXiv: [1207.5030 \[hep-ph\]](#).
- [30] S. Höche, F. Krauss, M. Schönherr and F. Siegert, *A critical appraisal of NLO+PS matching methods*, *JHEP* **09** (2012) 049, arXiv: [1111.1220 \[hep-ph\]](#).
- [31] S. Catani, F. Krauss, B. R. Webber and R. Kuhn, *QCD matrix elements + parton showers*, *JHEP* **11** (2001) 063, arXiv: [hep-ph/0109231 \[hep-ph\]](#).
- [32] S. Höche, F. Krauss, S. Schumann and F. Siegert, *QCD matrix elements and truncated showers*, *JHEP* **05** (2009) 053, arXiv: [0903.1219 \[hep-ph\]](#).
- [33] D. J. Lange, *The EvtGen particle decay simulation package*, *Nucl. Instrum. Meth. A* **462** (2001) 152.
- [34] ATLAS Collaboration, *The ATLAS Simulation Infrastructure*, *Eur. Phys. J. C* **70** (2010) 823, arXiv: [1005.4568 \[physics.ins-det\]](#).
- [35] S. Agostinelli et al., *GEANT4—a simulation toolkit*, *Nucl. Instrum. Meth. A* **506** (2003) 250.
- [36] ATLAS Collaboration, *The Pythia 8 A3 tune description of ATLAS minimum bias and inelastic measurements incorporating the Donnachie–Landshoff diffractive model*, ATL-PHYS-PUB-2016-017, 2016, URL: <https://cds.cern.ch/record/2206965>.
- [37] ATLAS Collaboration, *Performance of the ATLAS trigger system in 2015*, *Eur. Phys. J. C* **77** (2017) 317, arXiv: [1611.09661 \[hep-ex\]](#).
- [38] ATLAS Collaboration, *Performance of electron and photon triggers in ATLAS during LHC Run 2*, *Eur. Phys. J. C* **80** (2020) 47, arXiv: [1909.00761 \[hep-ex\]](#).
- [39] ATLAS Collaboration, *Performance of the ATLAS muon triggers in Run 2*, *JINST* **15** (2020) P09015, arXiv: [2004.13447 \[physics.ins-det\]](#).
- [40] ATLAS Collaboration, *Muon reconstruction performance of the ATLAS detector in proton-proton collision data at $\sqrt{s}=13$ TeV*, *Eur. Phys. J. C* **76** (2016) 292, arXiv: [1603.05598 \[hep-ex\]](#).

- [41] ATLAS Collaboration, *Muon reconstruction and identification efficiency in ATLAS using the full Run 2 pp collision data set at $\sqrt{s} = 13$ TeV*, *Eur. Phys. J. C* **81** (2021) 578, arXiv: [2012.00578 \[hep-ex\]](#).
- [42] ATLAS Collaboration, *Electron and photon performance measurements with the ATLAS detector using the 2015–2017 LHC proton-proton collision data*, *JINST* **14** (2019) P12006, arXiv: [1908.00005 \[hep-ex\]](#).
- [43] ATLAS Collaboration, *Jet reconstruction and performance using particle flow with the ATLAS Detector*, *Eur. Phys. J. C* **77** (2017) 466, arXiv: [1703.10485 \[hep-ex\]](#).
- [44] ATLAS Collaboration, *Jet energy scale and resolution measured in proton–proton collisions at $\sqrt{s} = 13$ TeV with the ATLAS detector*, *Eur. Phys. J. C* **81** (2021) 689, arXiv: [2007.02645 \[hep-ex\]](#).
- [45] ATLAS Collaboration, *Performance of pile-up mitigation techniques for jets in pp collisions at $\sqrt{s} = 8$ TeV using the ATLAS detector*, *Eur. Phys. J. C* **76** (2016) 581, arXiv: [1510.03823 \[hep-ex\]](#).
- [46] ATLAS Collaboration, *Forward jet vertex tagging using the particle flow algorithm*, ATL-PHYS-PUB-2019-026, 2019, URL: <https://cds.cern.ch/record/2683100>.
- [47] ATLAS Collaboration, *ATLAS flavour-tagging algorithms for the LHC Run 2 pp collision dataset*, *Eur. Phys. J. C* **83** (2023) 681, arXiv: [2211.16345 \[physics.data-an\]](#).
- [48] ATLAS Collaboration, *E_T^{miss} performance in the ATLAS detector using 2015-2016 LHC p-p collisions*, tech. rep. ATLAS-CONF-2018-023, CERN, 2018, URL: <http://cds.cern.ch/record/2625233>.
- [49] ATLAS Collaboration, *Search for supersymmetry at $\sqrt{s}=8$ TeV in final states with jets and two same-sign leptons or three leptons with the ATLAS detector*, *JHEP* **06** (2014) 035, arXiv: [1404.2500 \[hep-ex\]](#).
- [50] ATLAS Collaboration, *Measurement of $W^\pm Z$ production cross sections and gauge boson polarisation in pp collisions at $\sqrt{s} = 13$ TeV with the ATLAS detector*, *Eur. Phys. J. C* **79** (2019) 535, arXiv: [1902.05759 \[hep-ex\]](#).
- [51] ATLAS Collaboration, *Tools for estimating fake/non-prompt lepton backgrounds with the ATLAS detector at the LHC*, *JINST* **18** (2023) T11004, arXiv: [2211.16178 \[hep-ex\]](#).
- [52] A. Hoecker et al., *TMVA - Toolkit for Multivariate Data Analysis*, PoS ACAT (2007) 040, arXiv: [physics/0703039](#).
- [53] G. D’Agostini, *A Multidimensional unfolding method based on Bayes’ theorem*, *Nucl. Instrum. Meth. A* **362** (1995) 487.
- [54] T. Adye, *Unfolding algorithms and tests using RooUnfold*, Proceedings of the PHYSTAT 2011 Workshop, CERN, Geneva, Switzerland (2011) 313, arXiv: [1105.1160 \[physics.data-an\]](#).
- [55] ATLAS Collaboration, *Evaluating statistical uncertainties and correlations using the bootstrap method*, ATL-PHYS-PUB-2021-011, 2021, URL: <https://cds.cern.ch/record/2759945>.

- [56] J. Butterworth et al., *PDF4LHC recommendations for LHC Run II*, *J. Phys. G* **43** (2016) 023001, arXiv: [1510.03865 \[hep-ph\]](#).
- [57] B. Malaescu, *An Iterative, Dynamically Stabilized(IDS) Method of Data Unfolding*, Proceedings of the PHYSTAT 2011 Workshop, CERN, Geneva, Switzerland (2011) 271, arXiv: [1106.3107 \[physics.data-an\]](#).
- [58] ATLAS Collaboration, *Jet energy scale and resolution measured in proton–proton collisions at $\sqrt{s} = 13$ TeV with the ATLAS detector*, *Eur. Phys. J. C* **81** (2021) 689, arXiv: [2007.02645 \[hep-ex\]](#).
- [59] ATLAS Collaboration, *Measurement of the Inelastic Proton-Proton Cross Section at $\sqrt{s} = 13$ TeV with the ATLAS Detector at the LHC*, *Phys. Rev. Lett.* **117** (2016) 182002, arXiv: [1606.02625 \[hep-ex\]](#).
- [60] ATLAS Collaboration, *Multi-Boson Simulation for 13 TeV ATLAS Analyses*, ATL-PHYS-PUB-2016-002, 2016, URL: <http://cds.cern.ch/record/2119986>.
- [61] ATLAS Collaboration, *Luminosity determination in pp collisions at $\sqrt{s} = 13$ TeV using the ATLAS detector at the LHC*, *Eur. Phys. J. C* **83** (2023) 982, arXiv: [2212.09379 \[hep-ex\]](#).
- [62] G. Avoni et al., *The new LUCID-2 detector for luminosity measurement and monitoring in ATLAS*, *JINST* **13** (2018) P07017.
- [63] ATLAS Collaboration, *Measurement and interpretation of same-sign W boson pair production in association with two jets in pp collisions at $\sqrt{s} = 13$ TeV with the ATLAS detector*, (2023), arXiv: [2312.00420 \[hep-ex\]](#).
- [64] D. Rainwater, R. Szalapski and D. Zeppenfeld, *Probing color-singlet exchange in Z + 2-jet events at the CERN LHC*, *Phys. Rev. D* **54** (1996) 6680, arXiv: [hep-ph/9605444](#).
- [65] O. J. P. Éboli and M. C. Gonzalez-Garcia, *Classifying the bosonic quartic couplings*, *Phys. Rev. D* **93** (2016) 093013, arXiv: [1604.03555 \[hep-ph\]](#).
- [66] ATLAS Collaboration, *Combined effective field theory interpretation of Higgs boson and weak boson production and decay with ATLAS data and electroweak precision observables*, ATL-PHYS-PUB-2022-037, 2022, URL: <https://cds.cern.ch/record/2816369>.
- [67] CMS Collaboration, *Measurements of the $pp \rightarrow WZ$ inclusive and differential production cross sections and constraints on charged anomalous triple gauge couplings at $\sqrt{s} = 13$ TeV*, *JHEP* **04** (2019) 122, arXiv: [1901.03428 \[hep-ex\]](#).
- [68] R. Bellan et al., *A sensitivity study of VBS and diboson WW to dimension-6 EFT operators at the LHC*, *JHEP* **05** (2022) 039, arXiv: [2108.03199 \[hep-ph\]](#).
- [69] J. J. Ethier, R. Gomez-Ambrosio, G. Magni and J. Rojo, *SMEFT analysis of vector boson scattering and diboson data from the LHC Run II*, *Eur. Phys. J. C* **81** (2021) 560, arXiv: [2101.03180 \[hep-ph\]](#).
- [70] E. d. S. Almeida, O. J. P. Éboli and M. C. Gonzalez-Garcia, *Unitarity constraints on anomalous quartic couplings*, *Phys. Rev. D* **101** (2020) 113003, arXiv: [2004.05174 \[hep-ph\]](#).

- [71] ATLAS Collaboration, *ATLAS Computing Acknowledgements*, ATL-SOFT-PUB-2023-001, 2023,
URL: <https://cds.cern.ch/record/2869272>.

The ATLAS Collaboration

G. Aad ¹⁰³, E. Aakvaag ¹⁶, B. Abbott ¹²¹, S. Abdelhameed ^{117a}, K. Abeling ⁵⁵, N.J. Abicht ⁴⁹, S.H. Abidi ²⁹, M. Aboeela ⁴⁴, A. Aboulhorma ^{35e}, H. Abramowicz ¹⁵², H. Abreu ¹⁵¹, Y. Abulaiti ¹¹⁸, B.S. Acharya ^{69a,69b,k}, A. Ackermann ^{63a}, C. Adam Bourdarios ⁴, L. Adamczyk ^{86a}, S.V. Addepalli ²⁶, M.J. Addison ¹⁰², J. Adelman ¹¹⁶, A. Adiguzel ^{21c}, T. Adye ¹³⁵, A.A. Affolder ¹³⁷, Y. Afik ³⁹, M.N. Agaras ¹³, J. Agarwala ^{73a,73b}, A. Aggarwal ¹⁰¹, C. Agheorghiesei ^{27c}, A. Ahmad ³⁶, F. Ahmadov ^{38,x}, W.S. Ahmed ¹⁰⁵, S. Ahuja ⁹⁶, X. Ai ^{62e}, G. Aielli ^{76a,76b}, A. Aikot ¹⁶⁴, M. Ait Tamliah ^{35e}, B. Aitbenchikh ^{35a}, M. Akbiyik ¹⁰¹, T.P.A. Åkesson ⁹⁹, A.V. Akimov ³⁷, D. Akiyama ¹⁶⁹, N.N. Akolkar ²⁴, S. Aktas ^{21a}, K. Al Houry ⁴¹, G.L. Alberghi ^{23b}, J. Albert ¹⁶⁶, P. Albicocco ⁵³, G.L. Albouy ⁶⁰, S. Alderweireldt ⁵², Z.L. Alegria ¹²², M. Aleksa ³⁶, I.N. Aleksandrov ³⁸, C. Alexa ^{27b}, T. Alexopoulos ¹⁰, F. Alfonsi ^{23b}, M. Algren ⁵⁶, M. Alhroob ¹⁶⁸, B. Ali ¹³³, H.M.J. Ali ⁹², S. Ali ³¹, S.W. Alibocus ⁹³, M. Aliev ^{33c}, G. Alimonti ^{71a}, W. Alkahi ⁵⁵, C. Allaire ⁶⁶, B.M.M. Allbrooke ¹⁴⁷, J.F. Allen ⁵², C.A. Allendes Flores ^{138f}, P.P. Allport ²⁰, A. Aloisio ^{72a,72b}, F. Alonso ⁹¹, C. Alpigiani ¹³⁹, Z.M.K. Alsolami ⁹², M. Alvarez Estevez ¹⁰⁰, A. Alvarez Fernandez ¹⁰¹, M. Alves Cardoso ⁵⁶, M.G. Alvigi ^{72a,72b}, M. Aly ¹⁰², Y. Amaral Coutinho ^{83b}, A. Ambler ¹⁰⁵, C. Amelung ³⁶, M. Amerl ¹⁰², C.G. Ames ¹¹⁰, D. Amidei ¹⁰⁷, K.J. Amirie ¹⁵⁶, S.P. Amor Dos Santos ^{131a}, K.R. Amos ¹⁶⁴, S. An ⁸⁴, V. Ananiev ¹²⁶, C. Anastopoulos ¹⁴⁰, T. Andeen ¹¹, J.K. Anders ³⁶, S.Y. Andrean ^{47a,47b}, A. Andreazza ^{71a,71b}, S. Angelidakis ⁹, A. Angerami ^{41,z}, A.V. Anisenkov ³⁷, A. Annovi ^{74a}, C. Antel ⁵⁶, E. Antipov ¹⁴⁶, M. Antonelli ⁵³, F. Anulli ^{75a}, M. Aoki ⁸⁴, T. Aoki ¹⁵⁴, M.A. Aparo ¹⁴⁷, L. Aperio Bella ⁴⁸, C. Appelt ¹⁸, A. Apyan ²⁶, S.J. Arbiol Val ⁸⁷, C. Arcangeletti ⁵³, A.T.H. Arce ⁵¹, E. Arena ⁹³, J-F. Arguin ¹⁰⁹, S. Argyropoulos ⁵⁴, J.-H. Arling ⁴⁸, O. Arnaez ⁴, H. Arnold ¹⁴⁶, G. Artoni ^{75a,75b}, H. Asada ¹¹², K. Asai ¹¹⁹, S. Asai ¹⁵⁴, N.A. Asbah ³⁶, K. Assamagan ²⁹, R. Astalos ^{28a}, K.S.V. Astrand ⁹⁹, S. Atashi ¹⁶⁰, R.J. Atkin ^{33a}, M. Atkinson ¹⁶³, H. Atmani ^{35f}, P.A. Atmasiddha ¹²⁹, K. Augsten ¹³³, S. Auricchio ^{72a,72b}, A.D. Auriol ²⁰, V.A. Austrup ¹⁰², G. Avolio ³⁶, K. Axiotis ⁵⁶, G. Azuelos ^{109,ad}, D. Babal ^{28b}, H. Bachacou ¹³⁶, K. Bachas ^{153,o}, A. Bachi ³⁴, F. Backman ^{47a,47b}, A. Badea ³⁹, T.M. Baer ¹⁰⁷, P. Bagnaia ^{75a,75b}, M. Bahmani ¹⁸, D. Bahner ⁵⁴, K. Bai ¹²⁴, J.T. Baines ¹³⁵, L. Baines ⁹⁵, O.K. Baker ¹⁷³, E. Bakos ¹⁵, D. Bakshi Gupta ⁸, V. Balakrishnan ¹²¹, R. Balasubramanian ¹¹⁵, E.M. Baldin ³⁷, P. Balek ^{86a}, E. Ballabene ^{23b,23a}, F. Balli ¹³⁶, L.M. Baltos ^{63a}, W.K. Balunas ³², J. Balz ¹⁰¹, I. Bamwidhi ^{117b}, E. Banas ⁸⁷, M. Bandieramonte ¹³⁰, A. Bandyopadhyay ²⁴, S. Bansal ²⁴, L. Barak ¹⁵², M. Barakat ⁴⁸, E.L. Barberio ¹⁰⁶, D. Barberis ^{57b,57a}, M. Barbero ¹⁰³, M.Z. Barel ¹¹⁵, K.N. Barends ^{33a}, T. Barillari ¹¹¹, M-S. Barisits ³⁶, T. Barklow ¹⁴⁴, P. Baron ¹²³, D.A. Baron Moreno ¹⁰², A. Baroncelli ^{62a}, G. Barone ²⁹, A.J. Barr ¹²⁷, J.D. Barr ⁹⁷, F. Barreiro ¹⁰⁰, J. Barreiro Guimarães da Costa ^{14a}, U. Barron ¹⁵², M.G. Barros Teixeira ^{131a}, S. Barsov ³⁷, F. Bartels ^{63a}, R. Bartoldus ¹⁴⁴, A.E. Barton ⁹², P. Bartos ^{28a}, A. Basan ¹⁰¹, M. Baselga ⁴⁹, A. Bassalat ^{66,b}, M.J. Basso ^{157a}, R. Bate ¹⁶⁵, R.L. Bates ⁵⁹, S. Batlamous ¹⁰⁰, B. Batool ¹⁴², M. Battaglia ¹³⁷, D. Battulga ¹⁸, M. Baucé ^{75a,75b}, M. Bauer ³⁶, P. Bauer ²⁴, L.T. Bazzano Hurrell ³⁰, J.B. Beacham ⁵¹, T. Beau ¹²⁸, J.Y. Beaucamp ⁹¹, P.H. Beauchemin ¹⁵⁹, P. Bechtel ²⁴, H.P. Beck ^{19,n}, K. Becker ¹⁶⁸, A.J. Beddall ⁸², V.A. Bednyakov ³⁸, C.P. Bee ¹⁴⁶, L.J. Beemster ¹⁵, T.A. Beermann ³⁶, M. Begalli ^{83d}, M. Begel ²⁹, A. Behera ¹⁴⁶, J.K. Behr ⁴⁸, J.F. Beirer ³⁶, F. Beisiegel ²⁴, M. Belfkir ^{117b}, G. Bella ¹⁵², L. Bellagamba ^{23b}, A. Bellerive ³⁴, P. Bellos ²⁰, K. Beloborodov ³⁷, D. Benckekroun ^{35a}, F. Bendebba ^{35a}, Y. Benhammou ¹⁵²,

K.C. Benkendorfer ⁶¹, L. Beresford ⁴⁸, M. Beretta ⁵³, E. Bergeaas Kuutmann ¹⁶², N. Berger ⁴,
 B. Bergmann ¹³³, J. Beringer ^{17a}, G. Bernardi ⁵, C. Bernius ¹⁴⁴, F.U. Bernlochner ²⁴,
 F. Bernon ^{36,103}, A. Berrocal Guardia ¹³, T. Berry ⁹⁶, P. Berta ¹³⁴, A. Berthold ⁵⁰, S. Bethke ¹¹¹,
 A. Betti ^{75a,75b}, A.J. Bevan ⁹⁵, N.K. Bhalla ⁵⁴, S. Bhatta ¹⁴⁶, D.S. Bhattacharya ¹⁶⁷,
 P. Bhattarai ¹⁴⁴, K.D. Bhide ⁵⁴, V.S. Bhopatkar ¹²², R.M. Bianchi ¹³⁰, G. Bianco ^{23b,23a},
 O. Biebel ¹¹⁰, R. Bielski ¹²⁴, M. Biglietti ^{77a}, C.S. Billingsley ⁴⁴, M. Bindi ⁵⁵, A. Bingul ^{21b},
 C. Bini ^{75a,75b}, A. Biondini ⁹³, G.A. Bird ³², M. Birman ¹⁷⁰, M. Biros ¹³⁴, S. Biryukov ¹⁴⁷,
 T. Bisanz ⁴⁹, E. Bisceglie ^{43b,43a}, J.P. Biswal ¹³⁵, D. Biswas ¹⁴², I. Bloch ⁴⁸, A. Blue ⁵⁹,
 U. Blumenschein ⁹⁵, J. Blumenthal ¹⁰¹, V.S. Bobrovnikov ³⁷, M. Boehler ⁵⁴, B. Boehm ¹⁶⁷,
 D. Bogavac ³⁶, A.G. Bogdanchikov ³⁷, C. Bohm ^{47a}, V. Boisvert ⁹⁶, P. Bokan ³⁶, T. Bold ^{86a},
 M. Bomben ⁵, M. Bona ⁹⁵, M. Boonekamp ¹³⁶, C.D. Booth ⁹⁶, A.G. Borbély ⁵⁹,
 I.S. Bordulev ³⁷, H.M. Borecka-Bielska ¹⁰⁹, G. Borissov ⁹², D. Bortoletto ¹²⁷, D. Boscherini ^{23b},
 M. Bosman ¹³, J.D. Bossio Sola ³⁶, K. Bouaouda ^{35a}, N. Bouchhar ¹⁶⁴, L. Boudet ⁴,
 J. Boudreau ¹³⁰, E.V. Bouhova-Thacker ⁹², D. Boumediene ⁴⁰, R. Bouquet ^{57b,57a}, A. Boveia ¹²⁰,
 J. Boyd ³⁶, D. Boye ²⁹, I.R. Boyko ³⁸, L. Bozianu ⁵⁶, J. Bracinek ²⁰, N. Brahimi ⁴,
 G. Brandt ¹⁷², O. Brandt ³², F. Braren ⁴⁸, B. Brau ¹⁰⁴, J.E. Brau ¹²⁴, R. Brenner ¹⁷⁰,
 L. Brenner ¹¹⁵, R. Brenner ¹⁶², S. Bressler ¹⁷⁰, D. Britton ⁵⁹, D. Britzger ¹¹¹, I. Brock ²⁴,
 G. Brooijmans ⁴¹, E. Brost ²⁹, L.M. Brown ¹⁶⁶, L.E. Bruce ⁶¹, T.L. Bruckler ¹²⁷,
 P.A. Bruckman de Renstrom ⁸⁷, B. Brüers ⁴⁸, A. Bruni ^{23b}, G. Bruni ^{23b}, M. Bruschi ^{23b},
 N. Brusino ^{75a,75b}, T. Buanes ¹⁶, Q. Buat ¹³⁹, D. Buchin ¹¹¹, A.G. Buckley ⁵⁹, O. Bulekov ³⁷,
 B.A. Bullard ¹⁴⁴, S. Burdin ⁹³, C.D. Burgard ⁴⁹, A.M. Burger ³⁶, B. Burghgrave ⁸,
 O. Burlayenko ⁵⁴, J.T.P. Burr ³², J.C. Burzynski ¹⁴³, E.L. Busch ⁴¹, V. Büscher ¹⁰¹,
 P.J. Bussey ⁵⁹, J.M. Butler ²⁵, C.M. Buttar ⁵⁹, J.M. Butterworth ⁹⁷, W. Buttinger ¹³⁵,
 C.J. Buxo Vázquez ¹⁰⁸, A.R. Buzykaev ³⁷, S. Cabrera Urbán ¹⁶⁴, L. Cadamuro ⁶⁶, D. Caforio ⁵⁸,
 H. Cai ¹³⁰, Y. Cai ^{14a,14e}, Y. Cai ^{14c}, V.M.M. Cairo ³⁶, O. Cakir ^{3a}, N. Calace ³⁶,
 P. Calafiura ^{17a}, G. Calderini ¹²⁸, P. Calfayan ⁶⁸, G. Callea ⁵⁹, L.P. Caloba ^{83b}, D. Calvet ⁴⁰,
 S. Calvet ⁴⁰, M. Calvetti ^{74a,74b}, R. Camacho Toro ¹²⁸, S. Camarda ³⁶, D. Camarero Munoz ²⁶,
 P. Camarri ^{76a,76b}, M.T. Camerlingo ^{72a,72b}, D. Cameron ³⁶, C. Camincher ¹⁶⁶, M. Campanelli ⁹⁷,
 A. Camplani ⁴², V. Canale ^{72a,72b}, A.C. Canbay ^{3a}, E. Canonero ⁹⁶, J. Cantero ¹⁶⁴, Y. Cao ¹⁶³,
 F. Capocasa ²⁶, M. Capua ^{43b,43a}, A. Carbone ^{71a,71b}, R. Cardarelli ^{76a}, J.C.J. Cardenas ⁸,
 G. Carducci ^{43b,43a}, T. Carli ³⁶, G. Carlino ^{72a}, J.I. Carlotto ¹³, B.T. Carlson ^{130,p},
 E.M. Carlson ^{166,157a}, J. Carmignani ⁹³, L. Carminati ^{71a,71b}, A. Carnelli ¹³⁶, M. Carnesale ^{75a,75b},
 S. Caron ¹¹⁴, E. Carquin ^{138f}, S. Carrá ^{71a}, G. Carratta ^{23b,23a}, A.M. Carroll ¹²⁴, T.M. Carter ⁵²,
 M.P. Casado ^{13,h}, M. Caspar ⁴⁸, F.L. Castillo ⁴, L. Castillo Garcia ¹³, V. Castillo Gimenez ¹⁶⁴,
 N.F. Castro ^{131a,131e}, A. Catinaccio ³⁶, J.R. Catmore ¹²⁶, T. Cavaliere ⁴, V. Cavaliere ²⁹,
 N. Cavalli ^{23b,23a}, Y.C. Cekmecelioglu ⁴⁸, E. Celebi ^{21a}, S. Cella ³⁶, F. Celli ¹²⁷,
 M.S. Centonze ^{70a,70b}, V. Cepaitis ⁵⁶, K. Cerny ¹²³, A.S. Cerqueira ^{83a}, A. Cerri ¹⁴⁷,
 L. Cerrito ^{76a,76b}, F. Cerutti ^{17a}, B. Cervato ¹⁴², A. Cervelli ^{23b}, G. Cesarini ⁵³, S.A. Cetin ⁸²,
 D. Chakraborty ¹¹⁶, J. Chan ^{17a}, W.Y. Chan ¹⁵⁴, J.D. Chapman ³², E. Chapon ¹³⁶,
 B. Chargeishvili ^{150b}, D.G. Charlton ²⁰, M. Chatterjee ¹⁹, C. Chauhan ¹³⁴, Y. Che ^{14c},
 S. Chekanov ⁶, S.V. Chekulaev ^{157a}, G.A. Chelkov ^{38,a}, A. Chen ¹⁰⁷, B. Chen ¹⁵², B. Chen ¹⁶⁶,
 H. Chen ^{14c}, H. Chen ²⁹, J. Chen ^{62c}, J. Chen ¹⁴³, M. Chen ¹²⁷, S. Chen ¹⁵⁴, S.J. Chen ^{14c},
 X. Chen ^{62c,136}, X. Chen ^{14b,ac}, Y. Chen ^{62a}, C.L. Cheng ¹⁷¹, H.C. Cheng ^{64a}, S. Cheong ¹⁴⁴,
 A. Cheplakov ³⁸, E. Cheremushkina ⁴⁸, E. Cherepanova ¹¹⁵, R. Cherkaoui El Moursli ^{35e},
 E. Cheu ⁷, K. Cheung ⁶⁵, L. Chevalier ¹³⁶, V. Chiarella ⁵³, G. Chiarelli ^{74a}, N. Chiedde ¹⁰³,
 G. Chiodini ^{70a}, A.S. Chisholm ²⁰, A. Chitan ^{27b}, M. Chitishvili ¹⁶⁴, M.V. Chizhov ³⁸,
 K. Choi ¹¹, Y. Chou ¹³⁹, E.Y.S. Chow ¹¹⁴, K.L. Chu ¹⁷⁰, M.C. Chu ^{64a}, X. Chu ^{14a,14e},

J. Chudoba ¹³², J.J. Chwastowski ⁸⁷, D. Cieri ¹¹¹, K.M. Ciesla ^{86a}, V. Cindro ⁹⁴, A. Ciocio ^{17a}, F. Cirotto ^{72a,72b}, Z.H. Citron ¹⁷⁰, M. Citterio ^{71a}, D.A. Ciubotaru ^{27b}, A. Clark ⁵⁶, P.J. Clark ⁵², N. Clarke Hall ⁹⁷, C. Clarry ¹⁵⁶, J.M. Clavijo Columbie ⁴⁸, S.E. Clawson ⁴⁸, C. Clement ^{47a,47b}, J. Clercx ⁴⁸, Y. Coadou ¹⁰³, M. Cobal ^{69a,69c}, A. Coccaro ^{57b}, R.F. Coelho Barrue ^{131a}, R. Coelho Lopes De Sa ¹⁰⁴, S. Coelli ^{71a}, B. Cole ⁴¹, J. Collot ⁶⁰, P. Conde Muiño ^{131a,131g}, M.P. Connell ^{33c}, S.H. Connell ^{33c}, E.I. Conroy ¹²⁷, F. Conventi ^{72a,ae}, H.G. Cooke ²⁰, A.M. Cooper-Sarkar ¹²⁷, F.A. Corchia ^{23b,23a}, A. Cordeiro Oudot Choi ¹²⁸, L.D. Corpe ⁴⁰, M. Corradi ^{75a,75b}, F. Corriveau ^{105,v}, A. Cortes-Gonzalez ¹⁸, M.J. Costa ¹⁶⁴, F. Costanza ⁴, D. Costanzo ¹⁴⁰, B.M. Cote ¹²⁰, J. Couthures ⁴, G. Cowan ⁹⁶, K. Cranmer ¹⁷¹, D. Cremonini ^{23b,23a}, S. Crépe-Renaudin ⁶⁰, F. Crescioli ¹²⁸, M. Cristinziani ¹⁴², M. Cristoforetti ^{78a,78b}, V. Croft ¹¹⁵, J.E. Crosby ¹²², G. Crosetti ^{43b,43a}, A. Cueto ¹⁰⁰, Z. Cui ⁷, W.R. Cunningham ⁵⁹, F. Curcio ¹⁶⁴, J.R. Curran ⁵², P. Czodrowski ³⁶, M.M. Czurylo ³⁶, M.J. Da Cunha Sargedas De Sousa ^{57b,57a}, J.V. Da Fonseca Pinto ^{83b}, C. Da Via ¹⁰², W. Dabrowski ^{86a}, T. Dado ⁴⁹, S. Dahbi ¹⁴⁹, T. Dai ¹⁰⁷, D. Dal Santo ¹⁹, C. Dallapiccola ¹⁰⁴, M. Dam ⁴², G. D'amen ²⁹, V. D'Amico ¹¹⁰, J. Damp ¹⁰¹, J.R. Dandoy ³⁴, D. Dannheim ³⁶, M. Danninger ¹⁴³, V. Dao ¹⁴⁶, G. Darbo ^{57b}, S.J. Das ^{29,af}, F. Dattola ⁴⁸, S. D'Auria ^{71a,71b}, A. D'avanzo ^{72a,72b}, C. David ^{33a}, T. Davidek ¹³⁴, I. Dawson ⁹⁵, H.A. Day-hall ¹³³, K. De ⁸, R. De Asmundis ^{72a}, N. De Biase ⁴⁸, S. De Castro ^{23b,23a}, N. De Groot ¹¹⁴, P. de Jong ¹¹⁵, H. De la Torre ¹¹⁶, A. De Maria ^{14c}, A. De Salvo ^{75a}, U. De Sanctis ^{76a,76b}, F. De Santis ^{70a,70b}, A. De Santo ¹⁴⁷, J.B. De Vivie De Regie ⁶⁰, D.V. Dedovich ³⁸, J. Degen ⁹³, A.M. Deiana ⁴⁴, F. Del Corso ^{23b,23a}, J. Del Peso ¹⁰⁰, F. Del Rio ^{63a}, L. Delagrangé ¹²⁸, F. Deliot ¹³⁶, C.M. Delitzsch ⁴⁹, M. Della Pietra ^{72a,72b}, D. Della Volpe ⁵⁶, A. Dell'Acqua ³⁶, L. Dell'Asta ^{71a,71b}, M. Delmastro ⁴, P.A. Delsart ⁶⁰, S. Demers ¹⁷³, M. Demichev ³⁸, S.P. Denisov ³⁷, L. D'Erano ⁴⁰, D. Derendarz ⁸⁷, F. Derue ¹²⁸, P. Dervan ⁹³, K. Desch ²⁴, C. Deutsch ²⁴, F.A. Di Bello ^{57b,57a}, A. Di Ciaccio ^{76a,76b}, L. Di Ciaccio ⁴, A. Di Domenico ^{75a,75b}, C. Di Donato ^{72a,72b}, A. Di Girolamo ³⁶, G. Di Gregorio ³⁶, A. Di Luca ^{78a,78b}, B. Di Micco ^{77a,77b}, R. Di Nardo ^{77a,77b}, K.F. Di Pettillo ³⁹, M. Diamantopoulou ³⁴, F.A. Dias ¹¹⁵, T. Dias Do Vale ¹⁴³, M.A. Diaz ^{138a,138b}, F.G. Diaz Capriles ²⁴, M. Didenko ¹⁶⁴, E.B. Diehl ¹⁰⁷, S. Díez Cornell ⁴⁸, C. Diez Pardos ¹⁴², C. Dimitriadi ^{162,24}, A. Dimitrievska ²⁰, J. Dingfelder ²⁴, I-M. Dinu ^{27b}, S.J. Dittmeier ^{63b}, F. Dittus ³⁶, M. Divisek ¹³⁴, F. Djama ¹⁰³, T. Djobava ^{150b}, C. Doglioni ^{102,99}, A. Dohnalova ^{28a}, J. Dolejsi ¹³⁴, Z. Dolezal ¹³⁴, K. Domijan ^{86a}, K.M. Dona ³⁹, M. Donadelli ^{83d}, B. Dong ¹⁰⁸, J. Donini ⁴⁰, A. D'Onofrio ^{72a,72b}, M. D'Onofrio ⁹³, J. Dopke ¹³⁵, A. Doria ^{72a}, N. Dos Santos Fernandes ^{131a}, P. Dougan ¹⁰², M.T. Dova ⁹¹, A.T. Doyle ⁵⁹, M.A. Draguet ¹²⁷, E. Dreyer ¹⁷⁰, I. Drivas-koulouris ¹⁰, M. Drnevich ¹¹⁸, M. Drozdova ⁵⁶, D. Du ^{62a}, T.A. du Pree ¹¹⁵, F. Dubinin ³⁷, M. Dubovsky ^{28a}, E. Duchovni ¹⁷⁰, G. Duckeck ¹¹⁰, O.A. Ducu ^{27b}, D. Duda ⁵², A. Dudarev ³⁶, E.R. Duden ²⁶, M. D'uffizi ¹⁰², L. Duflost ⁶⁶, M. Dührssen ³⁶, I. Duminica ^{27g}, A.E. Dumitriu ^{27b}, M. Dunford ^{63a}, S. Dungs ⁴⁹, K. Dunne ^{47a,47b}, A. Duperrin ¹⁰³, H. Duran Yildiz ^{3a}, M. Düren ⁵⁸, A. Durglishvili ^{150b}, B.L. Dwyer ¹¹⁶, G.I. Dyckes ^{17a}, M. Dyndal ^{86a}, B.S. Dziedzic ³⁶, Z.O. Earnshaw ¹⁴⁷, G.H. Eberwein ¹²⁷, B. Eckerova ^{28a}, S. Eggebrecht ⁵⁵, E. Egidio Purcino De Souza ¹²⁸, L.F. Ehrke ⁵⁶, G. Eigen ¹⁶, K. Einsweiler ^{17a}, T. Ekelof ¹⁶², P.A. Ekman ⁹⁹, S. El Farkh ^{35b}, Y. El Ghazali ^{35b}, H. El Jarrari ³⁶, A. El Moussaouy ^{35a}, V. Ellajosyula ¹⁶², M. Ellert ¹⁶², F. Ellinghaus ¹⁷², N. Ellis ³⁶, J. Elmsheuser ²⁹, M. Elsayy ^{117a}, M. Elsing ³⁶, D. Emelianov ¹³⁵, Y. Enari ¹⁵⁴, I. Ene ^{17a}, S. Epari ¹³, P.A. Erland ⁸⁷, D. Ernani Martins Neto ⁸⁷, M. Errenst ¹⁷², M. Escalier ⁶⁶, C. Escobar ¹⁶⁴, E. Etzion ¹⁵², G. Evans ^{131a}, H. Evans ⁶⁸, L.S. Evans ⁹⁶, A. Ezhilov ³⁷, S. Ezzarqtouni ^{35a}, F. Fabbri ^{23b,23a},

L. Fabbri [id](#)^{23b,23a}, G. Facini [id](#)⁹⁷, V. Fadeyev [id](#)¹³⁷, R.M. Fakhruddinov [id](#)³⁷, D. Fakoudis [id](#)¹⁰¹,
 S. Falciano [id](#)^{75a}, L.F. Falda Ulhoa Coelho [id](#)³⁶, F. Fallavollita [id](#)¹¹¹, G. Falsetti [id](#)^{43b,43a}, J. Faltova [id](#)¹³⁴,
 C. Fan [id](#)¹⁶³, Y. Fan [id](#)^{14a}, Y. Fang [id](#)^{14a,14e}, M. Fanti [id](#)^{71a,71b}, M. Faraj [id](#)^{69a,69b}, Z. Farazpay [id](#)⁹⁸,
 A. Farbin [id](#)⁸, A. Farilla [id](#)^{77a}, T. Farooque [id](#)¹⁰⁸, S.M. Farrington [id](#)⁵², F. Fassi [id](#)^{35e}, D. Fassouliotis [id](#)⁹,
 M. Faucci Giannelli [id](#)^{76a,76b}, W.J. Fawcett [id](#)³², L. Fayard [id](#)⁶⁶, P. Federic [id](#)¹³⁴, P. Federicova [id](#)¹³²,
 O.L. Fedin [id](#)^{37,a}, M. Feickert [id](#)¹⁷¹, L. Feligioni [id](#)¹⁰³, D.E. Fellers [id](#)¹²⁴, C. Feng [id](#)^{62b}, M. Feng [id](#)^{14b},
 Z. Feng [id](#)¹¹⁵, M.J. Fenton [id](#)¹⁶⁰, L. Ferencz [id](#)⁴⁸, R.A.M. Ferguson [id](#)⁹², S.I. Fernandez Luengo [id](#)^{138f},
 P. Fernandez Martinez [id](#)¹³, M.J.V. Fernoux [id](#)¹⁰³, J. Ferrando [id](#)⁹², A. Ferrari [id](#)¹⁶², P. Ferrari [id](#)^{115,114},
 R. Ferrari [id](#)^{73a}, D. Ferrere [id](#)⁵⁶, C. Ferretti [id](#)¹⁰⁷, D. Fiacco [id](#)^{75a,75b}, F. Fiedler [id](#)¹⁰¹, P. Fiedler [id](#)¹³³,
 A. Filipčič [id](#)⁹⁴, E.K. Filmer [id](#)¹, F. Filthaut [id](#)¹¹⁴, M.C.N. Fiolhais [id](#)^{131a,131c,c}, L. Fiorini [id](#)¹⁶⁴,
 W.C. Fisher [id](#)¹⁰⁸, T. Fitschen [id](#)¹⁰², P.M. Fitzhugh [id](#)¹³⁶, I. Fleck [id](#)¹⁴², P. Fleischmann [id](#)¹⁰⁷, T. Flick [id](#)¹⁷²,
 M. Flores [id](#)^{33d,aa}, L.R. Flores Castillo [id](#)^{64a}, L. Flores Sanz De Acedo [id](#)³⁶, F.M. Follega [id](#)^{78a,78b},
 N. Fomin [id](#)¹⁶, J.H. Foo [id](#)¹⁵⁶, A. Formica [id](#)¹³⁶, A.C. Forti [id](#)¹⁰², E. Fortin [id](#)³⁶, A.W. Fortman [id](#)^{17a},
 M.G. Foti [id](#)^{17a}, L. Fountas [id](#)^{9,i}, D. Fournier [id](#)⁶⁶, H. Fox [id](#)⁹², P. Francavilla [id](#)^{74a,74b}, S. Francescato [id](#)⁶¹,
 S. Franchellucci [id](#)⁵⁶, M. Franchini [id](#)^{23b,23a}, S. Franchino [id](#)^{63a}, D. Francis [id](#)³⁶, L. Franco [id](#)¹¹⁴,
 V. Franco Lima [id](#)³⁶, L. Franconi [id](#)⁴⁸, M. Franklin [id](#)⁶¹, G. Frattari [id](#)²⁶, Y.Y. Frid [id](#)¹⁵², J. Friend [id](#)⁵⁹,
 N. Fritzsche [id](#)⁵⁰, A. Froch [id](#)⁵⁴, D. Froidevaux [id](#)³⁶, J.A. Frost [id](#)¹²⁷, Y. Fu [id](#)^{62a},
 S. Fuenzalida Garrido [id](#)^{138f}, M. Fujimoto [id](#)¹⁰³, K.Y. Fung [id](#)^{64a}, E. Furtado De Simas Filho [id](#)^{83e},
 M. Furukawa [id](#)¹⁵⁴, J. Fuster [id](#)¹⁶⁴, A. Gaa [id](#)⁵⁵, A. Gabrielli [id](#)^{23b,23a}, A. Gabrielli [id](#)¹⁵⁶, P. Gadow [id](#)³⁶,
 G. Gagliardi [id](#)^{57b,57a}, L.G. Gagnon [id](#)^{17a}, S. Gaid [id](#)¹⁶¹, S. Galantzan [id](#)¹⁵², E.J. Gallas [id](#)¹²⁷,
 B.J. Gallop [id](#)¹³⁵, K.K. Gan [id](#)¹²⁰, S. Ganguly [id](#)¹⁵⁴, Y. Gao [id](#)⁵², F.M. Garay Walls [id](#)^{138a,138b}, B. Garcia [id](#)²⁹,
 C. García [id](#)¹⁶⁴, A. Garcia Alonso [id](#)¹¹⁵, A.G. Garcia Caffaro [id](#)¹⁷³, J.E. García Navarro [id](#)¹⁶⁴,
 M. Garcia-Sciveres [id](#)^{17a}, G.L. Gardner [id](#)¹²⁹, R.W. Gardner [id](#)³⁹, N. Garelli [id](#)¹⁵⁹, D. Garg [id](#)⁸⁰,
 R.B. Garg [id](#)¹⁴⁴, J.M. Gargan [id](#)⁵², C.A. Garner [id](#)¹⁵⁶, C.M. Garvey [id](#)^{33a}, V.K. Gassmann [id](#)¹⁵⁹, G. Gaudio [id](#)^{73a},
 V. Gautam [id](#)¹³, P. Gauzzi [id](#)^{75a,75b}, I.L. Gavrilenko [id](#)³⁷, A. Gavrilyuk [id](#)³⁷, C. Gay [id](#)¹⁶⁵, G. Gaycken [id](#)⁴⁸,
 E.N. Gazis [id](#)¹⁰, A.A. Geanta [id](#)^{27b}, C.M. Gee [id](#)¹³⁷, A. Gekow [id](#)¹²⁰, C. Gemme [id](#)^{57b}, M.H. Genest [id](#)⁶⁰,
 A.D. Gentry [id](#)¹¹³, S. George [id](#)⁹⁶, W.F. George [id](#)²⁰, T. Geralis [id](#)⁴⁶, P. Gessinger-Befurt [id](#)³⁶,
 M.E. Geyik [id](#)¹⁷², M. Ghani [id](#)¹⁶⁸, K. Ghorbanian [id](#)⁹⁵, A. Ghosal [id](#)¹⁴², A. Ghosh [id](#)¹⁶⁰, A. Ghosh [id](#)⁷,
 B. Giacobbe [id](#)^{23b}, S. Giagu [id](#)^{75a,75b}, T. Giani [id](#)¹¹⁵, P. Giannetti [id](#)^{74a}, A. Giannini [id](#)^{62a}, S.M. Gibson [id](#)⁹⁶,
 M. Gignac [id](#)¹³⁷, D.T. Gil [id](#)^{86b}, A.K. Gilbert [id](#)^{86a}, B.J. Gilbert [id](#)⁴¹, D. Gillberg [id](#)³⁴, G. Gilles [id](#)¹¹⁵,
 L. Ginabat [id](#)¹²⁸, D.M. Gingrich [id](#)^{2,ad}, M.P. Giordani [id](#)^{69a,69c}, P.F. Giraud [id](#)¹³⁶, G. Giugliarelli [id](#)^{69a,69c},
 D. Giugni [id](#)^{71a}, F. Giuli [id](#)³⁶, I. Gkialas [id](#)^{9,i}, L.K. Gladilin [id](#)³⁷, C. Glasman [id](#)¹⁰⁰, G.R. Gledhill [id](#)¹²⁴,
 G. Glemža [id](#)⁴⁸, M. Glisic [id](#)¹²⁴, I. Gnesi [id](#)^{43b,e}, Y. Go [id](#)²⁹, M. Goblirsch-Kolb [id](#)³⁶, B. Gocke [id](#)⁴⁹,
 D. Godin [id](#)¹⁰⁹, B. Gokturk [id](#)^{21a}, S. Goldfarb [id](#)¹⁰⁶, T. Golling [id](#)⁵⁶, M.G.D. Gololo [id](#)^{33g}, D. Golubkov [id](#)³⁷,
 J.P. Gombas [id](#)¹⁰⁸, A. Gomes [id](#)^{131a,131b}, G. Gomes Da Silva [id](#)¹⁴², A.J. Gomez Delegido [id](#)¹⁶⁴,
 R. Gonçalves [id](#)^{131a}, L. Gonella [id](#)²⁰, A. Gongadze [id](#)^{150c}, F. Gonnella [id](#)²⁰, J.L. Gonski [id](#)¹⁴⁴,
 R.Y. González Andana [id](#)⁵², S. González de la Hoz [id](#)¹⁶⁴, R. Gonzalez Lopez [id](#)⁹³,
 C. Gonzalez Renteria [id](#)^{17a}, M.V. Gonzalez Rodrigues [id](#)⁴⁸, R. Gonzalez Suarez [id](#)¹⁶²,
 S. Gonzalez-Sevilla [id](#)⁵⁶, L. Goossens [id](#)³⁶, B. Gorini [id](#)³⁶, E. Gorini [id](#)^{70a,70b}, A. Gorišek [id](#)⁹⁴,
 T.C. Gosart [id](#)¹²⁹, A.T. Goshaw [id](#)⁵¹, M.I. Gostkin [id](#)³⁸, S. Goswami [id](#)¹²², C.A. Gottardo [id](#)³⁶,
 S.A. Gotz [id](#)¹¹⁰, M. Goughri [id](#)^{35b}, V. Goumarre [id](#)⁴⁸, A.G. Goussiou [id](#)¹³⁹, N. Govender [id](#)^{33c},
 I. Grabowska-Bold [id](#)^{86a}, K. Graham [id](#)³⁴, E. Gramstad [id](#)¹²⁶, S. Grancagnolo [id](#)^{70a,70b}, C.M. Grant [id](#)^{1,136},
 P.M. Gravila [id](#)^{27f}, F.G. Gravili [id](#)^{70a,70b}, H.M. Gray [id](#)^{17a}, M. Greco [id](#)^{70a,70b}, C. Grefe [id](#)²⁴,
 A.S. Grefsrud [id](#)¹⁶, I.M. Gregor [id](#)⁴⁸, K.T. Greif [id](#)¹⁶⁰, P. Grenier [id](#)¹⁴⁴, S.G. Grewe [id](#)¹¹¹, A.A. Grillo [id](#)¹³⁷,
 K. Grimm [id](#)³¹, S. Grinstein [id](#)^{13,r}, J.-F. Grivaz [id](#)⁶⁶, E. Gross [id](#)¹⁷⁰, J. Grosse-Knetter [id](#)⁵⁵,
 J.C. Grundy [id](#)¹²⁷, L. Guan [id](#)¹⁰⁷, J.G.R. Guerrero Rojas [id](#)¹⁶⁴, G. Guerrieri [id](#)^{69a,69c}, R. Gugel [id](#)¹⁰¹,
 J.A.M. Guhit [id](#)¹⁰⁷, A. Guida [id](#)¹⁸, E. Guilloton [id](#)¹⁶⁸, S. Guindon [id](#)³⁶, F. Guo [id](#)^{14a,14e}, J. Guo [id](#)^{62c},

L. Guo ⁴⁸, Y. Guo ¹⁰⁷, R. Gupta ¹³⁰, S. Gurbuz ²⁴, S.S. Gurdasani ⁵⁴, G. Gustavino ^{75a,75b},
 M. Guth ⁵⁶, P. Gutierrez ¹²¹, L.F. Gutierrez Zagazeta ¹²⁹, M. Gutsche ⁵⁰, C. Gutschow ⁹⁷,
 C. Gwenlan ¹²⁷, C.B. Gwilliam ⁹³, E.S. Haaland ¹²⁶, A. Haas ¹¹⁸, M. Habedank ⁴⁸,
 C. Haber ^{17a}, H.K. Hadavand ⁸, A. Hadeef ⁵⁰, S. Hadzic ¹¹¹, A.I. Hagan ⁹², J.J. Hahn ¹⁴²,
 E.H. Haines ⁹⁷, M. Haleem ¹⁶⁷, J. Haley ¹²², J.J. Hall ¹⁴⁰, G.D. Hallewell ¹⁰³, L. Halser ¹⁹,
 K. Hamano ¹⁶⁶, M. Hamer ²⁴, G.N. Hamity ⁵², E.J. Hampshire ⁹⁶, J. Han ^{62b}, K. Han ^{62a},
 L. Han ^{14c}, L. Han ^{62a}, S. Han ^{17a}, Y.F. Han ¹⁵⁶, K. Hanagaki ⁸⁴, M. Hance ¹³⁷,
 D.A. Hangal ⁴¹, H. Hanif ¹⁴³, M.D. Hank ¹²⁹, J.B. Hansen ⁴², P.H. Hansen ⁴², K. Hara ¹⁵⁸,
 D. Harada ⁵⁶, T. Harenberg ¹⁷², S. Harkusha ³⁷, M.L. Harris ¹⁰⁴, Y.T. Harris ¹²⁷, J. Harrison ¹³,
 N.M. Harrison ¹²⁰, P.F. Harrison ¹⁶⁸, N.M. Hartman ¹¹¹, N.M. Hartmann ¹¹⁰, R.Z. Hasan ^{96,135},
 Y. Hasegawa ¹⁴¹, S. Hassan ¹⁶, R. Hauser ¹⁰⁸, C.M. Hawkes ²⁰, R.J. Hawkings ³⁶,
 Y. Hayashi ¹⁵⁴, S. Hayashida ¹¹², D. Hayden ¹⁰⁸, C. Hayes ¹⁰⁷, R.L. Hayes ¹¹⁵, C.P. Hays ¹²⁷,
 J.M. Hays ⁹⁵, H.S. Hayward ⁹³, F. He ^{62a}, M. He ^{14a,14e}, Y. He ¹⁵⁵, Y. He ⁴⁸, Y. He ⁹⁷,
 N.B. Heatley ⁹⁵, V. Hedberg ⁹⁹, A.L. Heggelund ¹²⁶, N.D. Hehir ^{95,*}, C. Heidegger ⁵⁴,
 K.K. Heidegger ⁵⁴, J. Heilman ³⁴, S. Heim ⁴⁸, T. Heim ^{17a}, J.G. Heinlein ¹²⁹, J.J. Heinrich ¹²⁴,
 L. Heinrich ^{111,ab}, J. Hejbal ¹³², A. Held ¹⁷¹, S. Hellesund ¹⁶, C.M. Helling ¹⁶⁵,
 S. Hellman ^{47a,47b}, R.C.W. Henderson ⁹², L. Henkelmann ³², A.M. Henriques Correia ³⁶, H. Herde ⁹⁹,
 Y. Hernández Jiménez ¹⁴⁶, L.M. Herrmann ²⁴, T. Herrmann ⁵⁰, G. Herten ⁵⁴, R. Hertenberger ¹¹⁰,
 L. Hervas ³⁶, M.E. Hesping ¹⁰¹, N.P. Hessey ^{157a}, M. Hidaoui ^{35b}, N. Hidic ¹³⁴, E. Hill ¹⁵⁶,
 S.J. Hillier ²⁰, J.R. Hinds ¹⁰⁸, F. Hinterkeuser ²⁴, M. Hirose ¹²⁵, S. Hirose ¹⁵⁸,
 D. Hirschbuehl ¹⁷², T.G. Hitchings ¹⁰², B. Hiti ⁹⁴, J. Hobbs ¹⁴⁶, R. Hobincu ^{27e}, N. Hod ¹⁷⁰,
 M.C. Hodgkinson ¹⁴⁰, B.H. Hodgkinson ¹²⁷, A. Hoecker ³⁶, D.D. Hofer ¹⁰⁷, J. Hofer ⁴⁸,
 T. Holm ²⁴, M. Holzbock ¹¹¹, L.B.A.H. Hommels ³², B.P. Honan ¹⁰², J.J. Hong ⁶⁸, J. Hong ^{62c},
 T.M. Hong ¹³⁰, B.H. Hooberman ¹⁶³, W.H. Hopkins ⁶, M.C. Hoppesch ¹⁶³, Y. Horii ¹¹²,
 S. Hou ¹⁴⁹, A.S. Howard ⁹⁴, J. Howarth ⁵⁹, J. Hoya ⁶, M. Hrabovsky ¹²³, A. Hrynevich ⁴⁸,
 T. Hryn'ova ⁴, P.J. Hsu ⁶⁵, S.-C. Hsu ¹³⁹, T. Hsu ⁶⁶, M. Hu ^{17a}, Q. Hu ^{62a}, S. Huang ^{64b},
 X. Huang ^{14a,14e}, Y. Huang ¹⁴⁰, Y. Huang ¹⁰¹, Y. Huang ^{14a}, Z. Huang ¹⁰², Z. Hubacek ¹³³,
 M. Huebner ²⁴, F. Huegging ²⁴, T.B. Huffman ¹²⁷, C.A. Hugli ⁴⁸, M. Huhtinen ³⁶,
 S.K. Huiberts ¹⁶, R. Hulsken ¹⁰⁵, N. Huseynov ¹², J. Huston ¹⁰⁸, J. Huth ⁶¹, R. Hyneman ¹⁴⁴,
 G. Iacobucci ⁵⁶, G. Iakovidis ²⁹, L. Iconomidou-Fayard ⁶⁶, J.P. Iddon ³⁶, P. Iengo ^{72a,72b},
 R. Iguchi ¹⁵⁴, Y. Iiyama ¹⁵⁴, T. Iizawa ¹²⁷, Y. Ikegami ⁸⁴, N. Ilic ¹⁵⁶, H. Imam ^{35a},
 M. Ince Lezki ⁵⁶, T. Ingebretsen Carlson ^{47a,47b}, G. Introzzi ^{73a,73b}, M. Iodice ^{77a},
 V. Ippolito ^{75a,75b}, R.K. Irwin ⁹³, M. Ishino ¹⁵⁴, W. Islam ¹⁷¹, C. Issever ^{18,48}, S. Istin ^{21a,ah},
 H. Ito ¹⁶⁹, R. Iuppa ^{78a,78b}, A. Ivina ¹⁷⁰, J.M. Izen ⁴⁵, V. Izzo ^{72a}, P. Jacka ¹³², P. Jackson ¹,
 C.S. Jagfeld ¹¹⁰, G. Jain ^{157a}, P. Jain ⁴⁸, K. Jakobs ⁵⁴, T. Jakoubek ¹⁷⁰, J. Jamieson ⁵⁹,
 M. Javurkova ¹⁰⁴, L. Jeanty ¹²⁴, J. Jejelava ^{150a,y}, P. Jenni ^{54,f}, C.E. Jessiman ³⁴, C. Jia ^{62b},
 J. Jia ¹⁴⁶, X. Jia ⁶¹, X. Jia ^{14a,14e}, Z. Jia ^{14c}, C. Jiang ⁵², S. Jiggins ⁴⁸, J. Jimenez Pena ¹³,
 S. Jin ^{14c}, A. Jinaru ^{27b}, O. Jinnouchi ¹⁵⁵, P. Johansson ¹⁴⁰, K.A. Johns ⁷, J.W. Johnson ¹³⁷,
 D.M. Jones ¹⁴⁷, E. Jones ⁴⁸, P. Jones ³², R.W.L. Jones ⁹², T.J. Jones ⁹³, H.L. Joos ^{55,36},
 R. Joshi ¹²⁰, J. Jovicevic ¹⁵, X. Ju ^{17a}, J.J. Junggeburth ¹⁰⁴, T. Junkermann ^{63a},
 A. Juste Rozas ^{13,r}, M.K. Juzek ⁸⁷, S. Kabana ^{138e}, A. Kaczmarek ⁸⁷, M. Kado ¹¹¹,
 H. Kagan ¹²⁰, M. Kagan ¹⁴⁴, A. Kahn ¹²⁹, C. Kahra ¹⁰¹, T. Kaji ¹⁵⁴, E. Kajomovitz ¹⁵¹,
 N. Kakati ¹⁷⁰, I. Kalaitzidou ⁵⁴, C.W. Kalderon ²⁹, N.J. Kang ¹³⁷, D. Kar ^{33g}, K. Karava ¹²⁷,
 M.J. Kareem ^{157b}, E. Karentzos ⁵⁴, O. Karkout ¹¹⁵, S.N. Karpov ³⁸, Z.M. Karpova ³⁸,
 V. Kartvelishvili ⁹², A.N. Karyukhin ³⁷, E. Kasimi ¹⁵³, J. Katzy ⁴⁸, S. Kaur ³⁴, K. Kawade ¹⁴¹,
 M.P. Kawale ¹²¹, C. Kawamoto ⁸⁸, T. Kawamoto ^{62a}, E.F. Kay ³⁶, F.I. Kaya ¹⁵⁹, S. Kazakos ¹⁰⁸,
 V.F. Kazanin ³⁷, Y. Ke ¹⁴⁶, J.M. Keaveney ^{33a}, R. Keeler ¹⁶⁶, G.V. Kehris ⁶¹, J.S. Keller ³⁴,

A.S. Kelly⁹⁷, J.J. Kempster¹⁴⁷, P.D. Kennedy¹⁰¹, O. Kepka¹³², B.P. Kerridge¹³⁵, S. Kersten¹⁷²,
 B.P. Kerševan⁹⁴, L. Keszezhova^{28a}, S. Ketabchi Haghighat¹⁵⁶, R.A. Khan¹³⁰, A. Khanov¹²²,
 A.G. Kharlamov³⁷, T. Kharlamova³⁷, E.E. Khoda¹³⁹, M. Kholodenko³⁷, T.J. Khoo¹⁸,
 G. Khoriauli¹⁶⁷, J. Khubua^{150b}, Y.A.R. Khwaira¹²⁸, B. Kibirige^{33g}, D.W. Kim^{47a,47b},
 Y.K. Kim³⁹, N. Kimura⁹⁷, M.K. Kingston⁵⁵, A. Kirchhoff⁵⁵, C. Kirfel²⁴, F. Kirfel²⁴,
 J. Kirk¹³⁵, A.E. Kiryunin¹¹¹, C. Kitsaki¹⁰, O. Kivernyk²⁴, M. Klassen¹⁵⁹, C. Klein³⁴,
 L. Klein¹⁶⁷, M.H. Klein⁴⁴, S.B. Klein⁵⁶, U. Klein⁹³, P. Klimek³⁶, A. Klimentov²⁹,
 T. Klioutchnikova³⁶, P. Kluit¹¹⁵, S. Kluth¹¹¹, E. Kneringer⁷⁹, T.M. Knight¹⁵⁶, A. Knue⁴⁹,
 R. Kobayashi⁸⁸, D. Kobylanskii¹⁷⁰, S.F. Koch¹²⁷, M. Kocian¹⁴⁴, P. Kodyš¹³⁴,
 D.M. Koeck¹²⁴, P.T. Koenig²⁴, T. Koffas³⁴, O. Kolay⁵⁰, I. Koletsou⁴, T. Komarek¹²³,
 K. Köneke⁵⁴, A.X.Y. Kong¹, T. Kono¹¹⁹, N. Konstantinidis⁹⁷, P. Kontaxakis⁵⁶, B. Konya⁹⁹,
 R. Kopeliansky⁴¹, S. Koperny^{86a}, K. Korcyl⁸⁷, K. Kordas^{153,d}, A. Korn⁹⁷, S. Korn⁵⁵,
 I. Korolkov¹³, N. Korotkova³⁷, B. Kortman¹¹⁵, O. Kortner¹¹¹, S. Kortner¹¹¹,
 W.H. Kostecka¹¹⁶, V.V. Kostyukhin¹⁴², A. Kotsokechagia¹³⁶, A. Kotwal⁵¹, A. Koulouris³⁶,
 A. Kourkoumeli-Charalampidi^{73a,73b}, C. Kourkoumelis⁹, E. Kourlitis^{111,ab}, O. Kovanda¹²⁴,
 R. Kowalewski¹⁶⁶, W. Kozanecki¹³⁶, A.S. Kozhin³⁷, V.A. Kramarenko³⁷, G. Kramberger⁹⁴,
 P. Kramer¹⁰¹, M.W. Krasny¹²⁸, A. Krasznahorkay³⁶, A.C. Kraus¹¹⁶, J.W. Kraus¹⁷²,
 J.A. Kremer⁴⁸, T. Kresse⁵⁰, J. Kretschmar⁹³, K. Kreul¹⁸, P. Krieger¹⁵⁶,
 S. Krishnamurthy¹⁰⁴, M. Krivos¹³⁴, K. Krizka²⁰, K. Kroeninger⁴⁹, H. Kroha¹¹¹, J. Kroll¹³²,
 J. Kroll¹²⁹, K.S. Krowpman¹⁰⁸, U. Kruchonak³⁸, H. Krüger²⁴, N. Krumnack⁸¹, M.C. Kruse⁵¹,
 O. Kuchinskaia³⁷, S. Kудay^{3a}, S. Kuehn³⁶, R. Kuesters⁵⁴, T. Kuhl⁴⁸, V. Kukhtin³⁸,
 Y. Kulchitsky^{37,a}, S. Kuleshov^{138d,138b}, M. Kumar^{33g}, N. Kumari⁴⁸, P. Kumari^{157b},
 A. Kupco¹³², T. Kupfer⁴⁹, A. Kupich³⁷, O. Kuprash⁵⁴, H. Kurashige⁸⁵, L.L. Kurchaninov^{157a},
 O. Kurdysh⁶⁶, Y.A. Kurochkin³⁷, A. Kurova³⁷, M. Kuze¹⁵⁵, A.K. Kvam¹⁰⁴, J. Kvita¹²³,
 T. Kwan¹⁰⁵, N.G. Kyriacou¹⁰⁷, L.A.O. Laatu¹⁰³, C. Lacasta¹⁶⁴, F. Lacava^{75a,75b},
 H. Lacker¹⁸, D. Lacour¹²⁸, N.N. Lad⁹⁷, E. Ladygin³⁸, A. Lafarge⁴⁰, B. Laforge¹²⁸,
 T. Lagouri¹⁷³, F.Z. Lahbabi^{35a}, S. Lai⁵⁵, J.E. Lambert¹⁶⁶, S. Lammers⁶⁸, W. Lampl⁷,
 C. Lampoudis^{153,d}, G. Lamprinoudis¹⁰¹, A.N. Lancaster¹¹⁶, E. Lançon²⁹, U. Landgraf⁵⁴,
 M.P.J. Landon⁹⁵, V.S. Lang⁵⁴, O.K.B. Langrekken¹²⁶, A.J. Lankford¹⁶⁰, F. Lanni³⁶,
 K. Lantzsck²⁴, A. Lanza^{73a}, J.F. Laporte¹³⁶, T. Lari^{71a}, F. Lasagni Manghi^{23b},
 M. Lassnig³⁶, V. Latonova¹³², A. Laudrain¹⁰¹, A. Laurier¹⁵¹, S.D. Lawlor¹⁴⁰,
 Z. Lawrence¹⁰², R. Lazaridou¹⁶⁸, M. Lazzaroni^{71a,71b}, B. Le¹⁰², E.M. Le Boulicaut⁵¹,
 L.T. Le Pottier^{17a}, B. Leban^{23b,23a}, A. Lebedev⁸¹, M. LeBlanc¹⁰², F. Ledroit-Guillon⁶⁰,
 S.C. Lee¹⁴⁹, S. Lee^{47a,47b}, T.F. Lee⁹³, L.L. Leeuw^{33c}, H.P. Lefebvre⁹⁶, M. Lefebvre¹⁶⁶,
 C. Leggett^{17a}, G. Lehmann Miotto³⁶, M. Leigh⁵⁶, W.A. Leight¹⁰⁴, W. Leinonen¹¹⁴,
 A. Leisos^{153,q}, M.A.L. Leite^{83c}, C.E. Leitgeb¹⁸, R. Leitner¹³⁴, K.J.C. Leney⁴⁴, T. Lenz²⁴,
 S. Leone^{74a}, C. Leonidopoulos⁵², A. Leopold¹⁴⁵, C. Leroy¹⁰⁹, R. Les¹⁰⁸, C.G. Lester³²,
 M. Levchenko³⁷, J. Levêque⁴, L.J. Levinson¹⁷⁰, G. Levrini^{23b,23a}, M.P. Lewicki⁸⁷,
 C. Lewis¹³⁹, D.J. Lewis⁴, A. Li⁵, B. Li^{62b}, C. Li^{62a}, C-Q. Li¹¹¹, H. Li^{62a}, H. Li^{62b},
 H. Li^{14c}, H. Li^{14b}, H. Li^{62b}, J. Li^{62c}, K. Li¹³⁹, L. Li^{62c}, M. Li^{14a,14e}, S. Li^{14a,14e},
 S. Li^{62d,62c}, T. Li⁵, X. Li¹⁰⁵, Z. Li¹²⁷, Z. Li¹⁰⁵, Z. Li^{14a,14e}, S. Liang^{14a,14e}, Z. Liang^{14a},
 M. Liberatore¹³⁶, B. Liberti^{76a}, K. Lie^{64c}, J. Lieber Marin^{83e}, H. Lien⁶⁸, H. Lin¹⁰⁷,
 K. Lin¹⁰⁸, R.E. Lindley⁷, J.H. Lindon², E. Lipeles¹²⁹, A. Lipniacka¹⁶, A. Lister¹⁶⁵,
 J.D. Little⁶⁸, B. Liu^{14a}, B.X. Liu^{14d}, D. Liu^{62d,62c}, E.H.L. Liu²⁰, J.B. Liu^{62a},
 J.K.K. Liu³², K. Liu^{62d}, K. Liu^{62d,62c}, M. Liu^{62a}, M.Y. Liu^{62a}, P. Liu^{14a}, Q. Liu^{62d,139,62c},
 X. Liu^{62a}, X. Liu^{62b}, Y. Liu^{14d,14e}, Y.L. Liu^{62b}, Y.W. Liu^{62a}, J. Llorente Merino¹⁴³,
 S.L. Lloyd⁹⁵, E.M. Lobodzinska⁴⁸, P. Loch⁷, T. Lohse¹⁸, K. Lohwasser¹⁴⁰, E. Loiacono⁴⁸,

M. Lokajicek ^{132,*}, J.D. Lomas ²⁰, J.D. Long ¹⁶³, I. Longarini ¹⁶⁰, R. Longo ¹⁶³,
I. Lopez Paz ⁶⁷, A. Lopez Solis ⁴⁸, N. Lorenzo Martinez ⁴, A.M. Lory ¹¹⁰, M. Losada ^{117a},
G. Löschcke Centeno ¹⁴⁷, O. Loseva ³⁷, X. Lou ^{47a,47b}, X. Lou ^{14a,14e}, A. Lounis ⁶⁶,
P.A. Love ⁹², G. Lu ^{14a,14e}, M. Lu ⁶⁶, S. Lu ¹²⁹, Y.J. Lu ⁶⁵, H.J. Lubatti ¹³⁹, C. Luci ^{75a,75b},
F.L. Lucio Alves ^{14c}, F. Luehring ⁶⁸, I. Luise ¹⁴⁶, O. Lukianchuk ⁶⁶, O. Lundberg ¹⁴⁵,
B. Lund-Jensen ¹⁴⁵, N.A. Luongo ⁶, M.S. Lutz ³⁶, A.B. Lux ²⁵, D. Lynn ²⁹, R. Lysak ¹³²,
E. Lytken ⁹⁹, V. Lyubushkin ³⁸, T. Lyubushkina ³⁸, M.M. Lyukova ¹⁴⁶, M.Firdaus M. Soberi ⁵²,
H. Ma ²⁹, K. Ma ^{62a}, L.L. Ma ^{62b}, W. Ma ^{62a}, Y. Ma ¹²², J.C. MacDonald ¹⁰¹,
P.C. Machado De Abreu Farias ^{83e}, R. Madar ⁴⁰, T. Madula ⁹⁷, J. Maeda ⁸⁵, T. Maeno ²⁹,
H. Maguire ¹⁴⁰, V. Maiboroda ¹³⁶, A. Maio ^{131a,131b,131d}, K. Maj ^{86a}, O. Majersky ⁴⁸,
S. Majewski ¹²⁴, N. Makovec ⁶⁶, V. Maksimovic ¹⁵, B. Malaescu ¹²⁸, Pa. Malecki ⁸⁷,
V.P. Maleev ³⁷, F. Malek ^{60,m}, M. Mali ⁹⁴, D. Malito ⁹⁶, U. Mallik ⁸⁰, S. Maltezos ¹⁰,
S. Malyukov ³⁸, J. Mamuzic ¹³, G. Mancini ⁵³, M.N. Mancini ²⁶, G. Manco ^{73a,73b},
J.P. Mandalia ⁹⁵, I. Mandić ⁹⁴, L. Manhaes de Andrade Filho ^{83a}, I.M. Maniatis ¹⁷⁰,
J. Manjarres Ramos ⁹⁰, D.C. Mankad ¹⁷⁰, A. Mann ¹¹⁰, S. Manzoni ³⁶, L. Mao ^{62c},
X. Mapekula ^{33c}, A. Marantis ^{153,q}, G. Marchiori ⁵, M. Marcisovsky ¹³², C. Marcon ^{71a},
M. Marinescu ²⁰, S. Marium ⁴⁸, M. Marjanovic ¹²¹, A. Markhoos ⁵⁴, M. Markovitch ⁶⁶,
E.J. Marshall ⁹², Z. Marshall ^{17a}, S. Marti-Garcia ¹⁶⁴, J. Martin ⁹⁷, T.A. Martin ¹³⁵,
V.J. Martin ⁵², B. Martin dit Latour ¹⁶, L. Martinelli ^{75a,75b}, M. Martinez ^{13,r},
P. Martinez Agullo ¹⁶⁴, V.I. Martinez Outschoorn ¹⁰⁴, P. Martinez Suarez ¹³, S. Martin-Haugh ¹³⁵,
G. Martinovicova ¹³⁴, V.S. Martoiu ^{27b}, A.C. Martyniuk ⁹⁷, A. Marzin ³⁶, D. Mascione ^{78a,78b},
L. Masetti ¹⁰¹, T. Mashimo ¹⁵⁴, J. Masik ¹⁰², A.L. Maslennikov ³⁷, P. Massarotti ^{72a,72b},
P. Mastrandrea ^{74a,74b}, A. Mastroberardino ^{43b,43a}, T. Masubuchi ¹⁵⁴, T. Mathisen ¹⁶²,
J. Matousek ¹³⁴, N. Matsuzawa ¹⁵⁴, J. Maurer ^{27b}, A.J. Maury ⁶⁶, B. Maček ⁹⁴, D.A. Maximov ³⁷,
A.E. May ¹⁰², R. Mazini ¹⁴⁹, I. Maznas ¹¹⁶, M. Mazza ¹⁰⁸, S.M. Mazza ¹³⁷, E. Mazzeo ^{71a,71b},
C. Mc Ginn ²⁹, J.P. Mc Gowan ¹⁶⁶, S.P. Mc Kee ¹⁰⁷, C.C. McCracken ¹⁶⁵, E.F. McDonald ¹⁰⁶,
A.E. McDougall ¹¹⁵, J.A. Mcfayden ¹⁴⁷, R.P. McGovern ¹²⁹, R.P. Mckenzie ^{33g},
T.C. McLachlan ⁴⁸, D.J. McLaughlin ⁹⁷, S.J. McMahan ¹³⁵, C.M. Mcpartland ⁹³,
R.A. McPherson ^{166,v}, S. Mehlhase ¹¹⁰, A. Mehta ⁹³, D. Melini ¹⁶⁴, B.R. Mellado Garcia ^{33g},
A.H. Melo ⁵⁵, F. Meloni ⁴⁸, A.M. Mendes Jacques Da Costa ¹⁰², H.Y. Meng ¹⁵⁶, L. Meng ⁹²,
S. Menke ¹¹¹, M. Mentink ³⁶, E. Meoni ^{43b,43a}, G. Mercado ¹¹⁶, S. Merianos ¹⁵³,
C. Merlassino ^{69a,69c}, L. Merola ^{72a,72b}, C. Meroni ^{71a,71b}, J. Metcalfe ⁶, A.S. Mete ⁶,
E. Meuser ¹⁰¹, C. Meyer ⁶⁸, J-P. Meyer ¹³⁶, R.P. Middleton ¹³⁵, L. Mijović ⁵²,
G. Mikenberg ¹⁷⁰, M. Mikestikova ¹³², M. Mikuž ⁹⁴, H. Mildner ¹⁰¹, A. Milic ³⁶,
D.W. Miller ³⁹, E.H. Miller ¹⁴⁴, L.S. Miller ³⁴, A. Milov ¹⁷⁰, D.A. Milstead ^{47a,47b}, T. Min ^{14c},
A.A. Minaenko ³⁷, I.A. Minashvili ^{150b}, L. Mince ⁵⁹, A.I. Mincer ¹¹⁸, B. Mindur ^{86a},
M. Mineev ³⁸, Y. Mino ⁸⁸, L.M. Mir ¹³, M. Miralles Lopez ⁵⁹, M. Mironova ^{17a}, A. Mishima ¹⁵⁴,
M.C. Missio ¹¹⁴, A. Mitra ¹⁶⁸, V.A. Mitsou ¹⁶⁴, Y. Mitsumori ¹¹², O. Miu ¹⁵⁶,
P.S. Miyagawa ⁹⁵, T. Mkrtychyan ^{63a}, M. Mlinarevic ⁹⁷, T. Mlinarevic ⁹⁷, M. Mlynarikova ³⁶,
S. Mobius ¹⁹, P. Mogg ¹¹⁰, M.H. Mohamed Farook ¹¹³, A.F. Mohammed ^{14a,14e}, S. Mohapatra ⁴¹,
G. Mokgatitswane ^{33g}, L. Moleri ¹⁷⁰, B. Mondal ¹⁴², S. Mondal ¹³³, K. Mönig ⁴⁸,
E. Monnier ¹⁰³, L. Monsonis Romero ¹⁶⁴, J. Montejo Berlingen ¹³, M. Montella ¹²⁰,
F. Montekali ^{77a,77b}, F. Monticelli ⁹¹, S. Monzani ^{69a,69c}, N. Morange ⁶⁶,
A.L. Moreira De Carvalho ⁴⁸, M. Moreno Llácer ¹⁶⁴, C. Moreno Martinez ⁵⁶, P. Morettini ^{57b},
S. Morgenstern ³⁶, M. Morii ⁶¹, M. Morinaga ¹⁵⁴, F. Morodei ^{75a,75b}, L. Morvaj ³⁶,
P. Moschovakos ³⁶, B. Moser ³⁶, M. Mosidze ^{150b}, T. Moskalets ⁴⁴, P. Moskvitina ¹¹⁴,
J. Moss ^{31,j}, P. Moszkowicz ^{86a}, A. Moussa ^{35d}, E.J.W. Moyse ¹⁰⁴, O. Mtintsilana ^{33g},

S. Muanza ¹⁰³, J. Mueller ¹³⁰, D. Muenstermann ⁹², R. Müller ¹⁹, G.A. Mullier ¹⁶²,
 A.J. Mullin³², J.J. Mullin¹²⁹, D.P. Mungo ¹⁵⁶, D. Munoz Perez ¹⁶⁴, F.J. Munoz Sanchez ¹⁰²,
 M. Murin ¹⁰², W.J. Murray ^{168,135}, M. Muškinja ⁹⁴, C. Mwewa ²⁹, A.G. Myagkov ^{37,a},
 A.J. Myers ⁸, G. Myers ¹⁰⁷, M. Myska ¹³³, B.P. Nachman ^{17a}, O. Nackenhorst ⁴⁹, K. Nagai ¹²⁷,
 K. Nagano ⁸⁴, J.L. Nagle ^{29,af}, E. Nagy ¹⁰³, A.M. Nairz ³⁶, Y. Nakahama ⁸⁴, K. Nakamura ⁸⁴,
 K. Nakkalil ⁵, H. Nanjo ¹²⁵, E.A. Narayanan ¹¹³, I. Naryshkin ³⁷, L. Nasella ^{71a,71b},
 M. Naseri ³⁴, S. Nasri ^{117b}, C. Nass ²⁴, G. Navarro ^{22a}, J. Navarro-Gonzalez ¹⁶⁴, R. Nayak ¹⁵²,
 A. Nayaz ¹⁸, P.Y. Nechaeva ³⁷, S. Nechaeva ^{23b,23a}, F. Nechansky ⁴⁸, L. Nedic ¹²⁷, T.J. Neep ²⁰,
 A. Negri ^{73a,73b}, M. Negrini ^{23b}, C. Nellist ¹¹⁵, C. Nelson ¹⁰⁵, K. Nelson ¹⁰⁷, S. Nemecek ¹³²,
 M. Nessi ^{36,g}, M.S. Neubauer ¹⁶³, F. Neuhaus ¹⁰¹, J. Neundorf ⁴⁸, P.R. Newman ²⁰,
 C.W. Ng ¹³⁰, Y.W.Y. Ng ⁴⁸, B. Ngair ^{117a}, H.D.N. Nguyen ¹⁰⁹, R.B. Nickerson ¹²⁷,
 R. Nicolaidou ¹³⁶, J. Nielsen ¹³⁷, M. Niemeyer ⁵⁵, J. Niermann ⁵⁵, N. Nikiforou ³⁶,
 V. Nikolaenko ^{37,a}, I. Nikolic-Audit ¹²⁸, K. Nikolopoulos ²⁰, P. Nilsson ²⁹, I. Ninca ⁴⁸,
 G. Ninio ¹⁵², A. Nisati ^{75a}, N. Nishu ², R. Nisius ¹¹¹, J-E. Nitschke ⁵⁰, E.K. Nkadimeng ^{33g},
 T. Nobe ¹⁵⁴, T. Nommensen ¹⁴⁸, M.B. Norfolk ¹⁴⁰, B.J. Norman ³⁴, M. Noury ^{35a}, J. Novak ⁹⁴,
 T. Novak ⁹⁴, L. Novotny ¹³³, R. Novotny ¹¹³, L. Nozka ¹²³, K. Ntekas ¹⁶⁰,
 N.M.J. Nunes De Moura Junior ^{83b}, J. Ocariz ¹²⁸, A. Ochi ⁸⁵, I. Ochoa ^{131a}, S. Oerdek ^{48,s},
 J.T. Offermann ³⁹, A. Ogrodnik ¹³⁴, A. Oh ¹⁰², C.C. Ohm ¹⁴⁵, H. Oide ⁸⁴, R. Oishi ¹⁵⁴,
 M.L. Ojeda ⁴⁸, Y. Okumura ¹⁵⁴, L.F. Oleiro Seabra ^{131a}, I. Oleksiyuk ⁵⁶, S.A. Olivares Pino ^{138d},
 G. Oliveira Correa ¹³, D. Oliveira Damazio ²⁹, D. Oliveira Goncalves ^{83a}, J.L. Oliver ¹⁶⁰,
 Ö.O. Öncel ⁵⁴, A.P. O'Neill ¹⁹, A. Onofre ^{131a,131e}, P.U.E. Onyisi ¹¹, M.J. Oreglia ³⁹,
 G.E. Orellana ⁹¹, D. Orestano ^{77a,77b}, N. Orlando ¹³, R.S. Orr ¹⁵⁶, L.M. Osojnak ¹²⁹,
 R. Ospanov ^{62a}, G. Otero y Garzon ³⁰, H. Otono ⁸⁹, P.S. Ott ^{63a}, G.J. Ottino ^{17a}, M. Ouchrif ^{35d},
 F. Ould-Saada ¹²⁶, T. Ovsiannikova ¹³⁹, M. Owen ⁵⁹, R.E. Owen ¹³⁵, V.E. Ozcan ^{21a},
 F. Ozturk ⁸⁷, N. Ozturk ⁸, S. Ozturk ⁸², H.A. Pacey ¹²⁷, A. Pacheco Pages ¹³,
 C. Padilla Aranda ¹³, G. Padovano ^{75a,75b}, S. Pagan Griso ^{17a}, G. Palacino ⁶⁸, A. Palazzo ^{70a,70b},
 J. Pampel ²⁴, J. Pan ¹⁷³, T. Pan ^{64a}, D.K. Panchal ¹¹, C.E. Pandini ¹¹⁵, J.G. Panduro Vazquez ¹³⁵,
 H.D. Pandya ¹, H. Pang ^{14b}, P. Pani ⁴⁸, G. Panizzo ^{69a,69c}, L. Panwar ¹²⁸, L. Paolozzi ⁵⁶,
 S. Parajuli ¹⁶³, A. Paramonov ⁶, C. Paraskevopoulos ⁵³, D. Paredes Hernandez ^{64b},
 A. Pareti ^{73a,73b}, K.R. Park ⁴¹, T.H. Park ¹⁵⁶, M.A. Parker ³², F. Parodi ^{57b,57a}, E.W. Parrish ¹¹⁶,
 V.A. Parrish ⁵², J.A. Parsons ⁴¹, U. Parzefall ⁵⁴, B. Pascual Dias ¹⁰⁹, L. Pascual Dominguez ¹⁰⁰,
 E. Pasqualucci ^{75a}, S. Passaggio ^{57b}, F. Pastore ⁹⁶, P. Patel ⁸⁷, U.M. Patel ⁵¹, J.R. Pater ¹⁰²,
 T. Pauly ³⁶, C.I. Pazos ¹⁵⁹, J. Pearkes ¹⁴⁴, M. Pedersen ¹²⁶, R. Pedro ^{131a}, S.V. Peleganchuk ³⁷,
 O. Penc ³⁶, E.A. Pender ⁵², G.D. Penn ¹⁷³, K.E. Penski ¹¹⁰, M. Penzin ³⁷, B.S. Peralva ^{83d},
 A.P. Pereira Peixoto ¹³⁹, L. Pereira Sanchez ¹⁴⁴, D.V. Perepelitsa ^{29,af}, P. Perera ¹⁰⁴,
 E. Perez Codina ^{157a}, M. Perganti ¹⁰, H. Pernegger ³⁶, S. Perrella ^{75a,75b}, O. Perrin ⁴⁰,
 K. Peters ⁴⁸, R.F.Y. Peters ¹⁰², B.A. Petersen ³⁶, T.C. Petersen ⁴², E. Petit ¹⁰³, V. Petousis ¹³³,
 C. Petridou ^{153,d}, T. Petru ¹³⁴, A. Petrukhin ¹⁴², M. Pettee ^{17a}, A. Petukhov ³⁷, K. Petukhova ¹³⁴,
 R. Pezoa ^{138f}, L. Pezzotti ³⁶, G. Pezzullo ¹⁷³, T.M. Pham ¹⁷¹, T. Pham ¹⁰⁶, P.W. Phillips ¹³⁵,
 G. Piacquadio ¹⁴⁶, E. Pianori ^{17a}, F. Piazza ¹²⁴, R. Piegai ³⁰, D. Pietreanu ^{27b},
 A.D. Pilkington ¹⁰², M. Pinamonti ^{69a,69c}, J.L. Pinfeld ², B.C. Pinheiro Pereira ^{131a},
 A.E. Pinto Pinoargote ^{136,136}, L. Pintucci ^{69a,69c}, K.M. Piper ¹⁴⁷, A. Pirttikoski ⁵⁶, D.A. Pizzi ³⁴,
 L. Pizzimento ^{64b}, A. Pizzini ¹¹⁵, M.-A. Pleier ²⁹, V. Pleskot ¹³⁴, E. Plotnikova³⁸, G. Poddar ⁹⁵,
 R. Poettgen ⁹⁹, L. Poggioli ¹²⁸, I. Pokharel ⁵⁵, S. Polacek ¹³⁴, G. Polesello ^{73a}, A. Poley ^{143,157a},
 A. Polini ^{23b}, C.S. Pollard ¹⁶⁸, Z.B. Pollock ¹²⁰, E. Pompa Pacchi ^{75a,75b}, N.I. Pond ⁹⁷,
 D. Ponomarenko ¹¹⁴, L. Pontecorvo ³⁶, S. Popa ^{27a}, G.A. Popeneciu ^{27d}, A. Poreba ³⁶,
 D.M. Portillo Quintero ^{157a}, S. Pospisil ¹³³, M.A. Postill ¹⁴⁰, P. Postolache ^{27c}, K. Potamianos ¹⁶⁸,

P.A. Potepa ^{86a}, I.N. Potrap ³⁸, C.J. Potter ³², H. Potti ¹⁴⁸, J. Poveda ¹⁶⁴,
 M.E. Pozo Astigarraga ³⁶, A. Prades Ibanez ¹⁶⁴, J. Pretel ⁵⁴, D. Price ¹⁰², M. Primavera ^{70a},
 M.A. Principe Martin ¹⁰⁰, R. Privara ¹²³, T. Procter ⁵⁹, M.L. Proffitt ¹³⁹, N. Proklova ¹²⁹,
 K. Prokofiev ^{64c}, G. Proto ¹¹¹, J. Proudfoot ⁶, M. Przybycien ^{86a}, W.W. Przygoda ^{86b},
 A. Psallidas ⁴⁶, J.E. Puddefoot ¹⁴⁰, D. Pudzha ³⁷, D. Pyatiizbyantseva ³⁷, J. Qian ¹⁰⁷,
 D. Qichen ¹⁰², Y. Qin ¹³, T. Qiu ⁵², A. Quadt ⁵⁵, M. Queitsch-Maitland ¹⁰², G. Quetant ⁵⁶,
 R.P. Quinn ¹⁶⁵, G. Rabanal Bolanos ⁶¹, D. Rafanoharana ⁵⁴, F. Raffaelli ^{76a,76b}, F. Ragusa ^{71a,71b},
 J.L. Rainbolt ³⁹, J.A. Raine ⁵⁶, S. Rajagopalan ²⁹, E. Ramakoti ³⁷, I.A. Ramirez-Berend ³⁴,
 K. Ran ^{48,14e}, N.P. Rapheeha ^{33g}, H. Rasheed ^{27b}, V. Raskina ¹²⁸, D.F. Rassloff ^{63a},
 A. Rastogi ^{17a}, S. Rave ¹⁰¹, S. Ravera ^{57b,57a}, B. Ravina ⁵⁵, I. Ravinovich ¹⁷⁰, M. Raymond ³⁶,
 A.L. Read ¹²⁶, N.P. Readioff ¹⁴⁰, D.M. Rebuzzi ^{73a,73b}, G. Redlinger ²⁹, A.S. Reed ¹¹¹,
 K. Reeves ²⁶, J.A. Reidelsturz ¹⁷², D. Reikher ¹⁵², A. Rej ⁴⁹, C. Rembser ³⁶, M. Renda ^{27b},
 M.B. Rendel ¹¹¹, F. Renner ⁴⁸, A.G. Rennie ¹⁶⁰, A.L. Rescia ⁴⁸, S. Resconi ^{71a},
 M. Ressegotti ^{57b,57a}, S. Rettie ³⁶, J.G. Reyes Rivera ¹⁰⁸, E. Reynolds ^{17a}, O.L. Rezanova ³⁷,
 P. Reznicek ¹³⁴, H. Riani ^{35d}, N. Ribaric ⁹², E. Ricci ^{78a,78b}, R. Richter ¹¹¹, S. Richter ^{47a,47b},
 E. Richter-Was ^{86b}, M. Ridel ¹²⁸, S. Ridouani ^{35d}, P. Rieck ¹¹⁸, P. Riedler ³⁶, E.M. Riefel ^{47a,47b},
 J.O. Rieger ¹¹⁵, M. Rijssenbeek ¹⁴⁶, M. Rimoldi ³⁶, L. Rinaldi ^{23b,23a}, T.T. Rinn ²⁹,
 M.P. Rinnagel ¹¹⁰, G. Ripellino ¹⁶², I. Riu ¹³, J.C. Rivera Vergara ¹⁶⁶, F. Rizatdinova ¹²²,
 E. Rizvi ⁹⁵, B.R. Roberts ^{17a}, S.H. Robertson ^{105,v}, D. Robinson ³², C.M. Robles Gajardo ^{138f},
 M. Robles Manzano ¹⁰¹, A. Robson ⁵⁹, A. Rocchi ^{76a,76b}, C. Roda ^{74a,74b}, S. Rodriguez Bosca ³⁶,
 Y. Rodriguez Garcia ^{22a}, A. Rodriguez Rodriguez ⁵⁴, A.M. Rodríguez Vera ¹¹⁶, S. Roe ³⁶,
 J.T. Roemer ¹⁶⁰, A.R. Roepe-Gier ¹³⁷, J. Roggel ¹⁷², O. Røhne ¹²⁶, R.A. Rojas ¹⁰⁴,
 C.P.A. Roland ¹²⁸, J. Roloff ²⁹, A. Romaniouk ³⁷, E. Romano ^{73a,73b}, M. Romano ^{23b},
 A.C. Romero Hernandez ¹⁶³, N. Rompotis ⁹³, L. Roos ¹²⁸, S. Rosati ^{75a}, B.J. Rosser ³⁹,
 E. Rossi ¹²⁷, E. Rossi ^{72a,72b}, L.P. Rossi ⁶¹, L. Rossini ⁵⁴, R. Rosten ¹²⁰, M. Rotaru ^{27b},
 B. Rottler ⁵⁴, C. Rougier ⁹⁰, D. Rousseau ⁶⁶, D. Rouso ⁴⁸, A. Roy ¹⁶³, S. Roy-Garand ¹⁵⁶,
 A. Rozanov ¹⁰³, Z.M.A. Rozario ⁵⁹, Y. Rozen ¹⁵¹, A. Rubio Jimenez ¹⁶⁴, A.J. Ruby ⁹³,
 V.H. Ruelas Rivera ¹⁸, T.A. Ruggeri ¹, A. Ruggiero ¹²⁷, A. Ruiz-Martinez ¹⁶⁴, A. Rummler ³⁶,
 Z. Rurikova ⁵⁴, N.A. Rusakovich ³⁸, H.L. Russell ¹⁶⁶, G. Russo ^{75a,75b}, J.P. Rutherford ⁷,
 S. Rutherford Colmenares ³², M. Rybar ¹³⁴, E.B. Rye ¹²⁶, A. Ryzhov ⁴⁴, J.A. Sabater Iglesias ⁵⁶,
 P. Sabatini ¹⁶⁴, H.F-W. Sadrozinski ¹³⁷, F. Safai Tehrani ^{75a}, B. Safarzadeh Samani ¹³⁵, S. Saha ¹,
 M. Sahinsoy ¹¹¹, A. Saibel ¹⁶⁴, M. Saimpert ¹³⁶, M. Saito ¹⁵⁴, T. Saito ¹⁵⁴, A. Sala ^{71a,71b},
 D. Salamani ³⁶, A. Salnikov ¹⁴⁴, J. Salt ¹⁶⁴, A. Salvador Salas ¹⁵², D. Salvatore ^{43b,43a},
 F. Salvatore ¹⁴⁷, A. Salzburger ³⁶, D. Sammel ⁵⁴, E. Sampson ⁹², D. Sampsonidis ^{153,d},
 D. Sampsonidou ¹²⁴, J. Sánchez ¹⁶⁴, V. Sanchez Sebastian ¹⁶⁴, H. Sandaker ¹²⁶, C.O. Sander ⁴⁸,
 J.A. Sandesara ¹⁰⁴, M. Sandhoff ¹⁷², C. Sandoval ^{22b}, L. Sanfilippo ^{63a}, D.P.C. Sankey ¹³⁵,
 T. Sano ⁸⁸, A. Sansoni ⁵³, L. Santi ^{36,75b}, C. Santoni ⁴⁰, H. Santos ^{131a,131b}, A. Santra ¹⁷⁰,
 E. Sanzani ^{23b,23a}, K.A. Saoucha ¹⁶¹, J.G. Saraiva ^{131a,131d}, J. Sardain ⁷, O. Sasaki ⁸⁴,
 K. Sato ¹⁵⁸, C. Sauer ^{63b}, E. Sauvan ⁴, P. Savard ^{156,ad}, R. Sawada ¹⁵⁴, C. Sawyer ¹³⁵,
 L. Sawyer ⁹⁸, C. Sbarra ^{23b}, A. Sbrizzi ^{23b,23a}, T. Scanlon ⁹⁷, J. Schaarschmidt ¹³⁹,
 U. Schäfer ¹⁰¹, A.C. Schaffer ^{66,44}, D. Schaile ¹¹⁰, R.D. Schamberger ¹⁴⁶, C. Scharf ¹⁸,
 M.M. Schefer ¹⁹, V.A. Schegelsky ³⁷, D. Scheirich ¹³⁴, M. Schernau ¹⁶⁰, C. Scheulen ⁵⁵,
 C. Schiavi ^{57b,57a}, M. Schioppa ^{43b,43a}, B. Schlag ^{144,1}, K.E. Schleicher ⁵⁴, S. Schlenker ³⁶,
 J. Schmeing ¹⁷², M.A. Schmidt ¹⁷², K. Schmieden ¹⁰¹, C. Schmitt ¹⁰¹, N. Schmitt ¹⁰¹,
 S. Schmitt ⁴⁸, L. Schoeffel ¹³⁶, A. Schoening ^{63b}, P.G. Scholer ³⁴, E. Schopf ¹²⁷, M. Schott ²⁴,
 J. Schovancova ³⁶, S. Schramm ⁵⁶, T. Schroer ⁵⁶, H-C. Schultz-Coulon ^{63a}, M. Schumacher ⁵⁴,
 B.A. Schumm ¹³⁷, Ph. Schune ¹³⁶, A.J. Schuy ¹³⁹, H.R. Schwartz ¹³⁷, A. Schwartzman ¹⁴⁴,

T.A. Schwarz [ID107](#), Ph. Schwemling [ID136](#), R. Schwienhorst [ID108](#), A. Sciandra [ID29](#), G. Sciolla [ID26](#),
 F. Scuri [ID74a](#), C.D. Sebastiani [ID93](#), K. Sedlaczek [ID116](#), S.C. Seidel [ID113](#), A. Seiden [ID137](#),
 B.D. Seidlitz [ID41](#), C. Seitz [ID48](#), J.M. Seixas [ID83b](#), G. Sekhniadze [ID72a](#), L. Selem [ID60](#),
 N. Semprini-Cesari [ID23b,23a](#), D. Sengupta [ID56](#), V. Senthilkumar [ID164](#), L. Serin [ID66](#), M. Sessa [ID76a,76b](#),
 H. Severini [ID121](#), F. Sforza [ID57b,57a](#), A. Sfyrla [ID56](#), Q. Sha [ID14a](#), E. Shabalina [ID55](#), A.H. Shah [ID32](#),
 R. Shaheen [ID145](#), J.D. Shahinian [ID129](#), D. Shaked Renous [ID170](#), L.Y. Shan [ID14a](#), M. Shapiro [ID17a](#),
 A. Sharma [ID36](#), A.S. Sharma [ID165](#), P. Sharma [ID80](#), P.B. Shatalov [ID37](#), K. Shaw [ID147](#), S.M. Shaw [ID102](#),
 Q. Shen [ID62c,5](#), D.J. Sheppard [ID143](#), P. Sherwood [ID97](#), L. Shi [ID97](#), X. Shi [ID14a](#), C.O. Shimmin [ID173](#),
 J.D. Shinner [ID96](#), I.P.J. Shipsey [ID127](#), S. Shirabe [ID89](#), M. Shiyakova [ID38,t](#), M.J. Shochet [ID39](#),
 J. Shojaii [ID106](#), D.R. Shope [ID126](#), B. Shrestha [ID121](#), S. Shrestha [ID120,ag](#), M.J. Shroff [ID166](#), P. Sicho [ID132](#),
 A.M. Sickles [ID163](#), E. Sideras Haddad [ID33g](#), A.C. Sidley [ID115](#), A. Sidoti [ID23b](#), F. Siegert [ID50](#),
 Dj. Sijacki [ID15](#), F. Sili [ID91](#), J.M. Silva [ID52](#), I. Silva Ferreira [ID83b](#), M.V. Silva Oliveira [ID29](#),
 S.B. Silverstein [ID47a](#), S. Simion [ID66](#), R. Simoniello [ID36](#), E.L. Simpson [ID102](#), H. Simpson [ID147](#),
 L.R. Simpson [ID107](#), N.D. Simpson [ID99](#), S. Simsek [ID82](#), S. Sindhu [ID55](#), P. Sinervo [ID156](#), S. Singh [ID156](#),
 S. Sinha [ID48](#), S. Sinha [ID102](#), M. Sioli [ID23b,23a](#), I. Siral [ID36](#), E. Sitnikova [ID48](#), J. Sjölin [ID47a,47b](#),
 A. Skaf [ID55](#), E. Skorda [ID20](#), P. Skubic [ID121](#), M. Slawinska [ID87](#), V. Smakhtin [ID170](#), B.H. Smart [ID135](#),
 S.Yu. Smirnov [ID37](#), Y. Smirnov [ID37](#), L.N. Smirnova [ID37,a](#), O. Smirnova [ID99](#), A.C. Smith [ID41](#),
 D.R. Smith [ID160](#), E.A. Smith [ID39](#), H.A. Smith [ID127](#), J.L. Smith [ID102](#), R. Smith [ID144](#), M. Smizanska [ID92](#),
 K. Smolek [ID133](#), A.A. Snesarev [ID37](#), S.R. Snider [ID156](#), H.L. Snoek [ID115](#), S. Snyder [ID29](#), R. Sobie [ID166,v](#),
 A. Soffer [ID152](#), C.A. Solans Sanchez [ID36](#), E.Yu. Soldatov [ID37](#), U. Soldevila [ID164](#), A.A. Solodkov [ID37](#),
 S. Solomon [ID26](#), A. Soloshenko [ID38](#), K. Solovieva [ID54](#), O.V. Solovyanov [ID40](#), P. Sommer [ID36](#),
 A. Sonay [ID13](#), W.Y. Song [ID157b](#), A. Sopczak [ID133](#), A.L. Soppio [ID97](#), F. Sopkova [ID28b](#), J.D. Sorenson [ID113](#),
 I.R. Sotarriva Alvarez [ID155](#), V. Sothilingam [ID63a](#), O.J. Soto Sandoval [ID138c,138b](#), S. Sottocornola [ID68](#),
 R. Soualah [ID161](#), Z. Soumami [ID35e](#), D. South [ID48](#), N. Soybelman [ID170](#), S. Spagnolo [ID70a,70b](#),
 M. Spalla [ID111](#), D. Sperlich [ID54](#), G. Spigo [ID36](#), S. Spinali [ID92](#), D.P. Spiteri [ID59](#), M. Spousta [ID134](#),
 E.J. Staats [ID34](#), R. Stamen [ID63a](#), A. Stampekis [ID20](#), M. Standke [ID24](#), E. Stanecka [ID87](#),
 W. Stanek-Maslouska [ID48](#), M.V. Stange [ID50](#), B. Stanislaus [ID17a](#), M.M. Stanitzki [ID48](#), B. Stapf [ID48](#),
 E.A. Starchenko [ID37](#), G.H. Stark [ID137](#), J. Stark [ID90](#), P. Staroba [ID132](#), P. Starovoitov [ID63a](#), S. Stärz [ID105](#),
 R. Staszewski [ID87](#), G. Stavropoulos [ID46](#), J. Steentoft [ID162](#), P. Steinberg [ID29](#), B. Stelzer [ID143,157a](#),
 H.J. Stelzer [ID130](#), O. Stelzer-Chilton [ID157a](#), H. Stenzel [ID58](#), T.J. Stevenson [ID147](#), G.A. Stewart [ID36](#),
 J.R. Stewart [ID122](#), M.C. Stockton [ID36](#), G. Stoicea [ID27b](#), M. Stolarski [ID131a](#), S. Stonjek [ID111](#),
 A. Straessner [ID50](#), J. Strandberg [ID145](#), S. Strandberg [ID47a,47b](#), M. Stratmann [ID172](#), M. Strauss [ID121](#),
 T. Streblner [ID103](#), P. Strizenec [ID28b](#), R. Ströhmer [ID167](#), D.M. Strom [ID124](#), R. Stroynowski [ID44](#),
 A. Strubig [ID47a,47b](#), S.A. Stucci [ID29](#), B. Stugu [ID16](#), J. Stupak [ID121](#), N.A. Styles [ID48](#), D. Su [ID144](#),
 S. Su [ID62a](#), W. Su [ID62d](#), X. Su [ID62a](#), D. Suchy [ID28a](#), K. Sugizaki [ID154](#), V.V. Sulin [ID37](#), M.J. Sullivan [ID93](#),
 D.M.S. Sultan [ID127](#), L. Sultanaliyeva [ID37](#), S. Sultansoy [ID3b](#), T. Sumida [ID88](#), S. Sun [ID171](#),
 O. Sunneborn Gudnadottir [ID162](#), N. Sur [ID103](#), M.R. Sutton [ID147](#), H. Suzuki [ID158](#), M. Svatos [ID132](#),
 M. Swiatlowski [ID157a](#), T. Swirski [ID167](#), I. Sykora [ID28a](#), M. Sykora [ID134](#), T. Sykora [ID134](#), D. Ta [ID101](#),
 K. Tackmann [ID48,s](#), A. Taffard [ID160](#), R. Tafirout [ID157a](#), J.S. Tafoya Vargas [ID66](#), Y. Takubo [ID84](#),
 M. Talby [ID103](#), A.A. Talyshev [ID37](#), K.C. Tam [ID64b](#), N.M. Tamir [ID152](#), A. Tanaka [ID154](#), J. Tanaka [ID154](#),
 R. Tanaka [ID66](#), M. Tanasini [ID146](#), Z. Tao [ID165](#), S. Tapia Araya [ID138f](#), S. Tapprogge [ID101](#),
 A. Tarek Abouelfadl Mohamed [ID108](#), S. Tarem [ID151](#), K. Tariq [ID14a](#), G. Tarna [ID27b](#), G.F. Tartarelli [ID71a](#),
 M.J. Tartarin [ID90](#), P. Tas [ID134](#), M. Tasevsky [ID132](#), E. Tassi [ID43b,43a](#), A.C. Tate [ID163](#), G. Tateno [ID154](#),
 Y. Tayalati [ID35e,u](#), G.N. Taylor [ID106](#), W. Taylor [ID157b](#), R. Teixeira De Lima [ID144](#), P. Teixeira-Dias [ID96](#),
 J.J. Teoh [ID156](#), K. Terashi [ID154](#), J. Terron [ID100](#), S. Terzo [ID13](#), M. Testa [ID53](#), R.J. Teuscher [ID156,v](#),
 A. Thaler [ID79](#), O. Theiner [ID56](#), N. Themistokleous [ID52](#), T. Thevenaux-Pelzer [ID103](#), O. Thielmann [ID172](#),
 D.W. Thomas [ID96](#), J.P. Thomas [ID20](#), E.A. Thompson [ID17a](#), P.D. Thompson [ID20](#), E. Thomson [ID129](#),

R.E. Thornberry⁴⁴, C. Tian ^{62a}, Y. Tian ⁵⁵, V. Tikhomirov ^{37,a}, Yu.A. Tikhonov ³⁷, S. Timoshenko³⁷, D. Timoshyn ¹³⁴, E.X.L. Ting ¹, P. Tipton ¹⁷³, A. Tishelman-Charny ²⁹, S.H. Tlou ^{33g}, K. Todome ¹⁵⁵, S. Todorova-Nova ¹³⁴, S. Todt⁵⁰, L. Toffolin ^{69a,69c}, M. Togawa ⁸⁴, J. Tojo ⁸⁹, S. Tokár ^{28a}, K. Tokushuku ⁸⁴, O. Toldaiev ⁶⁸, R. Tombs ³², M. Tomoto ^{84,112}, L. Tompkins ^{144,1}, K.W. Topolnicki ^{86b}, E. Torrence ¹²⁴, H. Torres ⁹⁰, E. Torró Pastor ¹⁶⁴, M. Toscani ³⁰, C. Toscirci ³⁹, M. Tost ¹¹, D.R. Tovey ¹⁴⁰, I.S. Trandafir ^{27b}, T. Trefzger ¹⁶⁷, A. Tricoli ²⁹, I.M. Trigger ^{157a}, S. Trincaz-Duvoid ¹²⁸, D.A. Trischuk ²⁶, B. Trocmé ⁶⁰, L. Truong ^{33c}, M. Trzebinski ⁸⁷, A. Trzupiek ⁸⁷, F. Tsai ¹⁴⁶, M. Tsai ¹⁰⁷, A. Tsiamis ^{153,d}, P.V. Tsiareshka³⁷, S. Tsigaridas ^{157a}, A. Tsirigotis ^{153,q}, V. Tsiskaridze ¹⁵⁶, E.G. Tskhadadze ^{150a}, M. Tsopoulou ¹⁵³, Y. Tsujikawa ⁸⁸, I.I. Tsukerman ³⁷, V. Tsulaia ^{17a}, S. Tsuno ⁸⁴, K. Tsurii ¹¹⁹, D. Tsybychev ¹⁴⁶, Y. Tu ^{64b}, A. Tudorache ^{27b}, V. Tudorache ^{27b}, A.N. Tuna ⁶¹, S. Turchikhin ^{57b,57a}, I. Turk Cakir ^{3a}, R. Turra ^{71a}, T. Turtuvshin ^{38,w}, P.M. Tuts ⁴¹, S. Tzamarias ^{153,d}, E. Tzovara ¹⁰¹, F. Ukegawa ¹⁵⁸, P.A. Ulloa Poblete ^{138c,138b}, E.N. Umaka ²⁹, G. Unal ³⁶, A. Undrus ²⁹, G. Unel ¹⁶⁰, J. Urban ^{28b}, P. Urrejola ^{138a}, G. Usai ⁸, R. Ushioda ¹⁵⁵, M. Usman ¹⁰⁹, Z. Uysal ⁸², V. Vacek ¹³³, B. Vachon ¹⁰⁵, T. Vafeiadis ³⁶, A. Vaitkus ⁹⁷, C. Valderanis ¹¹⁰, E. Valdes Santurio ^{47a,47b}, M. Valente ^{157a}, S. Valentinetti ^{23b,23a}, A. Valero ¹⁶⁴, E. Valiente Moreno ¹⁶⁴, A. Vallier ⁹⁰, J.A. Valls Ferrer ¹⁶⁴, D.R. Van Arneman ¹¹⁵, T.R. Van Daalen ¹³⁹, A. Van Der Graaf ⁴⁹, P. Van Gemmeren ⁶, M. Van Rijnbach ³⁶, S. Van Stroud ⁹⁷, I. Van Vulpen ¹¹⁵, P. Vana ¹³⁴, M. Vanadia ^{76a,76b}, W. Vandelli ³⁶, E.R. Vandewall ¹²², D. Vannicola ¹⁵², L. Vannoli ⁵³, R. Vari ^{75a}, E.W. Varnes ⁷, C. Varni ^{17b}, T. Varol ¹⁴⁹, D. Varouchas ⁶⁶, L. Varriale ¹⁶⁴, K.E. Varvell ¹⁴⁸, M.E. Vasile ^{27b}, L. Vaslin ⁸⁴, G.A. Vasquez ¹⁶⁶, A. Vasyukov ³⁸, L.M. Vaughan ¹²², R. Vavricka¹⁰¹, T. Vazquez Schroeder ³⁶, J. Veatch ³¹, V. Vecchio ¹⁰², M.J. Veen ¹⁰⁴, I. Veliscek ²⁹, L.M. Veloce ¹⁵⁶, F. Veloso ^{131a,131c}, S. Veneziano ^{75a}, A. Ventura ^{70a,70b}, S. Ventura Gonzalez ¹³⁶, A. Verbytskyi ¹¹¹, M. Verducci ^{74a,74b}, C. Vergis ⁹⁵, M. Verissimo De Araujo ^{83b}, W. Verkerke ¹¹⁵, J.C. Vermeulen ¹¹⁵, C. Vernieri ¹⁴⁴, M. Vessella ¹⁰⁴, M.C. Vetterli ^{143,ad}, A. Vgenopoulos ^{153,d}, N. Viaux Maira ^{138f}, T. Vickey ¹⁴⁰, O.E. Vickey Boeriu ¹⁴⁰, G.H.A. Viehhauser ¹²⁷, L. Vigani ^{63b}, M. Villa ^{23b,23a}, M. Villaplana Perez ¹⁶⁴, E.M. Villhauer⁵², E. Vilucchi ⁵³, M.G. Vincter ³⁴, A. Visibile¹¹⁵, C. Vittori ³⁶, I. Vivarelli ^{23b,23a}, E. Voevodina ¹¹¹, F. Vogel ¹¹⁰, J.C. Voigt ⁵⁰, P. Vokac ¹³³, Yu. Volkotrub ^{86b}, J. Von Ahnen ⁴⁸, E. Von Toerne ²⁴, B. Vormwald ³⁶, V. Vorobel ¹³⁴, K. Vorobev ³⁷, M. Vos ¹⁶⁴, K. Voss ¹⁴², M. Vozak ¹¹⁵, L. Vozdecky ¹²¹, N. Vranjes ¹⁵, M. Vranjes Milosavljevic ¹⁵, M. Vreeswijk ¹¹⁵, N.K. Vu ^{62d,62c}, R. Vuillermet ³⁶, O. Vujinovic ¹⁰¹, I. Vukotic ³⁹, S. Wada ¹⁵⁸, C. Wagner¹⁰⁴, J.M. Wagner ^{17a}, W. Wagner ¹⁷², S. Wahdan ¹⁷², H. Wahlberg ⁹¹, M. Wakida ¹¹², J. Walder ¹³⁵, R. Walker ¹¹⁰, W. Walkowiak ¹⁴², A. Wall ¹²⁹, E.J. Wallin ⁹⁹, T. Wamorkar ⁶, A.Z. Wang ¹³⁷, C. Wang ¹⁰¹, C. Wang ¹¹, H. Wang ^{17a}, J. Wang ^{64c}, P. Wang ⁹⁷, R. Wang ⁶¹, R. Wang ⁶, S.M. Wang ¹⁴⁹, S. Wang ^{62b}, S. Wang ^{14a}, T. Wang ^{62a}, W.T. Wang ⁸⁰, W. Wang ^{14a}, X. Wang ^{14c}, X. Wang ¹⁶³, X. Wang ^{62c}, Y. Wang ^{62d}, Y. Wang ^{14c}, Z. Wang ¹⁰⁷, Z. Wang ^{62d,51,62c}, Z. Wang ¹⁰⁷, A. Warburton ¹⁰⁵, R.J. Ward ²⁰, N. Warrack ⁵⁹, S. Waterhouse ⁹⁶, A.T. Watson ²⁰, H. Watson ⁵⁹, M.F. Watson ²⁰, E. Watton ^{59,135}, G. Watts ¹³⁹, B.M. Waugh ⁹⁷, J.M. Webb ⁵⁴, C. Weber ²⁹, H.A. Weber ¹⁸, M.S. Weber ¹⁹, S.M. Weber ^{63a}, C. Wei ^{62a}, Y. Wei ⁵⁴, A.R. Weidberg ¹²⁷, E.J. Weik ¹¹⁸, J. Weingarten ⁴⁹, C. Weiser ⁵⁴, C.J. Wells ⁴⁸, T. Wenaus ²⁹, B. Wendland ⁴⁹, T. Wengler ³⁶, N.S. Wenke¹¹¹, N. Wermes ²⁴, M. Wessels ^{63a}, A.M. Wharton ⁹², A.S. White ⁶¹, A. White ⁸, M.J. White ¹, D. Whiteson ¹⁶⁰, L. Wickremasinghe ¹²⁵, W. Wiedenmann ¹⁷¹, M. Wielers ¹³⁵, C. Wiglesworth ⁴², D.J. Wilbern¹²¹, H.G. Wilkens ³⁶, J.J.H. Wilkinson ³², D.M. Williams ⁴¹, H.H. Williams¹²⁹, S. Williams ³², S. Willocq ¹⁰⁴, B.J. Wilson ¹⁰², P.J. Windischhofer ³⁹, F.I. Winkel ³⁰, F. Winklmeier ¹²⁴, B.T. Winter ⁵⁴, J.K. Winter ¹⁰²,

M. Wittgen¹⁴⁴, M. Wobisch⁹⁸, T. Wojtkowski⁶⁰, Z. Wolffs¹¹⁵, J. Wollrath¹⁶⁰, M.W. Wolter⁸⁷, H. Wolters^{131a,131c}, M.C. Wong¹³⁷, E.L. Woodward⁴¹, S.D. Worm⁴⁸, B.K. Wosiek⁸⁷, K.W. Woźniak⁸⁷, S. Wozniowski⁵⁵, K. Wraight⁵⁹, C. Wu²⁰, M. Wu^{14d}, M. Wu¹¹⁴, S.L. Wu¹⁷¹, X. Wu⁵⁶, Y. Wu^{62a}, Z. Wu⁴, J. Wuerzinger^{111,ab}, T.R. Wyatt¹⁰², B.M. Wynne⁵², S. Xella⁴², L. Xia^{14c}, M. Xia^{14b}, J. Xiang^{64c}, M. Xie^{62a}, S. Xin^{14a,14e}, A. Xiong¹²⁴, J. Xiong^{17a}, D. Xu^{14a}, H. Xu^{62a}, L. Xu^{62a}, R. Xu¹²⁹, T. Xu¹⁰⁷, Y. Xu^{14b}, Z. Xu⁵², Z. Xu^{14c}, B. Yabsley¹⁴⁸, S. Yacoob^{33a}, Y. Yamaguchi¹⁵⁵, E. Yamashita¹⁵⁴, H. Yamauchi¹⁵⁸, T. Yamazaki^{17a}, Y. Yamazaki⁸⁵, J. Yan^{62c}, S. Yan⁵⁹, Z. Yan¹⁰⁴, H.J. Yang^{62c,62d}, H.T. Yang^{62a}, S. Yang^{62a}, T. Yang^{64c}, X. Yang³⁶, X. Yang^{14a}, Y. Yang⁴⁴, Y. Yang^{62a}, Z. Yang^{62a}, W-M. Yao^{17a}, H. Ye^{14c}, H. Ye⁵⁵, J. Ye^{14a}, S. Ye²⁹, X. Ye^{62a}, Y. Yeh⁹⁷, I. Yeletsikh³⁸, B.K. Yeo^{17b}, M.R. Yexley⁹⁷, T.P. Yildirim¹²⁷, P. Yin⁴¹, K. Yorita¹⁶⁹, S. Younas^{27b}, C.J.S. Young³⁶, C. Young¹⁴⁴, C. Yu^{14a,14e}, Y. Yu^{62a}, M. Yuan¹⁰⁷, R. Yuan^{62d,62c}, L. Yue⁹⁷, M. Zaazoua^{62a}, B. Zabinski⁸⁷, E. Zaid⁵², Z.K. Zak⁸⁷, T. Zakareishvili¹⁶⁴, N. Zakharchuk³⁴, S. Zambito⁵⁶, J.A. Zamora Saa^{138d,138b}, J. Zang¹⁵⁴, D. Zanzi⁵⁴, O. Zaplatilek¹³³, C. Zeitnitz¹⁷², H. Zeng^{14a}, J.C. Zeng¹⁶³, D.T. Zenger Jr²⁶, O. Zenin³⁷, T. Ženiš^{28a}, S. Zenz⁹⁵, S. Zerradi^{35a}, D. Zerwas⁶⁶, M. Zhai^{14a,14e}, D.F. Zhang¹⁴⁰, J. Zhang^{62b}, J. Zhang⁶, K. Zhang^{14a,14e}, L. Zhang^{62a}, L. Zhang^{14c}, P. Zhang^{14a,14e}, R. Zhang¹⁷¹, S. Zhang¹⁰⁷, S. Zhang⁹⁰, T. Zhang¹⁵⁴, X. Zhang^{62c}, X. Zhang^{62b}, Y. Zhang^{62c}, Y. Zhang⁹⁷, Y. Zhang^{14c}, Z. Zhang^{17a}, Z. Zhang^{62b}, Z. Zhang⁶⁶, H. Zhao¹³⁹, T. Zhao^{62b}, Y. Zhao¹³⁷, Z. Zhao^{62a}, Z. Zhao^{62a}, A. Zhemchugov³⁸, J. Zheng^{14c}, K. Zheng¹⁶³, X. Zheng^{62a}, Z. Zheng¹⁴⁴, D. Zhong¹⁶³, B. Zhou¹⁰⁷, H. Zhou⁷, N. Zhou^{62c}, Y. Zhou^{14b}, Y. Zhou^{14c}, Y. Zhou⁷, C.G. Zhu^{62b}, J. Zhu¹⁰⁷, X. Zhu^{62d}, Y. Zhu^{62c}, Y. Zhu^{62a}, X. Zhuang^{14a}, K. Zhukov³⁷, N.I. Zimine³⁸, J. Zinsser^{63b}, M. Ziolkowski¹⁴², L. Živković¹⁵, A. Zoccoli^{23b,23a}, K. Zoch⁶¹, T.G. Zorbas¹⁴⁰, O. Zormpa⁴⁶, W. Zou⁴¹, L. Zwalinski³⁶.

¹Department of Physics, University of Adelaide, Adelaide; Australia.

²Department of Physics, University of Alberta, Edmonton AB; Canada.

^{3(a)}Department of Physics, Ankara University, Ankara; ^(b)Division of Physics, TOBB University of Economics and Technology, Ankara; Türkiye.

⁴LAPP, Université Savoie Mont Blanc, CNRS/IN2P3, Annecy; France.

⁵APC, Université Paris Cité, CNRS/IN2P3, Paris; France.

⁶High Energy Physics Division, Argonne National Laboratory, Argonne IL; United States of America.

⁷Department of Physics, University of Arizona, Tucson AZ; United States of America.

⁸Department of Physics, University of Texas at Arlington, Arlington TX; United States of America.

⁹Physics Department, National and Kapodistrian University of Athens, Athens; Greece.

¹⁰Physics Department, National Technical University of Athens, Zografou; Greece.

¹¹Department of Physics, University of Texas at Austin, Austin TX; United States of America.

¹²Institute of Physics, Azerbaijan Academy of Sciences, Baku; Azerbaijan.

¹³Institut de Física d'Altes Energies (IFAE), Barcelona Institute of Science and Technology, Barcelona; Spain.

^{14(a)}Institute of High Energy Physics, Chinese Academy of Sciences, Beijing; ^(b)Physics Department, Tsinghua University, Beijing; ^(c)Department of Physics, Nanjing University, Nanjing; ^(d)School of Science, Shenzhen Campus of Sun Yat-sen University; ^(e)University of Chinese Academy of Science (UCAS), Beijing; China.

¹⁵Institute of Physics, University of Belgrade, Belgrade; Serbia.

¹⁶Department for Physics and Technology, University of Bergen, Bergen; Norway.

- ¹⁷(*a*) Physics Division, Lawrence Berkeley National Laboratory, Berkeley CA; (*b*) University of California, Berkeley CA; United States of America.
- ¹⁸Institut für Physik, Humboldt Universität zu Berlin, Berlin; Germany.
- ¹⁹Albert Einstein Center for Fundamental Physics and Laboratory for High Energy Physics, University of Bern, Bern; Switzerland.
- ²⁰School of Physics and Astronomy, University of Birmingham, Birmingham; United Kingdom.
- ²¹(*a*) Department of Physics, Bogazici University, Istanbul; (*b*) Department of Physics Engineering, Gaziantep University, Gaziantep; (*c*) Department of Physics, Istanbul University, Istanbul; Türkiye.
- ²²(*a*) Facultad de Ciencias y Centro de Investigaciones, Universidad Antonio Nariño, Bogotá; (*b*) Departamento de Física, Universidad Nacional de Colombia, Bogotá; Colombia.
- ²³(*a*) Dipartimento di Fisica e Astronomia A. Righi, Università di Bologna, Bologna; (*b*) INFN Sezione di Bologna; Italy.
- ²⁴Physikalisches Institut, Universität Bonn, Bonn; Germany.
- ²⁵Department of Physics, Boston University, Boston MA; United States of America.
- ²⁶Department of Physics, Brandeis University, Waltham MA; United States of America.
- ²⁷(*a*) Transilvania University of Brasov, Brasov; (*b*) Horia Hulubei National Institute of Physics and Nuclear Engineering, Bucharest; (*c*) Department of Physics, Alexandru Ioan Cuza University of Iasi, Iasi; (*d*) National Institute for Research and Development of Isotopic and Molecular Technologies, Physics Department, Cluj-Napoca; (*e*) National University of Science and Technology Politehnica, Bucharest; (*f*) West University in Timisoara, Timisoara; (*g*) Faculty of Physics, University of Bucharest, Bucharest; Romania.
- ²⁸(*a*) Faculty of Mathematics, Physics and Informatics, Comenius University, Bratislava; (*b*) Department of Subnuclear Physics, Institute of Experimental Physics of the Slovak Academy of Sciences, Kosice; Slovak Republic.
- ²⁹Physics Department, Brookhaven National Laboratory, Upton NY; United States of America.
- ³⁰Universidad de Buenos Aires, Facultad de Ciencias Exactas y Naturales, Departamento de Física, y CONICET, Instituto de Física de Buenos Aires (IFIBA), Buenos Aires; Argentina.
- ³¹California State University, CA; United States of America.
- ³²Cavendish Laboratory, University of Cambridge, Cambridge; United Kingdom.
- ³³(*a*) Department of Physics, University of Cape Town, Cape Town; (*b*) iThemba Labs, Western Cape; (*c*) Department of Mechanical Engineering Science, University of Johannesburg, Johannesburg; (*d*) National Institute of Physics, University of the Philippines Diliman (Philippines); (*e*) University of South Africa, Department of Physics, Pretoria; (*f*) University of Zululand, KwaDlangezwa; (*g*) School of Physics, University of the Witwatersrand, Johannesburg; South Africa.
- ³⁴Department of Physics, Carleton University, Ottawa ON; Canada.
- ³⁵(*a*) Faculté des Sciences Ain Chock, Réseau Universitaire de Physique des Hautes Energies - Université Hassan II, Casablanca; (*b*) Faculté des Sciences, Université Ibn-Tofail, Kénitra; (*c*) Faculté des Sciences Semlalia, Université Cadi Ayyad, LPHEA-Marrakech; (*d*) LPMR, Faculté des Sciences, Université Mohamed Premier, Oujda; (*e*) Faculté des sciences, Université Mohammed V, Rabat; (*f*) Institute of Applied Physics, Mohammed VI Polytechnic University, Ben Guerir; Morocco.
- ³⁶CERN, Geneva; Switzerland.
- ³⁷Affiliated with an institute covered by a cooperation agreement with CERN.
- ³⁸Affiliated with an international laboratory covered by a cooperation agreement with CERN.
- ³⁹Enrico Fermi Institute, University of Chicago, Chicago IL; United States of America.
- ⁴⁰LPC, Université Clermont Auvergne, CNRS/IN2P3, Clermont-Ferrand; France.
- ⁴¹Nevis Laboratory, Columbia University, Irvington NY; United States of America.
- ⁴²Niels Bohr Institute, University of Copenhagen, Copenhagen; Denmark.
- ⁴³(*a*) Dipartimento di Fisica, Università della Calabria, Rende; (*b*) INFN Gruppo Collegato di Cosenza,

Laboratori Nazionali di Frascati; Italy.

⁴⁴Physics Department, Southern Methodist University, Dallas TX; United States of America.

⁴⁵Physics Department, University of Texas at Dallas, Richardson TX; United States of America.

⁴⁶National Centre for Scientific Research "Demokritos", Agia Paraskevi; Greece.

⁴⁷(^a) Department of Physics, Stockholm University; (^b) Oskar Klein Centre, Stockholm; Sweden.

⁴⁸Deutsches Elektronen-Synchrotron DESY, Hamburg and Zeuthen; Germany.

⁴⁹Fakultät Physik, Technische Universität Dortmund, Dortmund; Germany.

⁵⁰Institut für Kern- und Teilchenphysik, Technische Universität Dresden, Dresden; Germany.

⁵¹Department of Physics, Duke University, Durham NC; United States of America.

⁵²SUPA - School of Physics and Astronomy, University of Edinburgh, Edinburgh; United Kingdom.

⁵³INFN e Laboratori Nazionali di Frascati, Frascati; Italy.

⁵⁴Physikalisches Institut, Albert-Ludwigs-Universität Freiburg, Freiburg; Germany.

⁵⁵II. Physikalisches Institut, Georg-August-Universität Göttingen, Göttingen; Germany.

⁵⁶Département de Physique Nucléaire et Corpusculaire, Université de Genève, Genève; Switzerland.

⁵⁷(^a) Dipartimento di Fisica, Università di Genova, Genova; (^b) INFN Sezione di Genova; Italy.

⁵⁸II. Physikalisches Institut, Justus-Liebig-Universität Giessen, Giessen; Germany.

⁵⁹SUPA - School of Physics and Astronomy, University of Glasgow, Glasgow; United Kingdom.

⁶⁰LPSC, Université Grenoble Alpes, CNRS/IN2P3, Grenoble INP, Grenoble; France.

⁶¹Laboratory for Particle Physics and Cosmology, Harvard University, Cambridge MA; United States of America.

⁶²(^a) Department of Modern Physics and State Key Laboratory of Particle Detection and Electronics, University of Science and Technology of China, Hefei; (^b) Institute of Frontier and Interdisciplinary Science and Key Laboratory of Particle Physics and Particle Irradiation (MOE), Shandong University, Qingdao; (^c) School of Physics and Astronomy, Shanghai Jiao Tong University, Key Laboratory for Particle Astrophysics and Cosmology (MOE), SKLPPC, Shanghai; (^d) Tsung-Dao Lee Institute, Shanghai; (^e) School of Physics and Microelectronics, Zhengzhou University; China.

⁶³(^a) Kirchhoff-Institut für Physik, Ruprecht-Karls-Universität Heidelberg, Heidelberg; (^b) Physikalisches Institut, Ruprecht-Karls-Universität Heidelberg, Heidelberg; Germany.

⁶⁴(^a) Department of Physics, Chinese University of Hong Kong, Shatin, N.T., Hong Kong; (^b) Department of Physics, University of Hong Kong, Hong Kong; (^c) Department of Physics and Institute for Advanced Study, Hong Kong University of Science and Technology, Clear Water Bay, Kowloon, Hong Kong; China.

⁶⁵Department of Physics, National Tsing Hua University, Hsinchu; Taiwan.

⁶⁶IJCLab, Université Paris-Saclay, CNRS/IN2P3, 91405, Orsay; France.

⁶⁷Centro Nacional de Microelectrónica (IMB-CNM-CSIC), Barcelona; Spain.

⁶⁸Department of Physics, Indiana University, Bloomington IN; United States of America.

⁶⁹(^a) INFN Gruppo Collegato di Udine, Sezione di Trieste, Udine; (^b) ICTP, Trieste; (^c) Dipartimento Politecnico di Ingegneria e Architettura, Università di Udine, Udine; Italy.

⁷⁰(^a) INFN Sezione di Lecce; (^b) Dipartimento di Matematica e Fisica, Università del Salento, Lecce; Italy.

⁷¹(^a) INFN Sezione di Milano; (^b) Dipartimento di Fisica, Università di Milano, Milano; Italy.

⁷²(^a) INFN Sezione di Napoli; (^b) Dipartimento di Fisica, Università di Napoli, Napoli; Italy.

⁷³(^a) INFN Sezione di Pavia; (^b) Dipartimento di Fisica, Università di Pavia, Pavia; Italy.

⁷⁴(^a) INFN Sezione di Pisa; (^b) Dipartimento di Fisica E. Fermi, Università di Pisa, Pisa; Italy.

⁷⁵(^a) INFN Sezione di Roma; (^b) Dipartimento di Fisica, Sapienza Università di Roma, Roma; Italy.

⁷⁶(^a) INFN Sezione di Roma Tor Vergata; (^b) Dipartimento di Fisica, Università di Roma Tor Vergata, Roma; Italy.

⁷⁷(^a) INFN Sezione di Roma Tre; (^b) Dipartimento di Matematica e Fisica, Università Roma Tre, Roma; Italy.

- ⁷⁸(*a*) INFN-TIFPA; (*b*) Università degli Studi di Trento, Trento; Italy.
- ⁷⁹Universität Innsbruck, Department of Astro and Particle Physics, Innsbruck; Austria.
- ⁸⁰University of Iowa, Iowa City IA; United States of America.
- ⁸¹Department of Physics and Astronomy, Iowa State University, Ames IA; United States of America.
- ⁸²Istinye University, Sariyer, Istanbul; Türkiye.
- ⁸³(*a*) Departamento de Engenharia Elétrica, Universidade Federal de Juiz de Fora (UFJF), Juiz de Fora; (*b*) Universidade Federal do Rio De Janeiro COPPE/EE/IF, Rio de Janeiro; (*c*) Instituto de Física, Universidade de São Paulo, São Paulo; (*d*) Rio de Janeiro State University, Rio de Janeiro; (*e*) Federal University of Bahia, Bahia; Brazil.
- ⁸⁴KEK, High Energy Accelerator Research Organization, Tsukuba; Japan.
- ⁸⁵Graduate School of Science, Kobe University, Kobe; Japan.
- ⁸⁶(*a*) AGH University of Krakow, Faculty of Physics and Applied Computer Science, Krakow; (*b*) Marian Smoluchowski Institute of Physics, Jagiellonian University, Krakow; Poland.
- ⁸⁷Institute of Nuclear Physics Polish Academy of Sciences, Krakow; Poland.
- ⁸⁸Faculty of Science, Kyoto University, Kyoto; Japan.
- ⁸⁹Research Center for Advanced Particle Physics and Department of Physics, Kyushu University, Fukuoka ; Japan.
- ⁹⁰L2IT, Université de Toulouse, CNRS/IN2P3, UPS, Toulouse; France.
- ⁹¹Instituto de Física La Plata, Universidad Nacional de La Plata and CONICET, La Plata; Argentina.
- ⁹²Physics Department, Lancaster University, Lancaster; United Kingdom.
- ⁹³Oliver Lodge Laboratory, University of Liverpool, Liverpool; United Kingdom.
- ⁹⁴Department of Experimental Particle Physics, Jožef Stefan Institute and Department of Physics, University of Ljubljana, Ljubljana; Slovenia.
- ⁹⁵School of Physics and Astronomy, Queen Mary University of London, London; United Kingdom.
- ⁹⁶Department of Physics, Royal Holloway University of London, Egham; United Kingdom.
- ⁹⁷Department of Physics and Astronomy, University College London, London; United Kingdom.
- ⁹⁸Louisiana Tech University, Ruston LA; United States of America.
- ⁹⁹Fysiska institutionen, Lunds universitet, Lund; Sweden.
- ¹⁰⁰Departamento de Física Teórica C-15 and CIAFF, Universidad Autónoma de Madrid, Madrid; Spain.
- ¹⁰¹Institut für Physik, Universität Mainz, Mainz; Germany.
- ¹⁰²School of Physics and Astronomy, University of Manchester, Manchester; United Kingdom.
- ¹⁰³CPPM, Aix-Marseille Université, CNRS/IN2P3, Marseille; France.
- ¹⁰⁴Department of Physics, University of Massachusetts, Amherst MA; United States of America.
- ¹⁰⁵Department of Physics, McGill University, Montreal QC; Canada.
- ¹⁰⁶School of Physics, University of Melbourne, Victoria; Australia.
- ¹⁰⁷Department of Physics, University of Michigan, Ann Arbor MI; United States of America.
- ¹⁰⁸Department of Physics and Astronomy, Michigan State University, East Lansing MI; United States of America.
- ¹⁰⁹Group of Particle Physics, University of Montreal, Montreal QC; Canada.
- ¹¹⁰Fakultät für Physik, Ludwig-Maximilians-Universität München, München; Germany.
- ¹¹¹Max-Planck-Institut für Physik (Werner-Heisenberg-Institut), München; Germany.
- ¹¹²Graduate School of Science and Kobayashi-Maskawa Institute, Nagoya University, Nagoya; Japan.
- ¹¹³Department of Physics and Astronomy, University of New Mexico, Albuquerque NM; United States of America.
- ¹¹⁴Institute for Mathematics, Astrophysics and Particle Physics, Radboud University/Nikhef, Nijmegen; Netherlands.
- ¹¹⁵Nikhef National Institute for Subatomic Physics and University of Amsterdam, Amsterdam;

Netherlands.

¹¹⁶Department of Physics, Northern Illinois University, DeKalb IL; United States of America.

¹¹⁷^(a)New York University Abu Dhabi, Abu Dhabi;^(b)United Arab Emirates University, Al Ain; United Arab Emirates.

¹¹⁸Department of Physics, New York University, New York NY; United States of America.

¹¹⁹Ochanomizu University, Otsuka, Bunkyo-ku, Tokyo; Japan.

¹²⁰Ohio State University, Columbus OH; United States of America.

¹²¹Homer L. Dodge Department of Physics and Astronomy, University of Oklahoma, Norman OK; United States of America.

¹²²Department of Physics, Oklahoma State University, Stillwater OK; United States of America.

¹²³Palacký University, Joint Laboratory of Optics, Olomouc; Czech Republic.

¹²⁴Institute for Fundamental Science, University of Oregon, Eugene, OR; United States of America.

¹²⁵Graduate School of Science, Osaka University, Osaka; Japan.

¹²⁶Department of Physics, University of Oslo, Oslo; Norway.

¹²⁷Department of Physics, Oxford University, Oxford; United Kingdom.

¹²⁸LPNHE, Sorbonne Université, Université Paris Cité, CNRS/IN2P3, Paris; France.

¹²⁹Department of Physics, University of Pennsylvania, Philadelphia PA; United States of America.

¹³⁰Department of Physics and Astronomy, University of Pittsburgh, Pittsburgh PA; United States of America.

¹³¹^(a)Laboratório de Instrumentação e Física Experimental de Partículas - LIP, Lisboa;^(b)Departamento de Física, Faculdade de Ciências, Universidade de Lisboa, Lisboa;^(c)Departamento de Física, Universidade de Coimbra, Coimbra;^(d)Centro de Física Nuclear da Universidade de Lisboa, Lisboa;^(e)Departamento de Física, Universidade do Minho, Braga;^(f)Departamento de Física Teórica y del Cosmos, Universidad de Granada, Granada (Spain);^(g)Departamento de Física, Instituto Superior Técnico, Universidade de Lisboa, Lisboa; Portugal.

¹³²Institute of Physics of the Czech Academy of Sciences, Prague; Czech Republic.

¹³³Czech Technical University in Prague, Prague; Czech Republic.

¹³⁴Charles University, Faculty of Mathematics and Physics, Prague; Czech Republic.

¹³⁵Particle Physics Department, Rutherford Appleton Laboratory, Didcot; United Kingdom.

¹³⁶IRFU, CEA, Université Paris-Saclay, Gif-sur-Yvette; France.

¹³⁷Santa Cruz Institute for Particle Physics, University of California Santa Cruz, Santa Cruz CA; United States of America.

¹³⁸^(a)Departamento de Física, Pontificia Universidad Católica de Chile, Santiago;^(b)Millennium Institute for Subatomic physics at high energy frontier (SAPHIR), Santiago;^(c)Instituto de Investigación Multidisciplinario en Ciencia y Tecnología, y Departamento de Física, Universidad de La Serena;^(d)Universidad Andres Bello, Department of Physics, Santiago;^(e)Instituto de Alta Investigación, Universidad de Tarapacá, Arica;^(f)Departamento de Física, Universidad Técnica Federico Santa María, Valparaíso; Chile.

¹³⁹Department of Physics, University of Washington, Seattle WA; United States of America.

¹⁴⁰Department of Physics and Astronomy, University of Sheffield, Sheffield; United Kingdom.

¹⁴¹Department of Physics, Shinshu University, Nagano; Japan.

¹⁴²Department Physik, Universität Siegen, Siegen; Germany.

¹⁴³Department of Physics, Simon Fraser University, Burnaby BC; Canada.

¹⁴⁴SLAC National Accelerator Laboratory, Stanford CA; United States of America.

¹⁴⁵Department of Physics, Royal Institute of Technology, Stockholm; Sweden.

¹⁴⁶Departments of Physics and Astronomy, Stony Brook University, Stony Brook NY; United States of America.

- ¹⁴⁷Department of Physics and Astronomy, University of Sussex, Brighton; United Kingdom.
- ¹⁴⁸School of Physics, University of Sydney, Sydney; Australia.
- ¹⁴⁹Institute of Physics, Academia Sinica, Taipei; Taiwan.
- ¹⁵⁰^(a)E. Andronikashvili Institute of Physics, Iv. Javakhishvili Tbilisi State University, Tbilisi; ^(b)High Energy Physics Institute, Tbilisi State University, Tbilisi; ^(c)University of Georgia, Tbilisi; Georgia.
- ¹⁵¹Department of Physics, Technion, Israel Institute of Technology, Haifa; Israel.
- ¹⁵²Raymond and Beverly Sackler School of Physics and Astronomy, Tel Aviv University, Tel Aviv; Israel.
- ¹⁵³Department of Physics, Aristotle University of Thessaloniki, Thessaloniki; Greece.
- ¹⁵⁴International Center for Elementary Particle Physics and Department of Physics, University of Tokyo, Tokyo; Japan.
- ¹⁵⁵Department of Physics, Tokyo Institute of Technology, Tokyo; Japan.
- ¹⁵⁶Department of Physics, University of Toronto, Toronto ON; Canada.
- ¹⁵⁷^(a)TRIUMF, Vancouver BC; ^(b)Department of Physics and Astronomy, York University, Toronto ON; Canada.
- ¹⁵⁸Division of Physics and Tomonaga Center for the History of the Universe, Faculty of Pure and Applied Sciences, University of Tsukuba, Tsukuba; Japan.
- ¹⁵⁹Department of Physics and Astronomy, Tufts University, Medford MA; United States of America.
- ¹⁶⁰Department of Physics and Astronomy, University of California Irvine, Irvine CA; United States of America.
- ¹⁶¹University of Sharjah, Sharjah; United Arab Emirates.
- ¹⁶²Department of Physics and Astronomy, University of Uppsala, Uppsala; Sweden.
- ¹⁶³Department of Physics, University of Illinois, Urbana IL; United States of America.
- ¹⁶⁴Instituto de Física Corpuscular (IFIC), Centro Mixto Universidad de Valencia - CSIC, Valencia; Spain.
- ¹⁶⁵Department of Physics, University of British Columbia, Vancouver BC; Canada.
- ¹⁶⁶Department of Physics and Astronomy, University of Victoria, Victoria BC; Canada.
- ¹⁶⁷Fakultät für Physik und Astronomie, Julius-Maximilians-Universität Würzburg, Würzburg; Germany.
- ¹⁶⁸Department of Physics, University of Warwick, Coventry; United Kingdom.
- ¹⁶⁹Waseda University, Tokyo; Japan.
- ¹⁷⁰Department of Particle Physics and Astrophysics, Weizmann Institute of Science, Rehovot; Israel.
- ¹⁷¹Department of Physics, University of Wisconsin, Madison WI; United States of America.
- ¹⁷²Fakultät für Mathematik und Naturwissenschaften, Fachgruppe Physik, Bergische Universität Wuppertal, Wuppertal; Germany.
- ¹⁷³Department of Physics, Yale University, New Haven CT; United States of America.
- ^a Also Affiliated with an institute covered by a cooperation agreement with CERN.
- ^b Also at An-Najah National University, Nablus; Palestine.
- ^c Also at Borough of Manhattan Community College, City University of New York, New York NY; United States of America.
- ^d Also at Center for Interdisciplinary Research and Innovation (CIRI-AUTH), Thessaloniki; Greece.
- ^e Also at Centro Studi e Ricerche Enrico Fermi; Italy.
- ^f Also at CERN, Geneva; Switzerland.
- ^g Also at Département de Physique Nucléaire et Corpusculaire, Université de Genève, Genève; Switzerland.
- ^h Also at Departament de Física de la Universitat Autònoma de Barcelona, Barcelona; Spain.
- ⁱ Also at Department of Financial and Management Engineering, University of the Aegean, Chios; Greece.
- ^j Also at Department of Physics, California State University, Sacramento; United States of America.
- ^k Also at Department of Physics, King's College London, London; United Kingdom.
- ^l Also at Department of Physics, Stanford University, Stanford CA; United States of America.

- m* Also at Department of Physics, Stellenbosch University; South Africa.
- n* Also at Department of Physics, University of Fribourg, Fribourg; Switzerland.
- o* Also at Department of Physics, University of Thessaly; Greece.
- p* Also at Department of Physics, Westmont College, Santa Barbara; United States of America.
- q* Also at Hellenic Open University, Patras; Greece.
- r* Also at Institutio Catalana de Recerca i Estudis Avancats, ICREA, Barcelona; Spain.
- s* Also at Institut für Experimentalphysik, Universität Hamburg, Hamburg; Germany.
- t* Also at Institute for Nuclear Research and Nuclear Energy (INRNE) of the Bulgarian Academy of Sciences, Sofia; Bulgaria.
- u* Also at Institute of Applied Physics, Mohammed VI Polytechnic University, Ben Guerir; Morocco.
- v* Also at Institute of Particle Physics (IPP); Canada.
- w* Also at Institute of Physics and Technology, Mongolian Academy of Sciences, Ulaanbaatar; Mongolia.
- x* Also at Institute of Physics, Azerbaijan Academy of Sciences, Baku; Azerbaijan.
- y* Also at Institute of Theoretical Physics, Ilia State University, Tbilisi; Georgia.
- z* Also at Lawrence Livermore National Laboratory, Livermore; United States of America.
- aa* Also at National Institute of Physics, University of the Philippines Diliman (Philippines); Philippines.
- ab* Also at Technical University of Munich, Munich; Germany.
- ac* Also at The Collaborative Innovation Center of Quantum Matter (CICQM), Beijing; China.
- ad* Also at TRIUMF, Vancouver BC; Canada.
- ae* Also at Università di Napoli Parthenope, Napoli; Italy.
- af* Also at University of Colorado Boulder, Department of Physics, Colorado; United States of America.
- ag* Also at Washington College, Chestertown, MD; United States of America.
- ah* Also at Yeditepe University, Physics Department, Istanbul; Türkiye.
- * Deceased